1   **Theoretical estimates of equilibrium sulfur isotope effects in aqueous sulfur systems:**

2   **Highlighting the role of isomers in the sulfite and sulfoxylate systems**

3   D.L. Eldridge[a]*, W. Guo[b], J. Farquhar[a]

4   **Affiliations:**

5   [a] Department of Geology and ESSIC, University of Maryland, College Park, MD 20740, USA

6   [b] Department of Geology and Geophysics, Woods Hole Oceanographic Institution, Woods Hole, MA

7   02543, USA

8   *Corresponding Author: eldridge@umd.edu

9

10

11

12

13

14

15

16

17

18

19

20

21

22

23

24

25

26

27

28

Abstract

We present theoretical calculations for all three isotope ratios of sulfur ($^{33}S/^{32}S$, $^{34}S/^{32}S$, $^{36}S/^{32}S$) at the B3LYP/6-31+G(d,p) level of theory for aqueous sulfur compounds modeled in 30-40 H_2O clusters spanning the range of sulfur oxidation state (S^n, n = -2 to +6) for estimating equilibrium fractionation factors in aqueous systems. Computed $^{34}\beta$ values based on major isotope ($^{34}S/^{32}S$) reduced partition function ratios (RPFRs) scale to a first order with sulfur oxidation state and coordination, where $^{34}\beta$ generally increase with higher oxidation state and increasing coordination of the sulfur atom. Exponents defining mass dependent relationships based on β values ($^{x/34}\kappa$ = $\ln(^x\beta)/\ln(^{34}\beta)$, x = 33 or 36) conform to tight ranges over a wide range of temperature for all aqueous compounds ($^{33/34}\kappa \approx 0.5148\text{-}0.5159$, $^{36/34}\kappa \approx 1.89\text{-}1.90$ from T ≥ 0°C). The exponents converge near a singular value for all compounds at the high temperature limit ($^{33/34}\kappa_{T\to\infty}$ = 0.51587 ± 0.00003 and $^{36/34}\kappa_{T\to\infty}$ = 1.8905 ± 0.0002; 1 s.d. of all computed compounds), and typically follow trends based on oxidation state and coordination similar to those seen in $^{34}\beta$ values at lower temperatures. Theoretical equilibrium fractionation factors computed from these β-values are compared to experimental constraints for $HSO_3^-{}_{T(aq)}/SO_{2(g,\,aq)}$, $SO_{2(aq)}/SO_{2(g)}$, $H_2S_{(aq)}/H_2S_{(g)}$, $H_2S_{(aq)}/HS^-{}_{(aq)}$, $SO_4^{2-}{}_{(aq)}/H_2S_{T(aq)}$, $S_2O_3^{2-}{}_{(aq)}$ (intramolecular), and $S_2O_3^{2-}{}_{(aq)}/H_2S_{T(aq)}$, and generally agree within a reasonable estimation of uncertainties. We make predictions of fractionation factors where other constraints are unavailable. Isotope partitioning of the isomers of protonated compounds in the sulfite and sulfoxylate systems depend strongly on whether protons are bound to either sulfur or oxygen atoms. The magnitude of the $HSO_3^-{}_T/SO_3^{2-}$ major isotope ($^{34}S/^{32}S$) fractionation factor is predicted to increase with temperature from 0-70°C due to the combined effects of the large magnitude $(HS)O_3^-/SO_3^{2-}$ fractionation factor ($1000\ln^{34}\alpha_{(HS)bisulfite\text{-}sulfite}$ = 19.9 ‰, 25°C) relative to the $(HO)SO_2^-/SO_3^{2-}$ fractionation factor ($1000\ln^{34}\alpha_{(HO)bisulfite\text{-}sulfite}$ = -2.2 ‰, 25°C), and the increased stability of the $(HS)O_3^-$ isomer with increasing temperature. We argue that isomerization phenomenon should be considered in models of the sulfur cycle, including models that describe the overall sulfur isotope fractionations associated with microbial metabolism (e.g., microbial sulfate reduction).

1.0 Introduction

1.1 Overview

        Quantum mechanical electronic structure calculations of aqueous clusters complement experimental investigations of isotope effects in aqueous systems (e.g., Rustad et al., 2008; Rustad et al., 2010; Zeebe, 2009), and have been instrumental for predicting isotope effects when experimental determinations are unavailable (e.g., Li et al., 2009; Li and Liu, 2011). Theoretical approaches are especially useful for compounds like those of the sulfite and sulfoxylate systems that contain numerous compounds that are difficult to experimentally isolate and study directly. The aim of the present study is to: (1) provide an internally consistent set of constraints for equilibrium isotope fractionations among aqueous sulfur compounds relevant to low and high temperature conditions, emphasizing the poorly documented sulfite and sulfoxylate systems; (2) provide new constraints on the exponents of mass-dependence associated with equilibrium isotope fractionation in aqueous systems and their relationships to sulfur oxidation state and bonding environment; (3) compare our theoretical constraints to the available experimental datasets and make predictions where estimates are currently unavailable, and assess where future experimental work may be needed; and (4) illustrate the effects of isomerization on isotope partitioning in the sulfite system where isomerization leads to relatively large and apparently unusual effects in observable isotope fractionation behavior.

1.2 Sulfite and Sulfoxylate in the Sulfur Cycle

        The sulfite (denoted $SO_3^{2-}{}_T$) and sulfoxylate systems (denoted $SO_2^{2-}{}_T$) are the series of inorganic compounds and oxyanions that contain sulfur in the +4 and +2 oxidation states, respectively. These oxidation states are intermediate between the most common end member sulfur oxidation states of -2 as the most reduced (e.g., $H_2S/HS^-/S^{2-}$) and +6 as the most oxidized (e.g., SO_4^{2-}). Sulfite is a well-documented intermediate in a variety of settings where sulfur is cycled, and sulfoxylate species, while very rarely observed, are inferred to be a 'missing-link' oxidation state in sulfur redox processes between zero-valent sulfur compounds (e.g., generically as S^0) and those of the sulfite system.

1.2.1 Sulfite In the Sulfur Cycle

85   Sulfite *sensu lato* in natural environments is typically transient and does not comprise a

86   significant fraction of the bulk sulfur in Earth's surface environment but nevertheless plays essential

87   roles in the environmental cycling of sulfur and related elemental cycles. The hydrolysis and

88   subsequent oxidation of sulfur dioxide in atmospheric water droplets is a major pathway of acid-rain

89   formation (e.g., Brandt and van Eldik, 1995). Sulfite is a major intermediate in both the oxidative and

90   reductive portions of the sulfur cycle, including the microbial production and subsequent oxidation

91   of sulfide (HS$^-$/H$_2$S; Zhang and Millero, 1993; Zopfi et al., 2004). In marine sediments containing

92   relatively high amounts of organic matter, sulfide is generated as a byproduct of anaerobic

93   respiration (microbial sulfate reduction; MSR) and ca. 80-95% of the sulfide produced is eventually

94   re-oxidized through intermediates like sulfite back to sulfate (Jørgensen, 1977; Jørgensen, 1982;

95   Jørgensen et al., 1990; Canfield and Teske, 1996; Jørgensen and Nelson, 2004). Depending on the

96   conditions and biota present, the sulfite thus produced can support or supplement a variety of

97   metabolisms carried out by microorganisms that oxidize, reduce, and disproportionate sulfite and

98   other intermediate sulfur compounds for overall energy conservation and metabolic function.

99   At the intracellular level, sulfite (*sensu lato*) is a pivotal intermediate during microbial sulfate

100   reduction (MSR), which in general is responsible for the oxidation of much of the organic matter

101   contained in modern marine sediments (e.g., Bowels et al., 2014). Intracellular sulfite within a

102   sulfate reducing microorganism sits between two reversible transformations: (1) its production via

103   the reduction of activated sulfate (adenosine-5'-phosphosulfate; cleaving an S-O bond) and (2) its

104   reaction with the siroheme active site of dissimilatory sulfite reductase (dSiR) where it is reduced to

105   eventually form the end waste product sulfide via other enzymatically-bound intermediates like

106   sulfoxylate (S^{2+}) and zero-valent sulfur (S^0) (Parey et al., 2010). The sulfide thus produced and its

107   subsequent cycling in the environment places primary controls on the isotopic composition of

108   authigenic pyrite, which in sedimentary rocks serves as a major archive of the sulfur cycle through

109   geologic time. Isotope network models that attempt to constrain the overall sulfur isotope

110   fractionations that occur during the step-wise reduction of sulfate have relied on estimations of

111   fractionation factors involving sulfite compounds (e.g., Wing and Halevy, 2014), but these

112   fractionations have yet to be determined in detail. In particular, present network models simplify the

113   intracellular inorganic speciation of sulfite (assuming sulfite *sensu stricto* only, SO_3^{2-}) and have yet to

114   take into consideration the influence of bisulfite compounds (generically: HSO_3^-).

115   *1.2.2 Sulfur Isotope Partitioning in the Sulfite System*

116   Despite the recognized importance of sulfite in the overall cycling of sulfur, the

117   determination of the equilibrium isotope fractionations among various sulfite species has received

118   very little attention. To our knowledge, only one set of experimental constraints has been reported

119   (Eriksen, 1972a; Eriksen, 1972b; Eriksen, 1972c), suggesting a fractionation factor between bulk

120   bisulfite in solution and gaseous SO_2 ($1000\ln^{34}\alpha_{bisulfite\text{-}SO2(g)}$) of 10.9 ± 1.4 ‰ (1 s.d., 10 experiments)

121   at 25°C (Eriksen, 1972a). No resolvable change in this fractionation factor was observed over the

122   investigated temperature range of 25-45°C. Fractionations among aqueous sulfite species (e.g., the

123   bisulfite compounds and sulfite) are completely unconstrained. Given that these are the dominant

124   species under most natural conditions as well as within sulfate reducing organisms, these

125   fractionations are key to a detailed understanding of sulfite isotope systematics in natural systems.

126   *1.2.3 Sulfoxylate in the Sulfur Cycle*

127   Sulfoxylate species are difficult to detect and analyze and their role in the (bio)geochemical

128   cycling of sulfur is not well understood. Hoffmann and Lim (1979) were among the first to suggest

129   sulfoxylate as a reaction intermediate of the sulfide oxidation mechanism in a scheme of hypothetical

130   reactions known as the polar mechanism (*cf.* Zhang and Millero, 1993). In this scheme, sulfoxylate is

131   postulated to be among the initial products of oxidation, and a key intermediate in the formation of

132   sulfite species and thiosulfate that are commonly observed products of the reaction (e.g., Cline and

133   Richards, 1969; Chen and Morris, 1972; Zhang and Millero, 1993). Vairavamurthy and Zhou (1995)

134   confirmed the presence of an S^{2+} oxyanion during sulfide oxidation via sulfur k-edge X-Ray

135   Absorbance Near Edge Structure (S-XANES) spectroscopy and attributed it to the sulfoxylate (SO_2^{2-})

136   structure based on Fourier Transformed Infrared (FT-IR) spectroscopic analysis. Tossell (1997) later

137   compared the spectral observations of Vairavamurthy and Zhou (1995) and their pH dependence

138   with calculated vibrational frequencies of sulfoxylate compounds, and revised the species identified

139   by Vairavamurthy and Zhou (1995) to more likely be bisulfoxylate (HSO_2^-) where the proton is bound

140   to an oxygen atom (denoted $(HO)SO^-$). To date, the study of Vairavamurthy and Zhou (1995) appears

141   to be the only study to directly document sulfoxylate compounds in sulfur redox processes.

142   Sulfur in the +2 oxidation state is a hypothesized intracellular intermediate during MSR. In

143   recent biochemically-informed models (Oliveira et al., 2008; Parey et al., 2010; Bradley et al., 2011;

144   Wing and Halevy, 2014; Santos et al., 2015), the reduction of sulfite at the siroheme-[4Fe-4S]

145   catalytic site in dissimilatory sulfite reductase occurs stepwise, first producing a bound S^{2+}

146   intermediate, then a bound S^0-intermediate before eventually forming sulfide facilitated via a

147   complex mechanism involving a Dsr-related protein known as DsrC (Oliveira et al., 2008; Santos et

148   al., 2015). Reactions of these enzymatically-bound intermediate moieties (S^{2+}, S^0) via nucleophilic

149   attack by residual non-enzymatically bound sulfite species have been hypothesized pathways for the

150   generation of polythionates (principally trithionate, $S_3O_6^{2-}$) and thiosulfate ($S_2O_3^{2-}$) that have been

151   observed in some MSR culture experiments (Parey et al., 2010). If the hypothesized S^{2+}

152   intermediates detach from the catalytic site and form free aqueous species, they are likely to be

153   included within the sulfoxylate system. The speciation and isotope partitioning behavior of inorganic

154   sulfoxylate compounds in intracellular media may play additional roles in the distribution of sulfur

155   isotopes within the MSR framework, and remains to be investigated in detail.

156   **2.0 Background: Aqueous Sulfur Speciation**

157   *2.1 Sulfite System Chemistry*

158   Sulfite species are distributed in solution as a continuum that depends on pH, temperature,

159   ionic strength (μ), and total S(IV) concentration (see Figure 1). A summary of select equilibrium

160   quotients related to sulfite speciation is included in Table S.1. At $\mu \sim 0$ m and 25°C, dissolved SO_2

161   dominates sulfite solutions under extremely acidic conditions (pH < 1.9), bisulfite compounds

162   dominate at 1.9 < pH < 7.2, and sulfite *sensu stricto* at pH > 7.2 (Martell and Smith, 1982; Beyad et al.,

163   2014). The hypothetical sulfurous acid (two generic groups of isomers: $SO(OH)_2$ and $(HS)O_2OH$;

164   collectively H_2SO_3) may be intermediary in the hydrolysis of SO_2 to form bisulfite anions, but has

165   never been detected in solution (Gerding and Nijveld, 1936; Falk and Giguere, 1958; Zhang and

166   Ewing, 2002; Voegele et al., 2004). Sulfurous acid (and related isomers) is therefore unlikely to be a

167   significant component of the mass balance.

168   Bisulfite exists in two isomeric forms: one tetrahedral form where the proton is bound to the

169   sulfur—denoted herein as $(HS)O_3^-$—and another that is pyramidal where the proton is bound to one

170   of the oxygen atoms—denoted herein as $(HO)SO_2^-$ (Golding, 1960 and references therein; Connick et

171   al., 1982; Horner and Connick, 1986; Littlejohn et al., 1992; Risberg et al., 2007). The relative

172   proportions of the bisulfite isomers in solution is given by the isomerization quotient (Q_i), defined as:

173                      $(HS)O_3^- \rightleftharpoons (HO)SO_2^-$ $Q_i = [(HO)SO_2^-]/[(HS)O_3^-]$,   (1)

174   where brackets "[ ]" denote concentrations. Studies utilizing ^{17}O-NMR, IR-Raman, and sulfur k-edge

175   XANES spectroscopy have shown that the OH-bonded pyramidal isomer of bisulfite is the dominant

176   form in solution at low temperature, comprising ~72-84% of bisulfite at 25°C depending on ionic

177   strength (see Figure 1; Horner and Connick, 1986; Littlejohn et al., 1992; Risberg et al., 2007).

178   The relative proportion of the bisulfite isomers is temperature-dependent, and the

179   proportion of the HS-bonded isomer increases with increasing temperature (Horner and Connick,

180   1986; Littlejohn et al., 1992; Risberg et al., 2007). Horner and Connick (1986) and Littlejohn et al.

181   (1992) determined the quotient in a medium of relatively high ionic strength (μ = 1 m) over a total

182   temperature range of 2-67°C, from which the following temperature dependence is obtained (Figure

183   2):

184                $\ln Q_i = 1413(\pm119)/T - 3.1(\pm0.4)$ (T = 275-340 K; μ = 1 m)   (2)

185   The isomerization quotient may be a strong function of ionic strength as indicated by the much lower

186   Q_i more recently determined in a low-ionic strength medium at 25°C (*cf.* Risberg, 2007; Figures 1 and

187   2, Table S.1). This suggests that application of the quotients of Horner and Connick (1986) and

188   Littlejohn et al. (1992) to solutions of lower ionic strength may significantly underestimate the

189   amount of $(HS)O_3^-$ present in solution. However, the exact effect of ionic strength on the

190   isomerization quotient is yet to be quantified over a wide range of temperatures relevant to many

191   natural systems.

192   Bisulfite can also form dimers in solution (*cf.* Golding, 1960). The principle dimer of bisulfite

193   is $S_2O_5^{2-}$ known as pyrosulfite or disulfite, whose structure can be schematically illustrated as: (O_2S-

194    $SO_3)^{2-}$ (note, however, that an aqueous form with a bridging oxygen—$(O_2S-O-SO_2)^{2-}$—remains to be

195   ruled out in solution; *cf.* Williamson and Rimstidt, 1992).   The extent of dimerization varies as a

196   function of the total bisulfite concentration and is quantified as the dimerization quotient (Q_d):

197                   $2HSO_3^-{}_T \rightleftharpoons S_2O_5^{2-} + H_2O$ $Q_d = [S_2O_5^{2-}]/[HSO_3^-{}_T]^2$; (M^{-1})   (3)
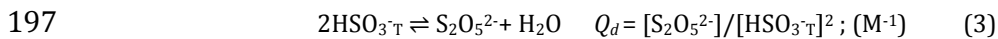
198   Studies directed at quantifying the dimerization quotient have produced varied results (see Table

199   S.1). Some of the discrepancies may have arisen from a variety of experimental errors in the earliest

200   determinations (see discussion in Connick et al., 1982). The existing experimental datasets indicate

201   that total bisulfite has to reach concentrations on the order of ≥ 0.1 M in order for significant

202   conversion to the dimer to occur. For example, the dimer comprises ≤1% of total bisulfite at $[HSO_3^-]_T$

203   ≤ 0.12 M at μ=1 *m* and ≤ 1% of total bisulfite at $[HSO_3^-]_T$ ≤ ~0.29 M at μ = 0 (using the quotients of

204   Connick et al., 1982). Recently, Beyad et al. (2014) found evidence for a protonated dimer ($HS_2O_5^-$)

205   via UV-spectrophotometric titrations and quantified its dissociation quotient (Table S.1).

206   *2.2 Sulfoxylate System Chemistry*

207   The sulfoxylate system comprises aqueous sulfur compounds and oxyanions in the 2+

208   oxidation state (S^{2+}), including compounds of the general compositions: H_2SO_2, HSO_2^-, and SO_2^{2-}.

209   Makarov et al. (2010) is among the few studies to report the acid dissociation quotients of H_2SO_2:

210   H_2SO_2 dominates at pH < 7.97, bisulfoxylate species (HSO_2^-) from 7.97 < pH < 13.55, and sulfoxylate

211   (SO_2^{2-}) at pH > 13.55 (T= 25°C, μ = 0.1 *m*; Makarov et al., 2010). Electronic structure calculations

212   have shown that the lowest energy configurations of H_2SO_2 in vacuum are rotamers of sulfoxylic acid

213   (denoted $S(OH)_2$), where the protons are bound to each of the oxygen atoms and differ structurally in

214   the relative orientation of the O-H bonds (Steiger and Steudel, 1992; Tossell, 1997; Napolion et al.,

215   2008; Crabtree et al., 2013). Other isomers of H_2SO_2 of potential significance are those termed

216   sulfinic acid, where one proton is bound to the sulfur atom and the other to one of the oxygen atoms

217   (denoted: $(HS)O_2H$). The relative stabilities of these isomers in solution are not constrained, nor are

218   the isomers of bisulfoxylate: $(HS)O_2^-$ and $(HO)SO^-$. Sulfur monoxide (SO) would be the hypothetical

219   unhydrolyzed component of the system (analogous to SO_2 in the sulfite system), but it is extremely

220   unstable and not known to undergo hydrolysis to form H_2SO_2 (Lyons and Nickless, 1968 and

221   references therein). Sulfur monoxide will not be considered a component of this system in this study.

222   *2.3 Aqueous Sulfide, Thiosulfate, and Sulfate*

223   Aqueous sulfide compounds (H_2S, HS^-, and S^{2-}) and sulfate (SO_4^{2-}) represent the lowest and

224   highest oxidation states of sulfur (-2 and +6, respectively), and are the most abundant forms of sulfur

225   in natural systems, either in aqueous or mineral form. Thiosulfate ($S_2O_3^{2-}$) is also a relatively

226   common mixed-valence intermediate in sulfur cycling processes (e.g., Jørgensen, 1990; Jørgensen

227   and Nelson, 2004; Zopfi et al., 2004).

228   The first acid dissociation quotient of H_2S is very close to neutral pH at 25°C and $\mu = 0$ m (H_2S

229     $\rightleftharpoons HS^-$ + H^+, pQ_{d1} = 6.98; Hershey et al., 1988). In the range of ca. 100-350°C, pQ_{d1} increases with

230   increasing temperature (e.g., at 300°C, p$Q_{d1} \approx 8.2$; Ellis and Giggenbach, 1971; Ohmoto and Lasaga,

231   1982). The second acid dissociation quotient ($HS^- \rightleftharpoons S^{2-} + H^+$, p$Q_{d2}$) is not as well constrained, but

232   likely to be on the order of p$Q_{d2} \approx$ 17-18 at 25°C (Ellis and Giggenbach, 1971; Schoonen and Barnes,

233   1988; Migdisov et al., 2002). Thus, S^{2-} may only comprise an appreciable component of aqueous

234   sulfide speciation in highly alkaline solutions possibly at high temperature (Ellis and Giggenbach,

235   1971). Under the conditions of most natural systems, aqueous sulfide is therefore predominately in

236   the form of H_2S or HS^- (and any ion pairs, e.g., $NaSH^0$).

237   Sulfuric acid (H_2SO_4) is a very strong acid and the doubly protonated form generally does not

238   form an appreciable component of the mass balance of sulfate solutions at low temperature but may

239   become a significant species in low pH solutions at high temperature (*cf.* Ohmoto and Lasaga, 1982

240   and references therein). The second acid dissociation quotient for sulfuric acid ($HSO_4^- \rightleftharpoons SO_4^{2-} + H^+$)

241   is pQ_{d2} = 1.99 ± 0.01 at 25°C and $\mu = 0$ m (Martell and Smith, 1982) but has values as high as 6.4 at

242   350°C (*cf.* Ohmoto and Lasaga, 1982 and references therein).

243   Thiosulfate ($S_2O_3^{2-}$, schematically: $S\text{-}SO_3^{2-}$) contains two sulfur atoms: one outer ("sulfanyl")

244   sulfur in a -1 oxidation state and another inner ("sulfonate") sulfur in a +5 oxidation state that is four-

245   fold coordinated with the sulfanyl sulfur and three oxygen atoms (Vairavamurthy et al., 1993). There

246   are many hypothetical forms of protonated thiosulfate: isomeric forms of $HS_2O_3^-$ (e.g., $(HS)SO_3^-$,

247     $S_2O_2OH^-$) and isomeric forms of $H_2S_2O_3$ (e.g., $(HS)SO_2(OH)$ and $S_2O(OH)_2$) (Steudel and Steudel, 2009).

248   Anhydrous forms of $H_2S_2O_3$ have been reported in syntheses as well as solid forms of $HS_2O_3^-$

249   ($[NH_4][HS_2O_3]$) (Steudel and Prenzel, 1989 and references therein) but protonated forms in the

250   aqueous phase are unstable, and have never been directly detected in solution via spectroscopic

251 techniques (e.g., Steudel and Prenzel, 1989; Steudel and Steudel, 2009). Acid dissociation quotients

252 for $H_2S_2O_3$ have been reported: $pQ_{d1} \approx 0.6$ and $pQ_{d2} = 1.6 \pm 0.1$ at 25°C and $\mu = 0$ m (Martell and Smith,

253 1982), and these pQ_d values may increase with increasing temperature over hydrothermal ranges (*cf.*

254 Ohmoto and Lasaga, 1982 and references therein).

255 **3.0 Methods**

256 *3.1 Overview: The Bigeleisen and Mayer Equation*

257   Theoretical calculations of equilibrium fractionation factors use the principles of quantum

258 mechanics to calculate the ground-state harmonic vibrational frequencies of molecules for use in the

259 Bigeleisen and Mayer equation (BM-equation), also referred to as the reduced partition function ratio

260 (RPFR; Bigeleisen and Mayer, 1947; Urey, 1947). These techniques have been widely applied since

261 the original derivation of the BM-equation and many extensive reviews cover this approach in detail

262 (e.g., Urey, 1947; Richet et al., 1977; Chacko et al., 2001; Wolfsberg et al., 2010; Liu et al., 2010). The

263 BM-equation or RPFR is given by:

$$\text{RPFR} = \frac{s}{s^*}\prod_i^l \frac{u_i^* \, e^{-u_i^*/2}(1-e^{-u_i})}{u_i \, e^{-u_i/2}(1-e^{-u_i^*})} \qquad (4)$$

264

265 Where * denotes terms related to the isotopically substituted molecule, s is the symmetry number,

266 and $u_i = hc\omega_i/kT$, where: k is the Boltzmann constant, h is the Planck constant, c is the speed of light, T

267 is temperature, and ω_i is the wave number for harmonic vibrational mode i (note vibrational

268 frequency $v_i = c\omega_i$) and the product is over all harmonic vibrational modes (number of modes equal

269 to $l = 3n - 6$ for a non-linear molecule and $l = 3n - 5$ for a linear molecule, where n is the number of

270 atoms in the molecule). In many cases, isotopic substitution does not change the symmetry of the

271 isotopologue and the quantity s/s^* is unity, leaving the RPFR in terms of harmonic vibrational

272 frequencies. In all cases, symmetry numbers do not influence isotope partitioning and merely

273 represent the relative probabilities of forming asymmetric vs. symmetric molecules (Bigeleisen and

274 Mayer, 1947).

275   RPFRs can be directly related to the commonly employed β-values for computing

276 equilibrium fractionation factors among compounds, where β-factors represent an equilibrium

277 fractionation factor between a compound (e.g., VY_n, where V and Y are generic elements) and an ideal

278   monoatomic gaseous reference (e.g., Y) (Richet et al., 1977). In our study, we focus on the

279   computation of RPFRs for singly substituted isotopologues such that β = RPFR when excess factors

280   are ignored (for a more detailed discussion of the relationship between β and RPFR, see: Richet et al.,

281   1977; Liu et al., 2010; Cao and Liu, 2011; Cao and Liu, 2012). Equilibrium fractionation factors

282   (denoted α) in this study are computed between two compounds based on singly substituted

283   isotopologues by taking the ratio of their respective β-values: $^x\alpha_{A\text{-}B} = {^x\beta_A}/{^x\beta_B}$, where x = 33, 34, or 36.

284   *3.2 Exponents defining mass-dependence relationships*

285   The mass dependence of an isotope effect relating a minor isotope fractionation factor and

286   the major isotope fractionation factor is given generally by an exponential relationship (*cf.* Craig,

287   1957; Matsuhisa et al., 1978; Clayton and Mayeda, 1996; Miller, 2002), which yields the following for

288   the sulfur isotope system under the condition of equilibrium:

289   $$^{33/34}\theta = \ln(^{33}\alpha_{A\text{-}B})/\ln(^{34}\alpha_{A\text{-}B}) \qquad (5)$$

290   $$^{36/34}\theta = \ln(^{36}\alpha_{A\text{-}B})/\ln(^{34}\alpha_{A\text{-}B}) \qquad (6)$$

291   The exponent is referred to as "θ" when computed from equilibrium fractionation factors between

292   two substances (here, compound "A" and compound "B"). Generally speaking, the capital delta

293   values commonly employed in multiple sulfur isotope studies ($\Delta^{33}S$ and $\Delta^{36}S$) are defined from such

294   exponential relationships as deviations from a reference exponent (e.g., $\Delta^{33}S_{A\text{-}B} = {^{33}\alpha_{A\text{-}B}} - ({^{34}\alpha_{A\text{-}B}})^{0.515}$

295   and $\Delta^{36}S_{A\text{-}B} = {^{36}\alpha_{A\text{-}B}} - ({^{34}\alpha_{A\text{-}B}})^{1.9}$), where the reference exponents are intended to represent the

296   approximate relationship of mass dependence for typical equilibrium isotope exchange reactions at

297   lower temperature (i.e., well below the high temperature limit). Similar exponential relationships

298   can be applied to β-values. Following Cao and Liu (2011), we adopt the kappa ("κ") notation to

299   describe these relationships: $^{33/34}\kappa = \ln(^{33}\beta)/\ln(^{34}\beta)$ and $^{36/34}\kappa = \ln(^{36}\beta)/\ln(^{34}\beta)$. Analogous to the

300   definition of β-values, κ-values describe the equilibrium exponent of mass dependence between a

301   compound of interest and an ideal gaseous monoatomic reference (Cao and Liu, 2011).

302   *3.3 Quantum Mechanical Software: Gaussian 09*

303   We use Gaussian 09 software (Frisch et al., 2010) at the B3LYP/6-31+G(d,p) level of theory

304   and basis set in this study to compute harmonic vibrational frequencies for use in the B-M equation.

305   The B3LYP method is a hybrid HF/B-LYP theoretical approach (employing the Becke and Lee, Yang,

306 & Parr 3-parameter gradient-corrected correlational functional; Lee et al., 1988; Becke, 1993;

307 Foresman and Frisch, 1996) that includes electron correlation. The basis set is the double-zeta Pople

308 basis set (6-31G) with diffuse functions added (+) to the non-hydrogen atoms (often required for

309 modeling anions) and polarization functions (p functions for all atoms, d functions for all non-

310 hydrogen atoms) for additional flexibility in the computation of molecular orbitals. Overall it is an

311 approach of low/moderate computational complexity and accuracy, chosen for reasons of

312 practicality given the relatively large molecular clusters modeled in this study.

313 *3.4 Explicit Solvation Model*

314   Optimization and frequency calculations were carried out with the sulfur molecules of

315 interest explicitly coordinated with water molecules in clusters containing up to 30-40 H_2O to

316 approximate the effects of solvation on molecular vibrations.   The construction of molecular clusters

317 involved the gradual addition of water molecules to sulfur solutes in an iterative series of

318 optimization calculations at lower levels of theory utilizing GaussView 5.0.9 and Gaussian 09

319 software (Frisch et al., 2010). First, the sulfur molecules of interest were coordinated with ca. 12-15

320 water molecules and optimized at relatively low levels of theory and basis set (B3LYP/6-31G(d)).

321 Following these initial optimization calculations, 2-5 water molecules were manually added to these

322 clusters and subsequently optimized at the same theoretical level. This procedure was then repeated

323 in a similar sequence of 2-5 H_2O-addition/optimization steps until the clusters reached a maximum

324 size of 30-40 depending on the solute and the required solvation coverage. The coordinates from the

325 B3LYP/6-31G(d)-level optimized geometries of the 30-40 H_2O solute clusters that resulted from this

326 step-wise cluster-building procedure were then used as the basis for the optimization and frequency

327 calculations at the B3LYP/6-31+(d,p) level that was used for computing fractionation factors in this

328 study. The majority of the optimization and frequency calculations were performed on a desktop

329 computer at the University of Maryland. For some of the sulfite calculations, coordinates from lower-

330 level B3LYP/6-31G(d) optimizations (computed at the University of Maryland) were run at the

331 B3LYP/6-31+G(d,p) level on the high performance computation cluster (Scylla) at the Woods Hole

332 Oceanographic Institution.

333 *3.5 Sources of Uncertainty*

334   Uncertainties in our theoretically estimated fractionation factors can derive from three main

335   sources: (1) errors arising from the harmonic and other approximations used in the derivation of the

336   Bigeleisen and Mayer equation (requiring higher-order corrections, e.g., for anharmonicity), (2)

337   inadequacies in the quantum mechanical theoretical method used to model the molecular system

338   (i.e., choice of theoretical method and basis set size), and (3) variability arising from the water cluster

339   geometry. All β-values and fractionation factors in this study are reported in the harmonic

340   approximation due to the inability to apply appropriate anharmonic corrections to our cluster

341   calculations at this time. We compute the anharmonic corrections to the ZPE (AnZPE) for a handful

342   of gaseous sulfur molecules (H_2S, $S(OH)_2$, $(HS)O_2H$, SO_2, SO_3) at the B3LYP/6-31+G(d,p) level to gain

343   insight into the magnitude of these corrections for more complex systems (section 5.1). We have

344   additionally chosen not to apply any scaling factors (harmonic or otherwise) to our harmonic

345   frequencies due to the potential issues associated with this practice (section 5.1), but we do discuss

346   the effects of harmonic scaling derived from high level gas phase calculations (CCSD/aug-cc-pVTZ) on

347   fractionation factors for individual systems to evaluate error arising from the chosen theoretical

348   method and basis set (following the approach of Li and Liu, 2011) (section 5.4). Unless otherwise

349   noted, all plotted and tabulated β-values and fractionation factors utilize un-scaled harmonic

350   frequencies at the B3LYP/6-31+G(d,p) level. We provide harmonic vibrational frequencies for all

351   computed clusters and compounds in a supplementary data file such that any user can scale the

352   frequencies in specific applications. To evaluate variability associated with cluster geometry, we

353   performed a series of at least duplicate constructions and optimizations of water clusters for a select

354   set of 30-40H_2O clusters in the sulfite system: SO_3^{2-}, $(HS)O_3^-$, $(HO)SO_2^-$, and the bisulfite dimer, $S_2O_5^{2-}$,

355   following the approach outlined in Section 3.4. Uncertainties derived from the above sources are

356   discussed in more detail in section 5.1.

357   **4.0 Results**

358   Optimized geometries of the 30-34H_2O molecular clusters of compounds in the sulfite,

359   sulfoxylate, and other systems (sulfide, thiosulfate, sulfate) are presented in Figure 3, Figure 4, and

360   Figure 5, respectively. These geometric parameters are also provided in Table S.2.

361   *4.1 $^{34}β$ values for aqueous sulfur compounds*

362   The major isotope $^{34}\beta$ values calculated at the B3LYP/6-31+G(d,p) level are presented in

363   Figure 6 as functions of inverse absolute temperature (1000/T; 273-373 K) for aqueous cluster

364   calculations, including the sulfite system, sulfoxylate system, sulfide system, sulfate, and thiosulfate

365   (inner 'sulfonate' sulfur, and the outer 'sulfanyl' sulfur). A tabulation of coefficients to polynomial fits

366   to the β values over 0-2000°C based on all three isotope ratios of sulfur is given in Table 1 in the form

367   of $A/T^4 + B/T^3 + C/T^2 + D/T + E$ (T in Kelvin).

368   Our calculated $^{34}\beta$ values generally scale with the oxidation state of sulfur, where higher

369   oxidation states generally have higher values than lower oxidation states, with the exception of the

370   two sulfur atoms in thiosulfate (-1 and +5; Vairavamurthy et al., 1993).   For a given temperature and

371   oxidation state of sulfur, our calculations predict that the magnitude of the $^{34}\beta$ increases with

372   increasing coordination of the sulfur atom. The species with the highest coordination of sulfur in

373   each system generally have the highest $^{34}\beta$ of their respective systems, and species of lower

374   coordination have lower $^{34}\beta$. For example, in the sulfite system, which contains the greatest diversity

375   in bonding arrangements around sulfur of any system in this study (triatomic bent, pyramidal, and

376   tetrahedral structures), the $^{34}\beta$ scale directly with coordination where: $^{34}\beta = (HS)O_3^- > SO_3^{2-} \approx$

377    $(HO)SO_2^- > SO_{2(aq)}$. Species where protonation occurs only on the oxygen atoms (i.e., $(HO)SO_2^-$,

378    $(HO)SO^-$, and $S(OH)_2$) typically exhibit very similar $^{34}\beta$ to their un-protonated counterparts.

379   The isotope partitioning behavior of the bisulfite dimer ($S_2O_5^{2-}$) warrants its own separate

380   description due to its unusual structure; it has been omitted from Figure 6 for simplicity of

381   presentation and due to difficulties in constraining its structure. The bisulfite dimer contains two

382   sulfur atoms that are coordinated differently in the molecule, where one sulfur atom (denoted "A") is

383   3-fold coordinated (one S and two O) and the other sulfur atom (denoted "B") is 4-fold coordinated

384   (one S and three O). We optimized four independently constructed $S_2O_5^{2-} \cdot nH_2O$ clusters (two n =30,

385   one n = 31, and one n=40) and found slight variability in the 4-fold coordinated site ($^{34}\beta$ = 1.0609-

386   1.0633; 25°C) that appears to correlate with the computed structure's S-S bond length, where higher

387    $^{34}\beta$ for this site corresponded to shorter S-S bond lengths (see Figure S.1). In contrast, the 3-fold

388   coordinated site's computed $^{34}\beta$ was found to be much more consistent between conformers ($^{34}\beta$ =

389   1.0438 ± 0.0003; 25°C; 1 s.e., all four computed conformers), and lower than any other species in the

390   sulfite system. In all cases, the calculated S-S bond lengths for the aqueous clusters—ranging

391   between 2.46-2.54 Å—are significantly longer than available experimental determinations in

392   crystalline solids (~2.2 Å; Zachariasen, 1932). Solvation could in principle affect the bond length but

393   we are unable to find any experimental constraints in the aqueous phase. We additionally note that

394   the precise structure of the aqueous dimer is perhaps contentious and forms with an S-O-S linkage

395   have yet to be ruled out (*cf.* Williamson and Rimstidt, 1992). For most discussions in this paper, we

396   will be using the conformer with the shortest S-S bond length and caution that the overall $^{34}\beta$ for

397   disulfite may be poorly constrained by our calculations due to a poorly constrained structure.

398   *4.2 $^{33/34}\kappa$ and $^{36/34}\kappa$ values for aqueous sulfur compounds*

399   In Figure 7, we plot the computed $^{33/34}\kappa = \ln(^{33}\beta)/\ln(^{34}\beta)$ and $^{36/34}\kappa = \ln(^{36}\beta)/\ln(^{34}\beta)$ as a

400   function of temperature for the explicitly solvated molecular water clusters and the related gaseous

401   species, which here only includes $SO_{2(g)}$ and $H_2S_{(g)}$. The exponents converge on or near a singular

402   value for all compounds at the high temperature limit: i.e., $^{33/34}\kappa_{T\rightarrow\infty}$ = 0.51587 ± 0.00003 and

403     $^{36/34}\kappa_{T\rightarrow\infty}$ = 1.8905 ± 0.0002 (1 s.d. from averaging the intercepts of the polynomial fits; Table 1), with

404   ranges of $^{33/34}\kappa_{T\rightarrow\infty}$ = 0.51582-0.51594 and $^{36/34}\kappa_{T\rightarrow\infty}$ = 1.8903-1.8913 (Table 1). These calculated

405   values are in generally good agreement with the high temperature limits that have been derived

406   based on the atomic masses of the four sulfur isotopes (*cf.* Matsuhisa et al., 1978; Young et al., 2002):

407                         $(1/m_{32} - 1/m_{33})/(1/m_{32}-1/m_{34})$ = 0.51588   (7)

408                         $(1/m_{32} - 1/m_{36})/(1/m_{32}-1/m_{34})$ = 1.8904   (8)

409   The variability (or noise) in our computed exponents as the high temperature limit is approached (*cf.*

410   Figure 7) is likely the result of error introduced by the cluster model and may relate specifically to

411   the multiple vibrational modes associated with the coordinated water molecules that contribute to

412   the overall β values. Such error may be most exemplified in the calculation of the atomic sulfide ion

413   ($S^{2-}\bullet30H_2O$)—a sulfur species that has no vibrational modes of its own—that displays the most

414   unusual behavior in $^{33/34}\kappa$ and $^{36/34}\kappa$ as the high temperature limit is approached.

415   At temperatures well-below the high temperature limit, $^{33/34}\kappa$ and $^{36/34}\kappa$ values follow

416   trends based on coordination and oxidation state similar to those seen in $^{34}\beta$ values as a function of

417   temperature (Figure 6), where the end-member oxidation states (sulfide species and sulfate)

418   generally represent end-member values and intermediate oxidation states plot successively in

419   between. Higher oxidation states tend to have lower $^{33/34}\kappa$ than lower oxidation states, and *vice versa*

420   for $^{36/34}\kappa$. For a given oxidation state, the more highly coordinated sulfur bonding sites generally

421   have lower $^{33/34}\kappa$ than lower coordinated sites and *vice versa* for $^{36/34}\kappa$, following similar

422   relationships to those observed in the magnitude of their $^{34}\beta$, but with some exceptions. Overall, the

423   exponents of mass dependence for sulfur compounds spanning the entire range of available

424   oxidation states define a narrow range of $^{33/34}\kappa$ =0.5148-0.5159 and $^{36/34}\kappa$ = 1.890-1.898 over a wide

425   range of temperature (T ≥ 0℃).

426   *4.3 Fractionations in the Sulfite System*

427   Triple sulfur isotope fractionations ($^{33}\alpha$ vs. $^{34}\alpha$) for aqueous species in the sulfite system

428   ($SO_{2(aq)}$, $(HO)SO_2^-$, two conformers of $(HS)O_3^-$, $S_2O_5^{2-}$, and two conformers of SO_3^{2-}) at 25℃ are

429   summarized in Figure 8. For purposes of illustration, fractionations are plotted relative to $SO_{2(aq)}$.

430   Fractionations among the major sulfite species in solution ($SO_{2(aq)}$, $(HO)SO_2^-$, and SO_3^{2-}) are relatively

431   small ($1000ln^{34}\alpha$ < 6 ‰). The fractionation between $(HO)SO_2^-$ and SO_3^{2-} at 25℃ is computed to be on

432   the order of -2.2 ‰ with corresponding $^{33/34}\theta$ = 0.51519 and $^{36/34}\theta$ = 1.8972. Fractionations between

433   the $(HS)O_3^-$ isomer and these species are much larger: at 25℃, the $1000ln^{34}\alpha$ between $(HS)O_3^-$ and

434     $SO_{2\,(aq)}$ is on the order of 25 ‰ ($^{33/34}\theta$ = 0.51488 and $^{36/34}\theta$ = 1.8975), and the $1000ln^{34}\alpha$ between

435     $(HS)O_3^-$ and SO_3^{2-} is 20 ‰ at 25℃ ($^{33/34}\theta$ = 0.51456 and $^{36/34}\theta$ =1.8993). The influence of the minor

436     $(HS)O_3^-$ isomer on overall isotope partitioning in this system will be a major focus of the discussion

437   (Section 5.4).

438   Fractionations involving the bisulfite dimer ($S_2O_5^{2-}$) are also presented in Figure 8. The 3-

439   fold coordinated site (with the most reproducible β between conformers) has a slightly lower

440   preference for heavier isotopes than $SO_{2(aq)}$, contrary to what would be expected from simple

441   coordination relationships. The 4-fold coordinated site has a β that is intermediary between the

442   pyramidal and tetrahedral sulfite species. When site-averaged, the isotopic composition of the dimer

443   is only slightly elevated from sulfite according to the conformer plotted in Figure 8. Given the inverse

444   correlation that we have observed between β values (namely that of the 4-fold coordinated site) and

445 S-S bond length, we expect this value to represent a minimum site-averaged fractionation factor for

446 the dimer if our calculations overestimate the S-S bond length.

447 *4.4 Fractionations in the Sulfoxylate System*

448 Triple sulfur isotope fractionations ($^{33}\alpha$ vs. $^{34}\alpha$) for aqueous species in the sulfoxylate system

449 (two isomers of H_2SO_2, $(HS)O_2^-$, $OS(OH)^-$, and SO_2^{2-}) at 25°C are summarized in Figure 9. For purposes

450 of illustration, fractionations are plotted relative to sulfoxylic acid, $S(OH)_2$. Similar to the sulfite

451 system, sulfoxylate species with similar coordination around the sulfur atom ($S(OH)_2$, $(HO)SO^-$, SO_2^{2-})

452 are minimally fractionated with respect to one another ($1000ln^{34}\alpha < 3$ ‰ at 25°C) and species where

453 protonation occurs on the sulfur atom (increasing coordination around sulfur) are significantly

454 fractionated from the other species. For example, the $1000ln^{34}\alpha$ between the two-fold coordinated

455 $(HO)SO^-$ and the two-fold coordinated $S(OH)_2$ is predicted to be -0.3 ‰ ($^{33/34}\theta = 0.51410$ and $^{36/34}\theta =$

456 1.8874), and the $1000ln^{34}\alpha$ between three-fold coordinated $(HS)O_2^-$ and the two-fold coordinated

457 $S(OH)_2$ is predicted to be 14.8 ‰ ($^{33/34}\theta = 0.51526$ and $^{36/34}\theta = 1.8950$).

458 *4.5 Fractionations in the Sulfide System*

459 Triple sulfur isotope fractionations ($^{33}\alpha$ vs. $^{34}\alpha$) for aqueous species in the sulfide system

460 (H_2S, HS^-, and S^{2-}) at 25°C are summarized in Figure 10. For purposes of illustration, fractionations

461 are plotted relative to the divalent sulfide anion, S^{2-}. Similar to the sulfite and sulfoxylate systems, the

462 magnitude of fractionation between sulfide species increases with coordination. In all cases,

463 fractionations are predicted to be relatively small in the sulfide system: at 25°C, the $1000ln^{34}\alpha$

464 between H_2S and HS^- is estimated to be on the order of 3.3 ‰ ($^{33/34}\theta = 0.51561$ and $^{36/34}\theta = 1.8916$),

465 and the $1000ln^{34}\alpha$ between HS^- and S^{2-} is on the order of 1.7 ‰ ($^{33/34}\theta = 0.51573$ and $^{36/34}\theta =$

466 1.8894).

467 *4.6 Fractionations Between Sulfate and the Sulfide Species*

468 Fractionations between the two end-member oxidation states of sulfur (S^{2-} and S^{6+}) yield the

469 largest equilibrium isotope fractionations in the aqueous sulfur system. The fractionation factor

470 between SO_4^{2-} and H_2S is ($1000ln(^{34}\alpha_{sulfate-H2S})$) is predicted to be 63.4 ‰ with corresponding $^{33/34}\theta =$

471 0.51475 and $^{36/34}\theta = 1.8981$ at 25°C. The fractionation factor between SO_4^{2-} and HS^- ($1000ln(^{34}\alpha_{sulfate-}$

472 $_{HS^-})$) is predicted to be 66.7 ‰ with corresponding $^{33/34}\theta = 0.51480$ and $^{36/34}\theta = 1.8978$ at 25°C.

473   Similarly, the fractionation factor between sulfate and the atomic sulfide dianion, S^{2-},

474   ($1000\ln(^{34}\alpha_{\text{sulfate-sulfide}})$) is predicted to be 68.4 ‰ with corresponding $^{33/34}\theta$ = 0.51482 and $^{36/34}\theta$ =

475   1.8976 at 25°C.

476   *4.7 Fractionations Within and Between Thiosulfate and the Major Sulfide Species*

477   The intramolecular fractionation factor between the outer ("sulfanyl") and inner

478   ("sulfonate") sulfur atoms in thiosulfate ($S_2O_3^{2-}$) ($1000\ln^{34}\alpha_{\text{outer-inner}}$) is predicted to be on the order of

479   -53.8 ‰ at 25°C, with corresponding $^{33/34}\theta$ = 0.51489 and $^{36/34}\theta$ = 1.8972. The fractionation factor

480   between the outer ("sulfanyl") sulfur atom in thiosulfate and H_2S ($1000\ln^{34}\alpha_{\text{outer-H2S}}$) is predicted to

481   be small and on the order of – 1.0 ‰ at 25°C, where the magnitude of the major isotope fractionation

482   factor increases with temperature (inverse temperature dependence) over the approximate

483   temperature range of ≈ -15 to 180°C to a maximum approaching $1000\ln^{34}\alpha_{\text{outer-H2S}}$ ≈ – 2 ‰ at ≈ 180°C.

484   This inverse temperature dependence is the consequence of a crossover in the direction of the

485    $^{34}\alpha_{\text{outer-H2S}}$ fractionation factor at sub-0°C temperature ($T_{\text{34/32-crossover}}$ ≈ -15°C). The fractionation factor

486   between the outer sulfur ("sulfanyl") atom in thiosulfate and the HS^- ion ($1000\ln^{34}\alpha_{\text{outer-HS-}}$) is

487   predicted to be 2.3 ‰ at 25°C (opposite in direction to the similar H_2S-based fractionation factor at

488   25°C), and also exhibits a crossover in proximity to ≈ 270°C. The exponents of mass dependence

489   ($^{33/34}\theta$ and $^{36/34}\theta$) associated with both $\alpha_{\text{outer-H2S}}$ and $\alpha_{\text{outer-HS-}}$ exhibit characteristic asymptotic

490   behavior at their respective crossover temperatures (*cf.* Deines, 2003; Otake et al., 2008) (not

491   shown) that lead to unusual exponents in proximity to the crossover temperature. For example, at

492   0°C, the $^{33/34}\theta$ and $^{36/34}\theta$ associated with $\alpha_{\text{outer-H2S}}$ are computed to be 0.5197 and 1.857, respectively.

493   Despite the unusual exponents associated with these crossovers, the capital delta values associated

494   with these fractionation factors are very near zero at all relevant temperatures: e.g., at T ≥ 0°C, $\Delta^{33}S$

495    $_{\text{outer-H2S}}$ ≤ - 0.002 ‰ and $\Delta^{36}S_{\text{outer-H2S}}$ ≤ - 0.02 ‰, and $\Delta^{33}S_{\text{outer-HS-}}$ ≈ 0.000 ‰ and $\Delta^{36}S_{\text{outer-HS-}}$ ≤ 0.01 ‰.

496   **5.0 Discussion**

497   *5.1 Uncertainties in estimated fractionation factors*

498   Uncertainties in our theoretically estimated fractionation factors can derive from three main

499   sources: (1) errors arising from the harmonic and other approximations in the derivation of the

500   Bigeleisen and Mayer equation (requiring higher-order corrections, e.g., for anharmonicity), (2)

501   inadequacies in the theoretical method (choice of theoretical method and basis set), and (3)

502   variability arising from the water cluster geometry. To quantitatively evaluate these uncertainties,

503   we adopt a similar approach to Li and Liu (2011), where a similar water cluster model was used to

504   calculate the equilibrium isotope fractionations among aqueous selenium compounds and anions.

505   *5.1.1 Harmonic approximation*

506   The BM-equation requires that harmonic frequencies be used to justify the various

507   approximations used in its derivation (*cf.* Rustad and Bylaska, 2007; Rustad et al., 2010; Liu et al.,

508   2010). We therefore use the calculated harmonic frequencies to calculate RPFRs/β-values and

509   isotope fractionation factors. An appropriate comparison of theoretically computed vibrational

510   frequencies to those derived from experiments is not possible at this time, because the conversion of

511   our computed harmonic frequencies to fundamental frequencies requires computation of

512   anharmonic constants (*cf.* Liu et al., 2010). The computation of anharmonic constants for large

513   molecular clusters is computationally laborious and is beyond our computational resources. We

514   therefore considered these computations beyond the scope of this study. Instead, we focus on

515   calculations of anharmonic corrections to the BM-equation (RPFR) for simple gaseous molecules to

516   gain insight into the magnitude of these corrections for more complex systems.

517   Liu et al. (2010) reviewed and applied a variety of anharmonic and higher-order corrections

518   to the BM-equation for simple gaseous molecules at the MP2/aug-cc-pVTZ level. They show that

519   many of these corrections are only significant when dealing with hydrogen-deuterium exchange

520   reactions. For example, the total $^{34}S/^{32}S$-based corrected partition function ratios (CPFR) for $H_2S_{(g)}$

521   and $SO_{2(g)}$ are shifted by 0.3 and 0.6 ‰ at 300 K from their uncorrected RPFR counterparts,

522   respectively, where the entirety of the correction for both compounds arises from the anharmonic

523   contribution to the zero point energy (AnZPE; Liu et al., 2010). We have computed the anharmonic

524   corrections to the ZPE (AnZPE) for a handful of gaseous sulfur molecules (H_2S, $S(OH)_2$, $(HS)O_2H$, SO_2,

525   SO_3) at the B3LYP/6-31+G(d,p) level and find that they are of a similar magnitude (H_2S, $S(OH)_2$,

526     $(HS)O_2H$, SO_2: ~ -0.5 ‰, SO_3: ~ -0.9 ‰; 25°C) (Figure S.2). Due to the low magnitude of these

527   corrections and the inability to apply appropriate anharmonic corrections to our cluster calculations

528 at this time, all RPFR/β values and fractionation factors in this study are reported in the harmonic

529 approximation.

530 *5.1.2 Theoretical level*

531 The theoretical method and basis set employed can lead to significant error in the computed

532 RPFRs and fractionation factors (*cf.* Rustad et al., 2008; Rustad et al., 2010). We evaluated the

533 potential error introduced by any inadequacies in our theoretical approach via harmonic frequency

534 scaling using high-level computations of simple neutral molecules modeled in the gas phase (*cf.* Li

535 and Liu, 2011). Note that this is not the same practice as scaling theoretical harmonic frequencies to

536 fit experimental fundamental frequencies that introduce anharmonic contributions to the theoretical

537 frequencies.

538 We computed harmonic frequencies for H_2S, S_2, SO_2, and SO at the CCSD/aug-cc-pVTZ level

539 and derived a first-order harmonic scaling factor for the B3LYP/6-31+G(d,p) level employed for our

540 water clusters on the order of 1.01-1.02 (i.e., a uniform 1-2% positive shift in the harmonic

541 frequencies; Figure S.3). The influence of this scaling factor on $^{34}\beta$ values and the computed

542 fractionation factors varies depending on the compound(s) and temperature considered, but is

543 generally magnified at lower temperatures. The effect of harmonic scaling is often negligible but can

544 be on the permil level for some computed fractionation factors that involve compounds with higher

545 magnitude $^{34}\beta$. For example, for the $SO_4^{2-}{}_{(30H2O)}$/$H_2S_{(30H2O)}$ equilibrium fractionation factor, applying a

546 harmonic frequency scaling factor of 1.02 results in a $\sim$2 ‰ increase in the $^{34}\alpha$ fractionation factor at

547 25°C from 1.0655 to 1.0677, but smaller shifts at higher temperatures (e.g. 1.1 and 0.6 ‰ positive

548 shift at 200°C and 400°C, respectively). In some cases (but not all), the small shifts arising from

549 harmonic frequency scaling places our theoretical fractionations factors in slightly better agreement

550 with experimental constraints (explored further for individual systems in Section 5.4).

551 The practice of harmonic frequency scaling may not be ideal because different vibrational

552 modes appear to scale slightly differently between computational methods (*cf.* Li and Liu, 2011).

553 Furthermore, gaseous molecules may not capture the full range of error introduced by the level of

554 theory and basis set employed in our aqueous cluster calculations, especially for the anions of more

555 varied geometric and electronic structure computed in our study. From our own calculations, it

556   appears that SO_2 may have a systematically higher scaling factor than the other compounds

557   investigated that may be on the order of 1.065, which is why when SO_2 is included in the regression

558   the net scaling factor increases from ~1.01 to ~1.02 (we show later that application of this higher

559   SO_2-specific scaling factor places estimates of the $SO_{2(aq)}/SO_{2(g)}$ fractionation factor in slightly better

560   agreement with experimental constraints, although overall the effect of the scaling is still only on the

561   ~0.2 ‰ magnitude at 25°C in the estimated fractionation factor). Due to these potential issues, we

562   have chosen to not apply a harmonic scaling factor in the computations of our reported β values but

563   we do discuss the effects of harmonic scaling on fractionation factors for individual systems (section

564   5.4).

565   *5.1.3 Cluster geometry*

566   Variability in the water cluster geometry surrounding the solute of interest is another

567   potential source of error/uncertainty in computed β values and fractionation factors. From previous

568   studies utilizing clusters manually constructed as in the present study (e.g., Li et al., 2009; Li and Liu,

569   2011) and clusters derived from molecular dynamics simulations (Rustad et al., 2008; Rustad et al.,

570   2010), it is generally understood that error/uncertainty arising from cluster geometries is relatively

571   small, and likely much lower than those associated with the theoretical approach (e.g., Rustad et al.,

572   2010). Most theoretical studies of compounds in water clusters where the centrally coordinated

573   element in the solute is undergoing isotope substitution have found that the variability in computed

574   β is generally at the 0.1 - 1 ‰ level (1 s.d.) from one cluster geometry to another for multiple

575   element systems (e.g., oxy-anions and compounds of C, Se, Ge, B; Rustad et al., 2008; Rustad et al.,

576   2010; Li et al., 2009; Li and Liu, 2011). We performed a series of at least duplicate constructions and

577   optimizations of water clusters (i.e., repeating the procedure of Section 3.4) for a select set of 30-

578    $40H_2O$ clusters in the sulfite system: SO_3^{2-}, $(HS)O_3^-$, $(HO)SO_2^-$, and the bisulfite dimer pyrosulfite,

579    $S_2O_5^{2-}$. Duplicate constructions and optimizations of $SO_3^{2-}\bullet 30H_2O$, $(HS)O_3^-\bullet 30H_2O$, and $(HO)SO_2^-$

580    $\bullet 34H_2O$ reveal that variability due to cluster geometry for aqueous sulfur compounds may also be

581   small: $(HS)O_3^-\bullet 30H_2O$: $^{34}\beta = 1.0721\pm0.0001$, $SO_3^{2-}\bullet 30H_2O$: $^{34}\beta = 1.0510\pm0.0003$, $(HO)SO_2^-\bullet 34H_2O$: $^{34}\beta$

582    $= 1.0487\pm0.0003$ (all at 25°C and 1 s.d.). The two sulfur atoms in the bisulfite dimer, labeled here as

583   'A' and 'B': $(O_2\text{-}^AS\text{-}^BS\text{-}O_3)^{2-}$, have similar reproducibility in their $^{34}\beta$ values between four separate

584   conformers ranging from 30-40 H_2O clusters: ^AS: $^{34}\beta = 1.0438 \pm 0.0003$ and ^BS: $^{34}\beta = 1.0622 \pm 0.0011$

585   (25℃, 1 s.e.), where the $^{34}\beta$ of the latter, higher-coordination site seems to vary systematically with

586   the computed S-S bond-length, and may be a special case (section 4.1).

587   Considering all of the uncertainties derived from the above sources, we estimate the overall

588   uncertainties associated with our theoretically computed fractionation factors ($^{34}\alpha$) for aqueous

589   sulfur systems to be on the order of $\sim$0.1 to 1-2 ‰, depending on temperature and the

590   compounds/system considered. The major source of uncertainty is believed to be from the potential

591   inadequacy of our theoretical approach (*cf.* Rustad et al., 2008; Rustad et al., 2010) and could

592   potentially be better constrained with more sophisticated computational methods. A major aim of

593   the present study is to explain the available experimental constraints for equilibrium fractionations

594   in the sulfite system in the context of the complex speciation of sulfite. Much of the uncertainty in

595   this analysis is dominated by uncertainties in experimental determinations of equilibrium quotients

596   (e.g. bisulfite isomerization) and experimental fractionation factors (e.g. approaching a few permil in

597   magnitude). Much of the uncertainties in the theoretically calculated fractionation factors discussed

598   above are either comparable to, or within this range. Therefore, we do not think the uncertainties in

599   the calculations will affect the main conclusions of the present study.

600   *5.2 General Trends in the Calculated $^{34}\beta$*

601   The general relationships in the computed $^{34}\beta$ for the hydrated sulfur species can be

602   explained by the general principles of stable isotope fractionation. The two primary factors

603   influencing the magnitude of $^{34}\beta$ (Figure 6) are: (1) the oxidation state of sulfur, and (2) the

604   coordination of sulfur, i.e., the number of bonds formed with other atoms. Both of these exert first

605   order controls on the bonding environment around sulfur, particularly on the bond

606   stiffness/strength, and are the primary factors in influencing the relative magnitudes of $^{34}\beta$ that we

607   have computed.

608   The oxidation state of the sulfur atom will affect the electron distribution throughout the

609   molecule and therefore the strength and nature of the bonds with the other atoms. The force

610   constants that describe the potential wells associated with the bonds (derived from the computation

611   of the multidimensional electronic potential energy surface) will generally be higher for bonds

612   associated with sulfur in higher oxidation states, meaning simply that the bonds will be more stiff.

613   Thus, species with higher oxidation state will generally have higher $^{34}\beta$ than those with lower

614   oxidation state in similarly coordinated structures. This is reflected in the significantly lower $^{34}\beta$ of

615   the sulfoxylate ion (SO_2^{2-}; S^{2+}) as compared to sulfur dioxide (SO_2; S^{4+}), which have similar bent

616   triatomic structures and two-fold coordination of the sulfur atom with bonds to oxygen atoms.

617   For a given oxidation state, the coordination of the sulfur exerts another first order control

618   on $^{34}\beta$. The Bigeleisen and Mayer equation describes the relationship between isotope partitioning

619   among molecules, zero point energies (ZPE), and molecular vibrations. The ZPE portion of the RPFR

620   reflects the contribution from all vibrational modes and scales with the sum of the frequency shifts.

621   Unless the bonds are weakened so much with increasing coordination that the adjusted sum of the

622   frequency shifts decreases, the RPFR may increase with coordination. From a simple vibrational

623   analysis of our solutes in vacuum, isotope substitution of the central sulfur atom in a bent (or linear

624   tri-atomic), pyramidal, or tetrahedral molecular structure generally affects the asymmetric

625   stretching and bending modes of the ground state vibrations the most and, therefore, contribute the

626   most to the overall magnitude of the RPFR/β-values of the molecule. The number of these stretching

627   and bending modes increases with increasing coordination of the central atom, and so all else being

628   equal, the RPFR/β-values (and therefore, preference for the heavy isotope) may increase with

629   increasing coordination. For example, the 2-fold coordinated $SO_{2(aq)}$ has a lower $^{34}\beta$ than the 3-fold

630   coordinated SO_3^{2-} and $(HO)SO_2^-$ molecules, which have lower $^{34}\beta$ than the 4-fold coordinated $(HS)O_3^-$

631   isomer of bisulfite (all S^{4+}). Variations from these relationships may be expected depending on the

632   elemental composition of the bonded atoms/groups that may affect bonding environment and the

633   manner in which frequency shifts are scaled.

634   Protonation of oxygen atoms has a smaller secondary effect on $^{34}\beta$ with respect to the

635   centrally coordinated sulfur. These small secondary effects are due to how protonation of the oxygen

636   atom affects its electron distribution and its bond to the sulfur atom. For example, the $^{34}\beta$ of the

637    $(HO)SO_2^-$ isomer of bisulfite differs by only $\sim$ -2 ‰ from that of the non-protonated sulfite (SO_3^{2-}) at

638   25°C. The slightly higher $^{34}\beta$ for the sulfite anion relative to the $(HO)SO_2^-$ isomer of bisulfite is likely

639   due to the slight weakening of the S-O bond corresponding to the protonated oxygen. This is

640   consistent with the slightly longer S-O bond length for the protonated oxygen atom (Figure 3; Table

641   S.2). Similarly, in the sulfoxylate system, the $^{34}\beta$ for (HO)SO$^-$ and S(OH)$_2$ are both lower than that for

642   SO$_2^{2-}$ and the corresponding S-OH bond lengths are longer than S-O bond lengths (Figure 4; Table

643   S.2). The $^{34}\beta$ for (HO)SO$^-$ and S(OH)$_2$ are nearly identical to one another (at 25°C: $^{34}\beta$ = 1.0240 and

644     $^{34}\beta$ = 1.0243, respectfully) and are likely within the uncertainties of the calculations. Multiple

645   rotamers of these types yielding different orientations of the protons and OH-bonds with respect to

646   the rest of the molecule are possible that will depend in large part on the water cluster geometry

647   (direct coordination with water molecules) in the case of these computed structures. Such variability

648   in structure would be expected to have small second order effects on the magnitude of $^{34}\beta$. For

649   example, our two optimized 34H$_2$O conformers of (HO)SO$_2^-$ do not have exactly the same structure

650   (slightly different orientations of the O-H bond relative to the rest of the molecule, i.e., O-S-O-H

651   dihedral ~49-71°) and yield highly reproducible $^{34}\beta$ ($^{34}\beta$ = 1.0487±0.0003 at 25°C, 1 s.d.).

652   *5.3 Exponents of Mass-Dependence: κ and θ*

653   We compute exponents of mass dependence for β values ($^{33/34}\kappa$ and $^{36/34}\kappa$) over a wide range

654   of temperature that conform to tight ranges (0.5148-0.5159 and 1.89-1.90, respectively; Figure 7).

655   The $^{33/34}\kappa$ for a given species is on a lower end of this range at low temperature and approaches the

656   high range at high temperature, and *vice versa* for $^{36/34}\kappa$. The relationships in $^{33/34}\kappa$ and $^{36/34}\kappa$ we

657   compute as a function of temperature for the diversity of aqueous sulfur compounds investigated

658   herein are straightforward consequences of ZPE differences among isotopomers varying as a

659   function of sulfur bonding environment (redox state, coordination, etc.).

660   The exponent of mass dependence computed for a fractionation factor between two

661   compounds (A and B; $^{33/34}\theta_{A-B}$ or $^{36/34}\theta_{A-B}$) generally follows:

662         $^{n/34}\theta_{A-B} = [^{n/34}\kappa_A \ln(^{34}\beta_A) - {}^{n/34}\kappa_B \ln(^{34}\beta_B)]/[\ln(^{34}\beta_A) - \ln(^{34}\beta_B)]$,   (9)

663   where n = 33 or 36 (we will focus on 33). Only when $^{33/34}\kappa_{(A)} = {}^{33/34}\kappa_{(B)}$ will $^{33/34}\theta_{A-B}$ be identical.

664   When $^{33/34}\kappa_{(A)} \neq {}^{33/34}\kappa_{(B)}$, the magnitude of $^{33/34}\theta_{A-B}$ will be slightly shifted to either higher or lower

665   values than either $^{33/34}\kappa_{(A)}$ or $^{33/34}\kappa_{(B)}$ depending on the relationships among the RPFRs/β-values (*cf.*

666   Matsuhisa et al., 1978). In the latter case, there are two primary examples to consider: (1) When $^{34}\beta_A$

667   > $^{34}\beta_B$ and the $^{33/34}\kappa_A < {}^{33/34}\kappa_B$, the computed $^{33/34}\theta_{A-B}$ will generally be slightly lower than either

668     $^{33/34}\kappa_A$ or $^{33/34}\kappa_B$; and (2) when $^{34}\beta_A > {}^{34}\beta_B$ and the $^{33/34}\kappa_A > {}^{33/34}\kappa_B$, the computed $^{33/34}\theta_{A\text{-}B}$ will

669   generally be slightly higher than either $^{33/34}\kappa_A$ or $^{33/34}\kappa_B$. The magnitudes of the shifts between $^{33/34}\kappa$

670   values and the $^{33/34}\theta$ corresponding to a fractionation factor between compounds are magnified at

671   lower temperature where differences in the magnitudes of β-values are largest (in the general case).

672   The shifts are additionally magnified under hypothetical conditions where the differences between

673     $^{33/34}\kappa_A$ and $^{33/34}\kappa_B$ are relatively large and differences between $^{34}\beta_A$ and $^{34}\beta_B$ are relatively small. For

674   most fractionation factors computed among compounds of different oxidation state at low/ambient

675   temperature, our calculations generally follow case (1). For example, at 0°C the fractionation factor

676   between sulfate (SO_4^{2-}; $^{34}\beta = 1.0910$, $^{33/34}\kappa = 0.5148$) and sulfide (H_2S; $^{34}\beta = 1.0142$, $^{33/34}\kappa = 0.5157$)

677   yields $^{33/34}\theta = 0.5146$, slightly lower than either compound's respective $^{33/34}\kappa$ values. An example of

678   case (2) is the fractionation factor between (HO)SO$_2^-$ isomer of bisulfite ($^{34}\beta = 1.0487$, $^{33/34}\kappa =$

679   0.51521; avg. of duplicate conformers, 25°C) and $SO_{2(aq)}$ ($^{34}\beta = 1.0454$, $^{33/34}\kappa = 0.51511$; 25°C), where

680     $^{33/34}\theta = 0.51652$. Due to the tight range in $^{33/34}\kappa$ and $^{36/34}\kappa$ that we compute over a relatively large

681   range in $^{34}\beta$ for various aqueous sulfur compounds, it may be generally concluded that our

682   calculations would not predict exponents of mass dependence associated with equilibrium isotope

683   fractionation factors significantly outside of the range of ca. $^{33/34}\theta \approx 0.514\text{-}0.516$ and $^{36/34}\theta \approx 1.89 -$

684   1.90 over a wide range of temperature (0°C →∞).

685   The major exception to this generality is for equilibrium isotope exchange reactions that are

686   predicted to have crossovers, i.e., a shift in the direction of an isotope effect where preference for

687   heavy isotopes undergoes inversion from one compound (or bonding environment) to the other at a

688   particular temperature. Our calculations predict crossovers in the isotope exchange reactions

689   between the outer ("sulfanyl") sulfur atom in thiosulfate and the two principle sulfide species (H_2S,

690   HS$^-$). Crossovers and their effects on the exponents of mass dependence have been described

691   previously in gas phase reactions for the sulfur isotope system (Deines, 2003; Otake et al., 2008).

692   Briefly, these effects relate to crossover temperatures being slightly different for exchange reactions

693   involving isotopes of different mass, i.e., $T_{33/32\text{-crossover}} \neq T_{34/32\text{-crossover}} \neq T_{36/32\text{-crossover}}$. As a crossover

694   temperature is approached, the exponents of mass dependence show asymptotic relationships where

695   the exponent can take any value between +∞ and -∞ (Deines, 2003; Otake et al., 2008). Crossovers

696   have been predicted in isotope exchange reactions involving H_2S and other reduced sulfur

697   compounds containing S-S bonds (S_2/H_2S, S_8/H_2S; Deines, 2003; Otake et al., 2008), and presumably

698   arise fundamentally from the competition between contributions from low frequency vibrational

699   modes (like those associated with S-S bonds) and high frequency modes in H_2S (and HS^-) to the

700   overall RPFRs as a function of temperature. Due to the small magnitude of the isotope effects in the

701   asymptotic crossover range, these effects are not substantially expressed (i.e., $\Delta^{33}S \approx 0$, $\Delta^{36}S \approx 0$, as

702   we have computed) without subsequent amplification via non-equilibrium isotope exchange

703   processes (e.g., a Rayleigh distillation process; Deines, 2003; Otake et al., 2008).

704   In a previous study, Otake et al. (2008) emphasized computations utilizing a non-

705   exponential formulation based on the approximation $^{33/34}\theta_{A-B} \approx (^{33}\alpha_{A-B} - 1)/(^{34}\alpha_{A-B} - 1)$ to argue that

706   their theoretical calculations of select sulfur compounds (modeled as either gas phase or in PCM

707   solvation models) predict a range of $^{33/34}\theta = 0.505$-0.516 for equilibrium fractionation factors

708   (including SO_4^{2-}-H_2S), where the reference exponent of 0.515 is approached at high temperature.

709   Computations of the mass dependence as $^{33/34}\theta_{A-B} = \ln(^{33}\alpha_{A-B})/\ln(^{34}\alpha_{A-B})$ calculated from the same

710   fractionation factors yields a much more narrow range of $^{33/34}\theta \approx 0.514$-$0.516$ over the same

711   temperature range. In other words, the so-called 'band of mass dependence' that Otake et al. (2008)

712   argued for as $^{33/34}\theta \approx 0.505$-$0.516$ for simple equilibrium isotope exchange reactions lowers to 0.514-

713   0.516 when the exponential definition of mass dependence is used. Note also that the computation of

714   the mass dependence as $(^{33}\alpha - 1)/(^{34}\alpha - 1)$ is valid to characterize effects associated with a Rayleigh

715   distillation process and not the condition of equilibrium isotope exchange.

716   *5.4 Comparisons to Available Experiments, and Predictions*

717   The validity of the theoretical fractionation factors can be assessed by comparison with

718   available experimental constraints, with particular focus on the sulfite system. Very little is known

719   about the behavior of sulfoxylate species in aqueous solutions (particularly the isomerization

720   quotients for the protonated species) and so we are only able to discuss the estimated ranges of

721   fractionations possible in this system. Calculations of the other sulfur compounds (sulfide, sulfate,

722   and thiosulfate) can also be compared to the available experimental datasets, including:

723   fractionations among sulfide species, fractionations between sulfate and sulfide species, the

724   intramolecular fractionation factor for thiosulfate, and fractionations between the sulfide species and

725   thiosulfate. We highlight potential experimental issues and include recommendations for future

726   experimental determinations where they may be needed.

727   *5.4.1 Sulfite System*

728   Experimental constraints for the equilibrium sulfur isotope partitioning in the aqueous

729   sulfite system are provided by Eriksen (1972a), Eriksen (1972b), and Eriksen (1972c). Eriksen

730   (1972a) explored fractionations between bulk bisulfite and gaseous SO_2 ($HSO_3^-_{TOTAL}/SO_{2(g)}$) at pH

731   =4.5 where bisulfite dominates, Eriksen (1972b) explored the fractionation between gaseous SO_2 and

732   aqueous SO_2 ($SO_{2(aq)}/SO_{2(g)}$) in acidic solutions (pH < 0.3), and Eriksen (1972c) explored

733   fractionations between bulk bisulfite and gaseous SO_2 as a function of the ratio of total bisulfite:

734     $SO_{2(aq)}$ (up to 10 M [HSO_3^-]; pH = <0.3 or 4.5), which was a study of the effect of dimerization on

735   isotope fractionations. With additional interpretation, the experiments presented in Eriksen (1972c)

736   yield constraints on both the $SO_{2(aq)}/SO_{2(g)}$ and $HSO_3^-_{TOTAL}/SO_{2(g)}$ fractionation factors. Additional

737   experimental constraints on the $SO_{2(aq)}/SO_{2(g)}$ fractionation factor are found in Chmielewski et al.

738   (2001).

739   *5.4.1.1 Bulk Bisulfite in Solution vs. $SO_{2(g)}$: Highlighting the role of bisulfite isomers*

740   In Figure 11, our calculated fractionation factors for bisulfite species vs. $SO_{2(g)}$ are plotted

741   with those from the experiments of Eriksen (1972a) and Eriksen(1972c) as a function of

742   temperature. Eriksen (1972a) chose experimental conditions to minimize the presence of dimers

743   and other sulfite species (pH = 4.5), so the experimentally determined fractionations should mostly

744   reflect those of the two bisulfite isomers and gaseous sulfur dioxide. The $^{34}\alpha_{bisulfite(bulk)-SO2(g)}$ of Eriksen

745   (1972a) appear to show a non-resolvable temperature dependence over the temperature range of

746   25-45°C. The constraints from Eriksen (1972c) were regressed from multiple experiments

747   performed over a range of $\chi_{HSO3T}:\chi_{SO2(aq)}$ and seem to indicate a slight normal temperature

748   dependence (these are discussed in more detail in section 5.4.1.2).

749   Using our theoretical calculations, we suggest that the experimental data can be explained in

750   terms of the isomerization of bisulfite. Using the experimental constraints for the isomerization

751   quotient for bisulfite as a function of temperature at 1 *m* ionic strength (Horner and Connick, 1986;

752   Littlejohn et al., 1992), we predict the $^{34}\alpha_{\text{bisulfite(bulk)-SO2(g)}}$ as the dashed curve in the figure via the

753   following relationship:

754        $$^{34}\alpha_{\text{bisulfite(bulk)-SO2(g)}} = [Q_i/(1+Q_i)^{34}\beta_{\text{(HO)bisulfite}} + 1/(1+Q_i)^{34}\beta_{\text{(HS)bisulfite}}]/^{34}\beta_{\text{SO2(g)}} \tag{10}$$

755   Where Q_i as a function of temperature is computed via the relationship: $\ln Q_i = 1413(\pm119)/\text{T} -$

756    $3.1(\pm0.4)$ (valid over $\sim$2-67°C, 1 m ionic strength; regressed from the combined datasets of Horner

757   and Connick, 1986; Littlejohn et al., 1992). The corresponding uncertainty envelope plotted in Figure

758   11 includes only the propagated uncertainty of the temperature dependence of the isomerization

759   quotient. The predicted $^{34}\alpha_{\text{bisulfite(bulk)-SO2(g)}}$ at $\mu = 1$ m has a temperature dependence that becomes

760   more shallow with increasing temperature, reflecting the higher proportion of the HS-isomer with

761   increasing temperature. This relationship is roughly consistent with the non-resolvable temperature

762   dependence of Eriksen (1972a) and Eriksen (1972c). When we apply an isomerization quotient to

763   our calculated fractionations performed in a low ionic strength medium ($\mu = 0$ m, T = 25°C; Risberg et

764   al., 2007), we obtain a fractionation factor that is $\sim$2.4 ‰ higher than that obtained from application

765   of the $\mu = 1$ m isomerization quotient (open square data point in Figure 11) and is indistinguishable

766   from the experimental constraint of Eriksen (1972a) at this temperature.

767   The experimental data fall within the range of our calculated theoretical estimates that

768   utilize the available experimental constraints of the relative mole fractions of bisulfite isomers

769   present in solution in media of 0 and 1 m ionic strength. The experiments of Eriksen (1972a, c) were

770   based on a distillation technique that required the solution to be constantly flushed (at an

771   unspecified, "slow" rate) with N_2 gas to strip SO_2 out of solution while simultaneously adding HCl to

772   keep pH constant. Such changes in ionic strength throughout experimental runs are a plausible

773   source of at least some of the variability in the experimentally determined fractionation factors. The

774   constant stripping of SO_2 from solution also requires that the rates of isotope exchange among the

775   aqueous sulfite species be sufficiently rapid at all times, and disequilibria among species and the SO_2

776   stripped from solution may be another source of variability in the experimental fractionation factors.

777   The complete effect of ionic strength on isomerization and isotope fractionations in this system

778   cannot be evaluated in full until the isomerization quotient is determined as a function of ionic

779   strength over a wide range of temperatures.

780	Despite the large uncertainties, it is clear from Figure 11 that: (1) we are able to reproduce

781	the general fractionation behavior in this system that has been determined experimentally, and (2)

782	isotope partitioning in this system is strongly influenced by the isomerization of bisulfite.

783	Furthermore, fractionations in the sulfite system involving bisulfite may be especially dependent on

784	ionic strength due to isomerization.

785	*5.4.1.2 Bisulfite Dimer: Bulk Bisulfite in Solution vs. SO$_{2(g)}$ as a function of pH and [HSO$_3^-$]$_T$*

786	Eriksen (1972c) measured the fractionation between gaseous SO$_2$ and bulk bisulfite as a

787	function of the molar ratio of aqueous SO$_2$ and total bisulfite by varying [HSO$_3^-$]$_T$ (1.5-10 M) and pH

788	(0.3 or 4.5). One of the primary aims of these experiments was to determine the effect of dimer

789	formation on the observable fractionations. Assuming full isotopic equilibration throughout

790	experimental runs, the experiments of Eriksen (1972c) should follow the simple mass balance

791	relationship:

792	$$^{34}\alpha_{S(IV)TOTAL(aq)-SO2(g)} = {}^{34}\alpha_{SO2(aq)/SO2(g)}\chi_{SO2(aq)} + {}^{34}\alpha_{HSO3\text{-}(T)/SO2(g)}\chi_{HSO3\text{-}(T)} + {}^{34}\alpha_{dimer/SO2(g)}\chi_{dimer} \qquad (11)$$

793	Where χ and $^{34}\alpha$ refer to the mole fraction and fractionation factor (based on $^{34}S/^{32}S$) of or between

794	the denoted species, respectively, and HSO$_3^-$$_{(T)}$ = (HO)SO$_2^-$ + (HS)O$_3^-$. In the absence of a dimer (or

795	significant influence thereof), measured fractionation factors between total S(IV) species in solution

796	and SO$_{2(g)}$ plotted against the mole fraction of total bisulfite species present should form a linear

797	array, i.e.:

798	$$^{34}\alpha_{S(IV)TOTAL(aq)-SO2(g)} = {}^{34}\alpha_{SO2(aq)/SO2(g)}\chi_{SO2(aq)} + {}^{34}\alpha_{HSO3\text{-}(T)/SO2(g)}(1 - \chi_{SO2(aq)}) \qquad (12)$$

799	Where $\chi_{HSO3(T)}$ = 1 - $\chi_{SO2(aq)}$ due to the negligible presence of SO$_3^{2-}$ at a pH of < 4.5. As Eriksen (1972c)

800	originally noted, this relationship can deviate from linear due to the power of two dependence on

801	[HSO$_3^-$$_{(T)}$] in the dimerization quotient if the system is driven to large conversion to the dimer (i.e.,

802	high [HSO$_3^-$$_{(T)}$]) and if the fractionation between the dimer and bisulfite (total of both isomers) is

803	relatively large.

804	Using the bisulfite dimer conformer computed to have the lowest S-S bond length, we

805	compute a theoretical fractionation factor at 25°C between the site-averaged dimer and bulk bisulfite

806	(considering both isomers) of 1000ln$^{34}\alpha_{dimer/HSO3\text{-}(T)}$ = - 1.6 ‰ (μ = 0 m; Q_i = 2.57 ± 0.5; Risberg et al.,

807	2007) and 1000ln$^{34}\alpha_{dimer/HSO3\text{-}(T)}$ = 0.9 ‰ (μ = 1 m; Q_i = 4.9 ± 0.1; Horner and Connick, 1986). This

808   indicates that the fractionation between the dimer and bulk bisulfite may be relatively small and

809   perhaps within the uncertainty of the theoretical calculations. The directionality of this overall

810   fractionation may additionally depend on the effects of ionic strength on the relative distribution of

811   bisulfite isomers.

812   We illustrate worked examples of the relationship between the $^{34}\alpha_{S(IV)(aq)/SO2(g)}$ and $\chi_{SO2(aq)}$

813   using our theoretical $^{34}\beta$ values and equilibrium quotients from the literature (μ = 0 m and 1 m) and

814   compare them with the experimental data of Eriksen (1972c) in Figure 12 under comparable

815   conditions. The smooth curves are based on our theoretical calculations where solid curves are the

816   linear arrays ignoring the dimer and the dashed curves are estimates with the dimer included. For

817   the calculations including the dimer (dashed), we assumed a pH range of 0-4.5 and we additionally

818   assume $[S(IV)]_T$ = 10 M (the highest of the Eriksen range) to examine the maximum possible

819   influence of the dimer. The thinnest dashed curves represent the same calculations as the thicker

820   dashed curves (pH = 0-4.5, $[S(IV)]_T$ = 10 M) except with an artificially increased site-averaged $^{34}\beta$ of

821   the dimer (equivalent to 5 ‰) for illustrative purposes due to the possibility that our theoretical

822   calculations are underestimating this value due to a poorly constrained structure for the dimer. Ionic

823   strength was not held constant in the experiments of Eriksen (1972c) and so the 0 m and 1 m are

824   shown for comparison, as these are the only conditions for which all equilibrium quotients

825   (dissociation, isomerization, dimerization) have been experimentally determined for computing mole

826   fractions.

827   The calculated fractionation trends in Figure 12 are generally consistent with the

828   experimental data of Eriksen (1972c), where the experimental data at relatively low $\chi_{SO2(aq)}$ appear to

829   plot in between our estimates using equilibrium quotients performed at 0 and 1 m ionic strength.

830   The presence of the dimer under conditions of $[S(IV)]_T$ = 10 M (thick dashed curves) affects the

831   overall fractionations between bulk bisulfite in solution and gaseous SO_2 at the sub-permil level,

832   which is well within the uncertainty of the experimental determinations. Eriksen (1972c) originally

833   noted that the effect of the dimer is either non-resolvable or insignificant given the seeming linearity

834   in the experimental dataset. Eriksen concluded that the fractionation factor between disulfite and

835 bisulfite might not be significantly higher than non-dimer bisulfite, which is generally consistent with

836 our theoretical calculations that take into consideration both isomers and the dimer.

837 Our theoretical calculations highlight the sensitivity of the fractionation trends in Figure 12

838 to the relative distributions of the bisulfite isomers. Depending on the ratio of the two isomers in

839 solution as a function of ionic strength, the dimer is computed to either dampen or enhance

840 fractionations between bulk aqueous S(IV) and $SO_{2(g)}$ in the modeled system. It is important to

841 reiterate, however, that our calculations of the dimer may overestimate the S-S bond length. From

842 the standpoint of our calculations, shortening the dimer S-S bond (all else being equal) may increase

843 the site-averaged $^{34}\beta$ for disulfite and change these calculated relationships depending on the

844 magnitude of the $^{34}\alpha$ between the dimer and the pooled isomers. Our calculations based on an

845 artificial increase in the site-averaged $^{34}\beta$ of the dimer (equivalent to 5 ‰) illustrate how computed

846 fractionation relationships may be influenced due to a potential overestimation of the dimer S-S bond

847 length. In this case, the fractionation factor $^{34}\alpha_{dimer/HSO3-(T)}$ is > 1 for both ionic strength conditions

848 and the overall influence of the dimer is to enhance fractionations between aqueous S(IV) and

849 gaseous SO_2. We cannot presently confirm the validity of our dimer calculations due to potentially

850 poor constraints on structure, and so it is possible that the dimer plays a different role than we have

851 computed.

852 Based on the seeming linearity of his dataset, Eriksen (1972c) reasoned that the dimer could

853 be ignored and he regressed his data presented in Figure 12 to obtain constraints for the $^{34}\alpha_{SO2(aq)-}$

854 $_{SO2(g)}$ and $^{34}\alpha_{HSO3(T)-SO2(g)}$ fractionation factors from the end member cases of $\chi_{SO2(aq)} = 0$ and $\chi_{SO2(aq)}=1$.

855 This yields $1000ln^{34}\alpha_{SO2(aq)-SO2(g)} = 0.9 \pm 0.4$ ‰ and $1000ln\,^{34}\alpha_{HSO3(T)-SO2(g)} = 9.9 \pm 1$ ‰ (1 s.e., note:

856 the latter fractionation determined this way at 25, 35, and 45°C are those that are plotted in Figure

857 11), where the latter is slightly lower in magnitude but unresolvable from the experiments reported

858 in Eriksen (1972a). These are highly comparable to our theoretical fractionation factors of

859 $1000ln^{34}\alpha_{SO2(aq)-SO2(g)} = 1.8$ ‰ and $1000ln^{34}\alpha_{HSO3(T)-SO2(g)}$ of 11.2 and 8.8 ‰ ($\pm$ 1 ‰, 1 s.e.) using

860 isomerization quotients determined at ionic strength of 0 and 1 m, respectively (see Section 5.4.1.3

861 for detailed discussion of the $SO_{2(aq)}/SO_{2(g)}$ fractionation factor). Although the estimates of Eriksen

862 (1972c) are within the uncertainty of the determinations from Eriksen (1972a), the slightly lower

863   magnitudes of Eriksen (1972c) may reflect the slight influence of the dimer on the bulk fractionation

864   behavior of the system. Further experimentation in this system may allow this hypothesis to be

865   tested.

866   *5.4.1.3 Solvated vs. Gaseous Sulfur Dioxide: $SO_{2(aq)}/SO_{2(g)}$*

867   Eriksen (1972b), Eriksen (1972c), and Chmielewski et al. (2001) provide estimates of the $^{34}\alpha$

868   fractionation factor between gaseous and solvated sulfur dioxide. These determinations are plotted

869   in Figure 13 with our computed $^{34}\alpha$ fractionation factor based on the $SO_{2(30H2O)}$ and $SO_{2(vacuum)}$

870   calculations. The experiments of Eriksen (1972b) overlap with our calculated fractionation factors

871   within experimental uncertainty but it is clear that the uncertainties in the experimental

872   fractionation factors (reflecting experimental reproducibility) may be as large or larger than the

873   magnitude of the fractionation factor itself and so make the comparison difficult. Estimates from the

874   Eriksen (1972c) experiments are reported to be more precise and seem to record an inverse

875   fractionation relationship with temperature, which is neither predicted from the theoretical

876   calculations nor is observed in the more recent and detailed experiments of Chmielewski et al.

877   (2001). Our calculations appear to agree with the experiments of Chmielewski et al. (2001) in terms

878   of both temperature dependence and magnitude, where the experiments are within ca. ≤ 0.5 ‰ of

879   the calculations. The ca. ≤ 0.5 ‰ offset between the Chmielewski et al. (2001) experiments and our

880   calculations is systematic and could be within the uncertainties/error of both determinations.

881   Application of the CCSD/aug-cc-pVTZ-derived harmonic scaling factor of 1.02 does not decrease the

882   offset with the experiments substantially (~0.1 ‰ at 25°C). Using only the SO_2 calculations in the gas

883   phase at the CCSD/aug-cc-pVTZ and B3LYP/6-31+G(d,p) level, we can derive a scaling factor on the

884   order of 1.065 for SO_2 alone that may be more appropriate to use in this case. When applied to our

885   harmonic frequencies, the estimated $SO_{2(aq)}/SO_{2(g)}$ fractionation factor shifts to better agreement

886   with the Chmielewski et al. (2001) experiments: $1000\ln(^{34}\alpha_{SO2\bullet30H2O/SO2(vacuum)})$ = 2.1 ‰ at 25°C.

887   An additional consideration is the pH of the experiments of Chmielewski et al., (2001) (not

888   reported) and whether or not any bisulfite may have been present in the experimental solutions that

889   may have biased the fractionation between aqueous S(IV) and gaseous SO_2 towards higher values.

890   Even between a pH of 0.5 and 1, bisulfite (sum of both isomers) comprises between ca. 4 and 12% of

891   the total S(IV) in solution at low ionic strength ($\mu = 0$ m; Beyad et al., 2014). With ca. 4 % of bisulfite

892   present in solution (corresponding to a pH ~ 0.5 at low ionic strength) and the remaining being

893     $SO_{2(aq)}$, we calculate a fractionation factor between S(IV) in solution and gaseous SO_2 of ~ 2.2 ‰ at

894   25°C based on our calculated $^{34}\beta$ values and assuming the isomerization quotient at low ionic

895   strength ($Q_i = 2.57 \pm 0.5$; Risberg et al., 2007), which is ~ 0.4 ‰ higher than our computed

896     $SO_{2(aq)}/SO_{2(g)}$ fractionation factor and can account for much of the apparent offset between theory

897   and experiment. We cannot uniquely attribute the offset between theory and experiment in this case

898   to either pH/speciation or error in the theoretical calculations but our analysis nevertheless further

899   highlights the strong role of speciation in influencing fractionation behavior in aqueous S(IV)

900   systems.

901   *5.4.1.4 Predicted Fractionations: $[HSO_3^-]_T/[SO_3^{2-}]$*

902   The isomerization of bisulfite appears to exert a strong influence on the observable

903   fractionations between bulk bisulfite and sulfur dioxide in the gas phase and there are similar

904   consequences for fractionation behavior between bulk bisulfite and sulfite in solution. Presently,

905   there do not appear to be any experimental constraints for fractionations among sulfite species in

906   solution and, thus, our theoretical estimates appear to represent the first constraints on these

907   fractionations. Figure 14 plots the calculated fractionation factors between bisulfite species and

908   sulfite as a function of temperature.

909   Using the isomerization quotients as a function of temperature at $\mu = 1$ m (Horner and

910   Connick, 1986; Littlejohn et al., 1992), we predict the $HSO_3^-{}_T$-SO_3^{2-} fractionation factor following a

911   similar relationship to that of equation 10 (Section 5.4.11):

912        $^{34}\alpha_{bisulfite(bulk)\text{-}sulfite} = [Q_i/(1+Q_i)\,^{34}\beta_{(HO)bisulfite} + 1/(1+Q_i)\,^{34}\beta_{(HS)bisulfite}]/^{34}\beta_{sulfite}$ (13)

913   With the similarly derived uncertainty envelope estimated only from the uncertainty of the

914   temperature dependence of the isomerization quotient. This prediction yields an apparent *increase*

915   in the bulk bisulfite-sulfite fractionation with increasing temperature. This apparent inverse-

916   fractionation with increasing temperature relationship is due to the combined effects of the small

917   magnitude of the $(HO)SO_2^-$-SO_3^{2-} fractionation factor relative to the $(HS)O_3^-$-SO_3^{2-} fractionation factor

918   and the increasing proportion of the $(HS)O_3^-$ isomer with increasing temperature. In this case, the

919   presence of the minor $(HS)O_3^-$ isomer is controlling: (1) the magnitude and potentially the direction

920   of the $HSO_{3\text{-}T}^-$-SO_3^{2-} fractionation factor, and (2) the apparent inverse-fractionation-temperature

921   relationship. It is expected that similar relationships would be observed under low-ionic strength

922   conditions, where the absolute magnitude of the fractionation may be slightly higher at any given

923   temperature due to an increase in the proportion of the $(HS)O_3^-$ isomer at low ionic strength (see

924   open square data point in Figure 14; Risberg et al., 2007). Table 2 contains a summary of computed

925   theoretical fractionations vs. the experiments of Eriksen (1972c) and Chmielewski et al., (2001) at

926   25°C.

927   *5.4.2 Sulfoxylate System: General Predictions*

928   As in the sulfite system, isotope partitioning in the sulfoxylate system will depend on the

929   isomerization of sulfoxylic acid and the bisulfoxylate species (the dominant forms of sulfoxylate

930   under most environmentally relevant conditions; Makarov et al., 2010), which is presently not

931   constrained in aqueous solutions. The 3-fold coordinated HS-bonded isomers in the sulfoxylate

932   system are computed to be highly fractionated (~14-15 ‰ at 25°C) relative to their respective two-

933   fold coordinated HO-bonded isomers (Figure 9). Depending on the relative stabilities of these

934   isomers, equilibrium isotope partitioning in the sulfoxylate system could be as equally (or more)

935   complex as the sulfite system. Similar effects relating to the relative distributions of isomers as a

936   function of temperature and ionic strength could come into play, leading to complex isotope

937   fractionations as a function of solution conditions. Research directed at determining the distribution

938   of these isomers in solution over a wide range of environmental conditions is needed before any

939   detailed assessment of isotope partitioning in this system can be made. The further detection and

940   quantification of unbound sulfoxylate species associated with chemical and enzymatic

941   transformations (e.g., dissimilatory sulfite reductase) would also allow an assessment of the

942   importance of these aqueous species in widespread sulfur cycling processes like dissimilatory sulfate

943   reduction.

944   *5.4.3 Sulfide System*

945   The major isotope fractionation factor ($^{34}\alpha$) between aqueous and gaseous H_2S ($H_2S_{(aq)}$-

946    $H_2S_{(g)}$) at low temperature (ca. 0-100°C) has been previously determined experimentally (Fry et al.,

947   1986; Geßler and von Gehlen, 1986; Szaran, 1996) and estimated theoretically by Czarnacki and

948   Halas (2012). A summary of these determinations and our own estimate from the H_2S_{30H2O}-H_2S_{vacuum}

949   calculations is presented in Figure 15. Our calculated $H_2S_{(aq)}$-$H_2S_{(g)}$ fractionation factor based on our

950   H_2S_{30H2O}-H_2S_{vacuum} calculations at the B3LYP/6-31+G(d,p) level of theory is indistinguishable from the

951   previous theoretical constraints based on the H_2S_{5H2O}- H_2S_{vacuum} calculations of Czarnacki and Halas

952   (2012) at both the B3LYP/6-311++G(d,p) and MP2/6-311++G(d,p) levels of theory, which represent

953   the largest basis set and explicit solvation (5 H_2O) applied in their study. Their calculations utilized a

954   larger basis set (and a higher-level theoretical method in the case of the MP2 calculations)—

955   implementing the triple zeta basis set, rather than double zeta, with diffuse functions added to the

956   hydrogen atoms—but much smaller H_2O clusters than what we have computed. Their H_2O

957   computations coordinated the H_2S molecule in ring structures ranging from 2-5 H_2O molecules that

958   did not approximate a complete solvation shell. Their theoretical estimates are effectively identical

959   to our own and, taken together, broadly agree with the available experimental constraints, although

960   the experimental constraints exhibit considerable variability from study to study.

961   The most detailed experimental constraints as a function of temperature come from Geßler

962   and von Gehlen (1986) and display a very similar temperature dependence to the theoretical

963   constraints and quantitatively agree with the theoretical estimates within about ~0.3 ‰ at all

964   determined temperatures. The slight ~0.3 ‰ offset is systematic and may be reasonably assumed to

965   be within the uncertainties of the respective experimental and theoretical approaches. The

966   determinations of Szaran (1996) are typically higher in magnitude and appear to display a steeper

967   temperature dependence than either the theoretical estimates or Geßler and von Gehlen (1986);

968   because of this disagreement (especially with respect to the temperature dependence), it may be

969   reasonably assumed that the experiments of Szaran (1996) do not represent true equilibrium values.

970   The singular determination of Fry et al. (1986) at 22°C is slightly lower than the Geßler and von

971   Gehlen (1986) but is still within the uncertainty of their data.

972   Fry et al. (1986) and Geßler and von Gehlen (1986) also provided constraints on the $H_2S_{(aq)}$-

973   $HS^-_{(aq)}$ fractionation factor by measuring the isotopic fractionation between gaseous H_2S and

974   dissolved sulfide in solution as a function of pH at ca. room temperature (22°C and 20°C,

975 respectively). Their determinations are plotted with our theoretical estimate from our H_2S_{30H2O}-HS$^-$

976 $_{30H2O}$ calculations in Figure 16. In either experimental case, the fractionation factor was estimated by

977 coupling the determinations of the fractionation factor $H_2S_{(aq)}$-$H_2S_{(g)}$ at low pH, then measuring the

978 same fractionation in solutions of higher pH where both $H_2S_{(aq)}$ and $HS^-_{(aq)}$ are present in solution,

979 utilizing information about the dissociation quotient ($H_2S_{(aq)} \rightleftharpoons HS^-_{(aq)} + H^+$, estimated as $\log Q_{d1} \sim 7$ in

980 either case) to back out an estimate for the $H_2S_{(aq)}$-$HS^-_{(aq)}$ fractionation factor by either simple mass

981 balance calculations (Fry et al., 1986) or graphically in the case of Geßler and von Gehlen (1986).

982 These two experimental investigations yield slightly different estimates for the $H_2S_{(aq)}$-$HS^-_{(aq)}$

983 fractionation factor at ca. room temperature in solution: Fry et al. (1986) obtain a $^{34}\alpha$ for $H_2S_{(aq)}$-HS$^-$

984 $_{(aq)}$ of 1.0026 ± 0.0002 (1 s.d., two experiments) at 22°C and Geßler and von Gehlen (1986) estimate a

985 value of ~ 1.0046 at 20°C. Our theoretical value falls in between these estimates ($^{34}\alpha = 1.0033$ at

986 20°C).

987   A primary difference between the experimental approaches of Fry et al. (1986) and Geßler

988 and von Gehlen (1986) is in how pH was adjusted and the resulting changes in ionic strength that

989 ensued. We hypothesize that changes in the dissociation quotient due to ionic strength could have

990 lead to an overestimation of the $H_2S_{(aq)}$-$HS^-_{(aq)}$ fractionation factor by Geßler and von Gehlen (1986)

991 and may also have influenced the determination in Fry et al. (1986). Fry et al. (1986) did not

992 completely describe the ionic strength conditions of their experiments, only that they worked from

993 stock sulfide solutions (very basic when prepared from Na_2S crystals) and adjusted to the desired pH

994 using phosphoric acid. They computed their $H_2S_{(aq)}$-$HS^-_{(aq)}$ fractionation factor using a dissociation

995 quotient for low ionic strength media ($\log Q_{d1} = 7.04$; consistent with the thermodynamic value of

996 7.02 at 22°C and $\mu = 0$ *m;* Hershey et al., 1988). From the description of the Fry et al. (1986)

997 experiments, it is difficult to assess how ionic strength may have influenced their results, but because

998 much more detail is provided in the Geßler and von Gehlen (1986) study, we can make quantitative

999 reinterpretations of their data.

1000   Geßler and von Gehlen (1986) measured fractionations between $H_2S_{(g)}$ and $H_2S_{(aq)T}$ ($H_2S_{(aq)T}$

1001 $= H_2S_{(aq)} + HS^-_{(aq)}$) at 20°C as a function of pH utilizing different concentrations of NaOH (up to 2 M

1002 NaOH for the highest pH measurements), significantly changing ionic strength from experiment to

1003 experiment. At 20°C, the first dissociation quotient of $H_2S_{(aq)}$ (Q_{d1}) varies as a function of ionic

1004 strength from pQ_{d1} = 7.05 at μ = 0 m to 6.72 at μ = 1 m (Hershey et al., 1988; NaCl media) and it

1005 appears Geßler and von Gehlen (1986) assumed a constant logQ_{d1} ~ 7 for their graphical estimation.

1006 We re-estimate the $H_2S_{(ag)}$/HS$^-_{(aq)}$ fractionation factor at 20°C from their data using the following

1007 simple mass balance relationship (solving for $^{34}\alpha_{HS-/H2S(aq)}$):

1008 $^{34}\alpha_{TOTAL(aq)/H2S(g)} = {}^{34}\alpha_{H2S(aq)/H2S(g)}[\chi_{H2S(aq)} + {}^{34}\alpha_{HS-/H2S(aq)}(\chi_{HS-(aq)})]$ (14)

1009 Where $\chi_{H2S(aq)}$ and $\chi_{HS-(aq)}$ are the mole fractions of H_2S and HS$^-$ in solution, which we estimated here

1010 by utilizing the Q_{d1} as function of ionic strength from Hershey et al. (1988), and estimating the ionic

1011 strength from the reported NaOH concentration (ignoring the slight difference between molarity and

1012 molality) and the reported pH. The $^{34}\alpha_{TOTAL(aq)-H2S(g)}$ is the measured fractionation between total

1013 aqueous sulfide and $H_2S_{(g)}$ at a given pH and [NaOH] and $^{34}\alpha_{H2S(aq)-H2S(g)}$= 1.0008 (approximately

1014 invariant over the ionic strength range ~0-2 M; Geßler and von Gehlen, 1986). These data are not

1015 tabulated in the original publication and, thus, the $^{34}\alpha_{TOTAL(aq)-H2S(g)}$, pH, and [NaOH] were estimated

1016 from the published figures (corresponding to the experiments performed at [NaOH] = 0.05, 0.2, 0.5,

1017 1.0, 1.5, and 2.0 M). This procedure yields a re-estimated $^{34}\alpha$ between $H_2S_{(aq)}$/HS$^-_{(aq)}$ of about 1.0040

1018 ± 0.0003 (1 s.d. of 6 experiments), slightly lower than their estimated value of 1.0046, and consistent

1019 with our interpretation that their usage of a constant Q_{d1} over an ionic strength range of ~0-2 M lead

1020 to an overestimation of the fractionation factor. This re-estimated fractionation factor is plotted

1021 Figure 16 in addition to their original estimate. Our theoretical estimation based on the HS$^-_{30H2O}$ and

1022 H_2S_{30H2O} calculations plots directly in between the Fry et al. (1986) determination and our re-

1023 estimated value from Geßler and von Gehlen (1986) and is within ~0.7 ‰ of each. Future

1024 experimental investigations of these fractionation factors as a function of temperature and ionic

1025 strength will allow for a more detailed comparison to our theoretical constraints.

1026 *5.4.4 Equilibrium Isotope Effect between sulfate and sulfide*

1027   Our calculations of the $^{34}\beta$ of sulfide species (principally H_2S_{30H2O} and HS$^-_{30H2O}$) and the

1028 sulfate anion ($SO_4{}^{2-}_{30H2O}$) can be used to provide new constraints on the equilibrium isotope effect

1029 between the two end-member oxidation states of sulfur for use in both high-temperature and low-

1030 temperature (principally biological) applications. Figure 17 plots the computed $^{33}\alpha$ and $^{34}\alpha$ for $SO_4{}^{2-}$

1031 $_{30H2O}$-H_2S_{30H2O} (solid grey curves) and $SO_4^{2-}{}_{30H2O}$-$HS^-{}_{30H2O}$ (dashed grey curves) along with the

1032   empirical relation derived from experimental data compiled in Ohmoto and Lasaga (1982) (solid

1033   black line, ~200-400°C) and the recent experiments of Syverson et al. (2015), which were the first to

1034   measure $^{33}\alpha$ fractionations in this system. (Calculations of the S^{2-} ion are not included due to its likely

1035   negligible abundance over a wide range of pH and T conditions; Ellis and Giggenbach, 1971;

1036   Schoonen and Barnes, 1988; Migdisov et al., 2002). Due to the extremely low rates of isotope

1037   exchange between sulfide species and sulfate at low temperature (*cf.* Ohmoto and Lasaga, 1982), the

1038   experimental constraints all fall within the 200-400°C temperature range. Ohmoto and Lasaga

1039   (1982) reported an experiment performed at 100°C but it did not come at all close to equilibrating;

1040   the measured fractionation between sulfate and sulfide after 240 hours of reaction time only

1041   approached ~4 ‰. The reported fractionation factor for 100°C in their paper ($^{34}\alpha$ $_{sulfate-sulfide}$ ~ 1.048)

1042   is simply the value calculated from their extrapolated empirical temperature dependence over the

1043   200-400°C range, from with they estimated a rate for isotopic exchange at this temperature based on

1044   how far the experimental fractionation was from the extrapolated value.

1045   The estimate from our $SO_4^{2-}{}_{30H2O}$-H_2S_{30H2O} calculations is consistent with the empirical

1046   relationship of Ohmoto and Lasaga (1982) over the 200-400°C temperature range, where the

1047   maximum displacement of the two curves approaches ~1 ‰ at the lowest temperature in this range

1048   (200°C). Additionally, the Ohmoto and Lasaga (1982) curve plots in between the computed

1049   fractionation factors for $SO_4^{2-}{}_{30H2O}$-H_2S_{30H2O} and $SO_4^{2-}{}_{30H2O}$-$HS^-{}_{30H2O}$. As inferred from their tabulated

1050   data, the experiments from which Ohmoto and Lasaga (1982) derived this empirical relation were

1051   mostly performed at low *in situ* pH conditions (where H_2S is dominant) but some of the experiments

1052   were performed at higher pH where the HS^- ion may have been present in appreciable amounts; the

1053 $SO_4^{2-}{}_{30H2O}$-$HS^-{}_{30H2O}$ curves are presented mostly for reference and to illustrate the effects of simple

1054   speciation. The experiments from which this relation is derived may also have exhibited more

1055   complex *in situ* speciation than we have calculated (e.g., ion pairs of HS^- and SO_4^{2-} with Na^+ and

1056   protonated forms of sulfate, principally HSO_4^-). We would expect the differences in the SO_4^{2-}-H_2S and

1057   the HSO_4^--H_2S fractionation factor to be minimal (especially over 200-400°C) because protonation is

1058   on one of the oxygen atoms in sulfate (*cf.* sulfite and sulfoxylate species as computed here) and

1059　perhaps similarly small for ion pairs forming with sulfate for similar reasons. The formation of ion

1060　pairs that involve direct interactions with sulfur, such as $NaSH^0$, may have greater effects.

1061　Complications due to our relatively simplified treatment of speciation may account for some of the

1062　small displacement between the theoretical and empirical curves. Errors in the empirically derived

1063　relationship may also be present (e.g., biased high due to quenching effects, disequilibrium, etc.)—

1064　noting that Ohmoto and Lasaga (1982) had only the major isotope ratio, $^{34}S/^{32}S$, with which to judge

1065　equilibrium from the available experiments.

1066　　　　The small, apparent divergence of the Ohmoto and Lasaga (1982)-derived sulfate/sulfide

1067　fractionation factor and our own based on the $SO_4{}^{2-}{}_{30H2O}$-H_2S_{30H2O} calculations at the low temperature

1068　end (~200°C) may also be within the uncertainty of the theoretical calculations. The combination of

1069　effects related to anharmonicity, inadequacies in the theoretical method, and cluster geometry

1070　variability may contribute permil level error/uncertainty in computed fractionation factors. To

1071　explore this more quantitatively, we will focus on errors arising from inadequacies in the theoretical

1072　method that may represent the major source of error in the calculations. When we apply our

1073　CCSD/aug-cc-pVTZ-derived harmonic scaling factor of 1.01-1.02 to the harmonic frequencies for the

1074　$SO_4{}^{2-}$ and H_2S $30H_2O$ clusters, the resulting fractionation factors appear to come into more

1075　quantitative agreement with the Ohmoto and Lasaga (1982) curve over the entire experimental

1076　temperature range (Figure S.4), which might suggest much of the apparent discrepancy results from

1077　inadequacies in the theoretical method employed in the present study. Since the discrepancy is small

1078　(sub-permil), we cannot rule out contributions from the other factors discussed above.

1079　　　　For comparison, we also plot in Figure S.4 other theoretical estimates based on our own

1080　calculations of $H_2S_{(vacuum)}$ and $SO_4{}^{2-}{}_{(vacuum)}$ using the IEF-PCM solvation model (without any form of

1081　frequency scaling) and previous theoretical calculations utilizing experimentally-derived

1082　fundamental frequencies and frequency shifts for the minor isotopes (Ono et al., 2007), both of which

1083　are several permil displaced from the experimental constraints and our $30H_2O$ cluster calculations.

1084　Comparison to our IEF-PCM calculations further emphasizes the long-understood need for explicit

1085　solvation models in placing theoretical fractionation factors more quantitatively in-line with

1086　experimental fractionation factors in aqueous systems.

1087   Our theoretical predictions also appear to be in reasonably good agreement with the recent

1088   experimental constraints of Syverson et al. (2015) who investigated equilibrium isotope

1089   fractionations ($^{33}\alpha$ and $^{34}\alpha$) in the H_2S-SO_4^{2-}-FeS_2 system at 300°C and 350°C. Their constraints at

1090   350°C are perhaps more quantitatively robust as these experiments were pursued at longer run

1091   times than the lower temperature experiments, and also in greater numbers. The starting solutions

1092   were comprised of sodium thiosulfate in acidic ferrous solutions. Upon ramping up the temperature

1093   to experimental conditions, thiosulfate undergoes quantitative hydrolytic disproportionation to

1094   sulfate and sulfide in 1:1 molar ratios. Since the sulfate and sulfide produced this way tended to have

1095   resolvable $\Delta^{33}S$ values as judged from the shortest experimental runs (a mass-conservation

1096   disequilibrium effect), this approach allowed for the direct monitoring of equilibrium. Figure 17

1097   shows all of their reported fractionations between sulfate and sulfide, which represent a wide range

1098   of experimental run times (ranging from < 1hr up to 4,297 hours as the longest experimental run).

1099   The lowest fractionations measured were typically those that were run for the shortest times and

1100   had not achieved isotopic equilibrium. The data points plotted as black circles are from end-run

1101   experimental analyses that indicated isotopic equilibrium between sulfate and sulfide by way of

1102   identical $\Delta^{33}S$ values between sulfate and sulfide within analytical uncertainty (their experiments

1103   labeled: 2-4, 4-4). When taken as an average for the 350°C determination, the demonstrably

1104   equilibrated experiments yield fractionation factors of $^{33}\alpha_{sulfate-sulfide}$ = 1.0091 ± 0.0003 and $^{34}\alpha_{sulfate-}$

1105 $_{sulfide}$ = 1.0176 ± 0.0006 (1 s.d.), which agree well with our estimated $^{33}\alpha_{sulfate-sulfide}$ = 1.0087 and

1106 $^{34}\alpha_{sulfate-sulfide}$ = 1.0170 from the $SO_4^{2-}{}_{30H2O}$-H_2S_{30H2O} calculations. We note that application of the

1107   CCSD/aug-cc-pVTZ-derived 1.01-1.02 harmonic scaling factors puts the theoretical fractionation

1108   factors at $^{33}\alpha_{sulfate-sulfide}$ = 1.0089-1.0091 and $^{34}\alpha_{sulfate-sulfide}$ = 1.0173-1.0177 from the $SO_4^{2-}{}_{30H2O}$-

1109 H_2S_{30H2O} calculations at 350°C.

1110   The apparent agreement with high temperature experiments suggest that our calculations

1111   may yield reasonable estimations of these fractionations at low-temperature conditions as well (*cf.*

1112   Schauble, 2004), although it is important to note that any systematic errors in the calculations will

1113   scale inversely with temperature. Due to the extremely low rates of isotope exchange between sulfate

1114   and sulfide at low temperature, the only other low temperature constraints have relied either on BM

1115 calculations utilizing experimental vibrational spectra (fundamental frequencies) and frequency

1116 shifts for the minor isotopes via force field models (e.g., Sakai, 1968; Farquhar et al., 2003; Ono et al.,

1117 2007) or, in perhaps the least ideal case, extrapolating the empirical temperature dependence of

1118 high-temperature constraints to low temperatures (from Ohmoto and Lasaga, 1982). Neither

1119 approach is strictly valid—for example, computing RPFRs from experimental fundamental

1120 frequencies via the BM-equation violates the harmonic oscillator approximations used in its

1121 derivation (*cf.* Liu et al., 2010)—and so our calculations may provide some of the most reliable

1122 estimates to date at low-temperature within the harmonic approximation. The low temperature

1123 fractionations computed via our calculations will likely have the most applicability to network

1124 models of isotope partitioning for sulfate reducing organisms (*cf.* Wing and Halevy, 2014), as well as

1125 the estimation of sulfate-sulfide equilibration rates from non-equilibrated low-temperature

1126 experiments (*cf.* approach of Ohmoto and Lasaga, 1982).

1127 Figure 18 presents the data of Figure 17 with an expanded temperature range (down to the

1128 equivalent of 0°C) and includes data from recent experiments from sulfate reducing organisms that

1129 have produced the largest fractionations between sulfate and sulfide that have been measured to

1130 date (Canfield et al., 2010; Sim et al., 2011a; Leavitt et al., 2013). It has been postulated that the

1131 maximum isotope fractionations possible in a sulfate reducing organism approach the equilibrium

1132 fractionation factor between sulfate and sulfide species at the given growth temperature (*cf.*, Sim et

1133 al., 2011a; Wing and Halevy, 2014), which is based on the consistency between some of the largest

1134 fractionations observed in certain cultures of sulfate reducers and the available constraints on

1135 equilibrium fractionations. Using the Sim et al. (2011a) and Sim et al. (2011b) pure culture

1136 (*Desulfovibrio* sp., DMSS-1) dataset as an example (also, see Leavitt et al., 2013 and Wing and Halevy,

1137 2014), as cell specific sulfate reduction rates approach extremely low values, the magnitude of the

1138 observed $^{33}S/^{32}S$- and $^{34}S/^{32}S$-based fractionation factors between sulfate and sulfide appear to

1139 approach near their expected equilibrium values (Figure 18; see also Figure S.5). The largest

1140 fractionation reported between sulfate and sulfide from the Sim et al. dataset is $^{34}\alpha_{\text{sulfate-sulfide}}$ ~1.0656

1141 ± 0.0003 with a corresponding observed $^{33}S/^{32}S$- and $^{34}S/^{32}S$-based exponent of 0.5142 ± 0.0002

1142 (~20°C; Sim et al., 2011a). From this perspective, at 20°C our calculations would predict a $^{34}\alpha_{\text{sulfate-}}$

1143 ₛᵤₗfᵢdₑ for $SO_4^{2-}{}_{30H2O}$-H_2S_{30H2O} of 1.0674 and a $SO_4^{2-}{}_{30H2O}$-$HS^-{}_{30H2O}$ 1.0709, with corresponding $^{33/34}\theta_{sulfate-}$

1144 ₛᵤₗfᵢdₑ of 0.5147 and 0.5148, respectively. We note that applying our CCSD/aug-cc-pVTZ-derived

1145 harmonic scaling factors of 1.01-1.02 will increase the $^{34}S/^{32}S$-based fractionation factor estimates

1146 slightly: for $SO_4^{2-}{}_{30H2O}$-H_2S_{30H2O} = 1.0685-1.0696 and $SO_4^{2-}{}_{30H2O}$-$HS^-{}_{30H2O}$ = 1.0720-1.0732 at 20°C,

1147 which may be appropriate in this case due to the enhanced agreement with Ohmoto and Lasaga

1148 (1982) at high temperature. Our calculations do not confirm or sufficiently test any hypotheses

1149 regarding the controls on fractionation magnitudes in sulfate reducing organisms, but may provide

1150 end-member constraints for isotope fractionation network models that use equilibrium fractionation

1151 factors (e.g., Wing and Halevy, 2014).

1152 *5.4.5 Fractionations Within and Between Thiosulfate and the Major Sulfide Species*

1153   The isotope fractionations associated with isotope exchange between the "outer" (**S**-SO_3^{2-};

1154 "sulfane") and "inner" (S-**S**O_3^{2-}; "sulfonate") sulfur atoms in thiosulfate ($S_2O_3^{2-}$), as well as those

1155 between these two sites and aqueous sulfide (i.e., $H_2S_{(aq)}$/$HS^-{}_{(aq)}$) have been studied experimentally

1156 (Uyama et al., 1985) and reinterpreted in terms of exchange rates and slightly revised equilibrium

1157 fractionation factors in follow up studies (Chu and Ohmoto, 1991; Chu et al., 2004). Figure 19 plots

1158 the experimentally derived fractionation factors ($^{34}\alpha$) for S-**S**O_3^{2-}/**S**-SO_3^{2-}, S-**S**O_3^{2-}/H_2S, and **S**-SO_3^{2-}

1159 /H_2S (100-170°C, as compiled/evaluated in Chu et al., 2004; bold and underline emphasizes the

1160 sulfur site undergoing exchange in thiosulfate) along with the same fractionation factors computed

1161 from our $S_2O_3^{2-}{}_{(30H2O)}$ and $H_2S_{(30H2O)}$ cluster calculations (the same calculations involving $HS^-{}_{(30H2O)}$

1162 have been omitted for simplicity of graphical presentation, but see discussion below). In terms of

1163 fractionation magnitude, the fractionation between the intramolecular sites of thiosulfate appear to

1164 be in the most agreement between the experimental dataset and our own calculations, where a

1165 slightly steeper temperature dependence is predicted from our calculations than appears to be

1166 represented in the experimental dataset.

1167   The fractionations predicted from our calculations and the experiments between the two

1168 sulfur sites in thiosulfate and H_2S appear to be systematically shifted by a few permil but agree in

1169 their temperature dependence. The experimental dataset of Uyama et al. (1985) seems to indicate

1170 that the **S**-SO_3^{2-}/H_2S fractionation factor increases in magnitude with increasing temperature over

1171 the 100-170°C range, which the calculations also predict; we find this to be related to a crossover at

1172 sub-0°C temperature. These offsets in the magnitude of the fractionation factors between theory and

1173 experiment appear to be the largest we have observed in our overall study and may be on the high

1174 end of the estimated uncertainties in the calculations.

1175 The relatively large offset (few permil) between theory and experiment in the

1176 thiosulfate/sulfide system may reflect speciation. The experiments were done under *in situ* pH

1177 conditions that were circumneutral (ca. 5.4-7.2) where HS⁻ may be present at appreciable levels at

1178 the experimental temperatures (*cf.* Ellis and Giggenbach, 1971; Hershey et al., 1988). However, the

1179 computed fractionations between the two sulfur sites in thiosulfate and HS⁻ do not bring the

1180 calculated fractionation factors in better agreement with the experiments. Due to the HS⁻ ion having

1181 a lower $^{34}\beta$ than H_2S, predicted fractionations between S-$\underline{S}O_3^{2-}$/HS⁻, and $\underline{S}$-SO_3^{2-}/HS⁻ are shifted

1182 upward relative to the H_2S counterparts in Figure 19, in the opposite direction needed to agree with

1183 the experimental datasets. The formation of NaSH⁰ ion pairs could, in principle, explain some of the

1184 offset, but we have not computed this species. In order for the NaSH⁰ ion pair to account for the

1185 several permil offset alone, it would need to be a major species under the experimental conditions

1186 and/or have a comparable (or higher) $^{34}\beta$ than H_2S.

1187 Applying the harmonic frequency scaling factor of 1.01-1.02 to the frequencies of the sulfide

1188 and thiosulfate 30H_2O clusters also shifts the predicted fractionation factors in the opposite direction

1189 of the experimental constraints on the order of 1-2 ‰ for the S-$\underline{S}O_3^{2-}$/H_2S and S-$\underline{S}O_3^{2-}$/$\underline{S}$-SO_3^{2-}

1190 fractionation factors, and has negligible effect on the smaller $\underline{S}$-SO_3^{2-}/H_2S fractionation factor. Based

1191 on our simple treatment, error arising from the employed theoretical method alone may not be able

1192 to explain the systematic offset between theory and experiment. Based on the present constraints,

1193 we cannot rule out contributions from experimental error (e.g., the influence of other sulfur

1194 compounds being present, either under experimental conditions or produced/decomposed upon

1195 quenching or processing), complex speciation effects, and other errors arising from the calculations

1196 (e.g., anharmonic effects and cluster geometry variability) in describing the apparent offset between

1197 theory and experiment. The offset is somewhat puzzling given the relatively good agreement

1198 between our theoretical calculations and the experiments of the intramolecular fractionation factor

1199   for thiosulfate, as well as the H_2S/HS^- fractionation factor (Section 5.4.3), and may indicate further

1200   experimentation is warranted in these systems.

1201   *5.5 Further Implications of Isomerization: Relative Reactivity of $(HO)SO_2^-$ and $(HS)O_3^-$*

1202   On the molecular and mechanistic level, the two isomers of bisulfite have been hypothesized

1203   to have different reactivity towards oxidants due to the absence of the lone pair of electrons on sulfur

1204   in the tetrahedral $(HS)O_3^-$ form, where the pyramidal $(HO)SO_2^-$ containing the lone electron pair on

1205   the sulfur atom might be expected to be more reactive (e.g., Yiin et al., 1987; Brandt and van Eldik,

1206   1995). In other words, the $(HS)O_3^-$ isomer is hypothesized to be sterically hindered in terms of

1207   reactions requiring access to the sulfur atom, which could be relevant for all redox reactions

1208   involving sulfite and bisulfite species (noting that, from this perspective, $(HO)SO_2^-$ and SO_3^{2-} would be

1209   expected to behave more similarly in reactions, at least relative to $(HS)O_3^-$). This hypothesis can be

1210   extended to the relative reactivity of the isomers towards the active binding sites of intracellular

1211   enzymes in biological redox processes (e.g., the heme sites in reductases like dissimilatory sulfite

1212   reductase and MccA where binding occurs directly to the sulfur atom; Parey et al., 2010; Hermann et

1213   al., 2015), because the lone pair of electrons would be necessary for bond formation to the Fe in the

1214   heme groups.

1215   To our knowledge, this hypothesis has yet to be tested rigorously and would be expected to

1216   depend on the energetics and rates of tautomerization (i.e., the intramolecular transfer of the proton

1217   from the sulfur atom to the oxygen atom):

1218 $(HS)O_3^- \rightarrow (HO)SO_2^-$ $k_{tautomerization}$ (15)
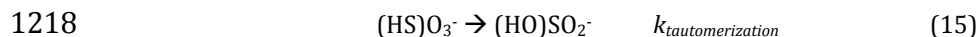
1219   Where $k_{tautomerization}$ represents the rate constant in the direction as indicated. If tautomerization

1220   occurs rapidly, perhaps the $(HS)O_3^-$ isomer could tautomerize prior to (or during) a reaction to

1221   expose the sulfur atom and its lone pair of electrons for binding or electron transfer in a way that led

1222   to minimal discrimination between $(HS)O_3^-$ and $(HO)SO_2^-$ during chemical reactions. Alternatively, if

1223   tautomerization was slow, the rates of tautomerization might inhibit reactions involving $(HS)O_3^-$ and

1224   lead to an overall discrimination between $(HS)O_3^-$ and $(HO)SO_2^-$.

1225   There are several consequences of the hypothesis that relatively slow tautomerization could

1226   lead to a discrimination between the bisulfite isomers during chemical reactions and, in particular,

1227   inhibit the reactivity for the $(HS)O_3^-$ isomer. From the standpoint of isotope mass balance, assuming

1228   that the bisulfite pool is at isotopic equilibrium prior to reaction, a preference for the $(HO)SO_2^-$

1229   isomer (or SO_3^{2-}) upon reaction would mean that the chemical reaction preferentially samples a

1230   fractionated portion of the total sulfite pool, which our calculations predict to be due almost

1231   exclusively to the presence of the $(HS)O_3^-$ isomer that has a high $^{34}\beta$ and shifts the other sulfite

1232   species towards isotopically lighter values (relative to the total S^{4+} composition). If the isotope effect

1233   associated with the chemical reaction is a so-called *normal* kinetic isotope effect (i.e., the typical case

1234   in which the light isotopomers react more readily than heavy isotopomers due to the predominating

1235   influence of weakly bound transition state(s)), slow tautomerization could lead to an apparent boost

1236   in the magnitude of the instantaneous fractionation between the bulk bisulfite pool and the pooled

1237   product. However, should the reaction be associated with a so-called *inverse* isotope effect (i.e., the

1238   atypical case of the heavy isotopomer reacting more readily than the light isotopomer), the effect of

1239   sluggish tautomerization would be less-straightforward: it could either lead to a dampening of

1240   magnitude of the apparent fractionation, or could possibly even lead to an apparent reversal in the

1241   direction of the fractionation (from inverse to normal) depending on the relative magnitudes of the

1242   fractionation associated with the KIE vs. that associated with the EIEs among the sulfite species. The

1243   complex speciation of sulfite species in solution may contribute to considerable ambiguity in the

1244   meaning of measured isotope effects associated with unidirectional reactions involving sulfite under

1245   solution conditions of mixed-species, potentially obscuring any observation of primary kinetic

1246   isotope effects.

1247   We consider a simple qualitative example to illustrate hypothetical effects associated with

1248   bisulfite isomerization within the basic framework of sulfate reduction. For the sake of this exercise,

1249   we first assume that equilibration rates between the sulfite and bisulfite isomers are sufficiently fast

1250   that they are in chemical and isotopic equilibrium at all times over all respiration rates and residence

1251   times of sulfite species within the cell. We consider a pool of sulfite species being generated via the

1252   reduction of APS. Upon the cleavage of the S-O bonds, the sulfite species would enter solution as

1253   inorganic anions and immediately undergo hydrolysis reactions to form the different bisulfite

1254   isomers, the relative equilibrium distribution of which would depend on the pH, temperature, and

1255   ionic strength conditions of the intracellular aqueous environment. Once equilibrated chemically

1256   and isotopically, this pool would be characterized by an isotopically light pool of sulfite *sensu stricto*

1257   and $(HO)SO_2^-$ and a relatively heavy pool of $(HS)O_3^-$. The magnitude of the bulk fractionation would

1258   depend on the relative distribution of these species and therefore depend on the temperature, ionic

1259   strength, and pH of the intracellular environment. If the active siroheme site of dissimilatory sulfite

1260   reductase discriminated between the aqueous sulfite species and showed a preference for sulfite

1261   *sensu stricto* and/or $(HO)SO_2^-$, the unidirectional reduction of this sulfite could introduce an apparent

1262   amplification in the instantaneous fractionation that eventually forms sulfide (all else being equal),

1263   which considering mass balance could amount to an amplification on the level of several permil

1264   depending on conditions. In this simple case of hypothetical species discrimination, the $(HS)O_3^-$

1265   isomer would effectively be acting as a relative dynamic 'sink' for heavy isotopes within the

1266   metabolism. An effect of this kind would be sensitive to temperature due to the increasing

1267   proportion of the $(HS)O_3^-$ isomer with increasing temperature, which would be significant for sulfate

1268   reducers that grow at higher temperatures.

1269   Even given little to no species discrimination with respect to enzymatic redox

1270   transformations involving the sulfite species, the presence of the $(HS)O_3^-$ isomer would be predicted

1271   to cause shifts in the isotopic mass balance between the bulk intracellular sulfite pool and other

1272   downstream and upstream pools in the metabolism. In this case, the magnitudes of these effects

1273   would likely depend on the rates of isotopic equilibrium among the sulfite species, especially in how

1274   these rates compare to the residence time of total sulfite in the cell. Since the residence time of

1275   sulfite species will vary as a function of cell specific reduction rate (which, in turn, is controlled by a

1276   wide variety of extra- and intra-cellular environmental and metabolic conditions; *cf.* Wing and

1277   Halevy, 2014), the magnitudes of any of the hypothetical effects associated with the $(HS)O_3^-$ isomer

1278   could vary over wide ranges of growth conditions.

1279   **6.0 Conclusion**

1280   The calculations presented here provide some of the most detailed constraints on sulfur

1281   isotope partitioning in the sulfite system available to date, and provide new constraints on

1282   fractionation factors involving many of the major aqueous sulfur compounds relevant to

1283 hydrothermal and (bio)geochemical cycles. From a detailed comparison to the experimental datasets

1284 of Eriksen, the calculations reveal that the isomerization of bisulfite is a major control on isotope

1285 partitioning in this system. However, much uncertainty still exists in the isomerization quotient as a

1286 function of temperature over a wide range of ionic strength. Future research should be directed at

1287 constraining this quotient over a wide range of conditions (temperature and ionic strength) to more

1288 precisely determine its influence in the sulfur cycle. Further detailed experimentation of the

1289 equilibrium isotope effects in the sulfite system as a function of temperature and ionic strength could

1290 test the predictions made by our theoretical calculations. Due to the complexity of sulfite solutions,

1291 precise and species-specific determinations of isotope partitioning in the sulfite system will be

1292 reliant upon the combination of experimental and theoretical techniques.

1293 The pH and ionic strength dependency of sulfur isotope partitioning in the sulfite system is

1294 predicted to be significant due to the complex speciation of sulfite. Treating the sulfite system in

1295 isotope partitioning models strictly as the pyramidal sulfite anion (SO_3^{2-}) (e.g., network models of

1296 sulfate reducing metabolisms) is clearly invalid for most conditions relevant to natural systems,

1297 particularly intracellular conditions where pH is typically circum-neutral. Future treatment and

1298 applications should include all relevant species. Assumptions about similarity in structure between

1299 sulfite species and their isotope partitioning behavior should be avoided in any future experimental

1300 approaches. It remains to be shown whether or not the two structural isomers of bisulfite behave

1301 differently during chemical reactions, but if they do, there could be consequences in isotope

1302 fractionations associated with chemical reactions in sulfite media where both isomers are present.

1303 Calculations of the isotope partitioning behavior of the sulfoxylate species have been

1304 included here in the hopes of igniting research towards their further characterization in aqueous

1305 solutions. As in the sulfite system, isotope partitioning among sulfoxylate species will strongly

1306 depend on the isomerization of the protonated species, principally H_2SO_2 (sulfoxylic and sulfinic

1307 acid) and bisulfoxylate species. Techniques exist for producing these compounds via the

1308 decomposition of organic precursors (e.g., thiourea dioxide; Svarovsky et al., 2000; Makarov et al.,

1309 2002; Makarov et al., 2010) and so their characterization in aqueous solutions should be possible, in

1310 principle. If such species do indeed exist within the MSR framework, their characterization could

1311   allow for an even more elaborate understanding of sulfate reduction metabolisms. The role these

1312   compounds play in other redox processes (e.g., sulfide oxidation) could further be illuminated and

1313   allow for detailed understandings of their mechanisms as well.

1314   **Acknowledgements**

1320   **Figure Captions**

1321   **Figure 1:** Mole fraction of sulfite species ($\chi_{S(IV)}$) as a function of pH at 25°C, highlighting the isomers of

1322   bisulfite (not including bisulfite dimers for simplicity; $[S^{4+}]_T <$ ~0.1 M). The solid black curves are

1323   computed using dissociation and isomerization quotients determined at an ionic strength of zero

1324   (Damian Risberg et al., 2007; Beyad et al., 2014; Martell and Smith, 1982) and the gray curves at an

1325   ionic strength of 1 m (Horner and Connick, 1986; Millero et al., 1989).

1326   **Figure 2:** Experimental constraints on the bisulfite isomerization quotient as a function of

1327   temperature, defined as $Q_i = [(HO)SO_2^-]/[(HS)O_3^-]$. The $\mu = 1$ m constraints are from Horner and

1328   Connick (1986) (black circles) and Littlejohn et al. (1992) (white circles), and the $\mu = 0$ m constraint

1329   is from Risberg et al. (2007) (white square). The least-squares linear regression of the 1 m

1330   constraints yields: $\ln Q_i = 1413(\pm119)/T - 3.1(\pm0.4)$ (valid over $\approx$ 0-67°C).

1331   **Figure 3:** Optimized geometries of sulfite species in $30H_2O$-$34H_2O$ clusters. (A) Sulfur dioxide

1332   ($SO_{2(aq)} \cdot 30H_2O$), (B) sulfite *sensu stricto* ($SO_3^{2-} \cdot 30H_2O$), (C) OH isomer of bisulfite ($(HO)SO_2^- \cdot 34H_2O$),

1333   (D) HS isomer of bisulfite ($(HS)O_3^- \cdot 30H_2O$), and (E) the bisulfite dimer, disulfite ($S_2O_5^{2-} \cdot 30H_2O$)

1334   containing the shortest computed S-S bond length. Geometries can also be found in Table S.2.

1335   **Figure 4:** Optimized geometries of sulfoxylate species in $30H_2O$ clusters. (A) Sulfoxylic acid ($S(OH)_2$),

1336   (B) sulfinic acid ($(HS)O_2H$), (C) OH isomer of bisulfoxylate ($(HO)SO^-$), (D) SH isomer of bisulfoxylate

1337   ($(HS)O_2^-$), and (E) sulfoxylate (SO_2^{2-}). Geometries can also be found in Table S.2.

1338 **Figure 5:** Optimized geometries of sulfide species, sulfate, and thiosulfate in $30H_2O$ clusters. (A)

1339 Hydrogen sulfide (H_2S), (B) bisulfide (HS^-), (C) sulfide dianion (S^{2-}), (D) sulfate (SO_4^{2-}), and (E)

1340 thiosulfate ($S_2O_3^{2-}$). Geometries can also be found in Table S.2.

1341 **Figure 6:** Computed theoretical $^{34}\beta$-values for aqueous sulfur compounds modeled in 30-34 H_2O

1342 clusters at the B3LYP/6-31+G(d,p) level of theory over T = 0-100°C.

1343 **Figure 7:** Exponents of mass dependence based on β-values computed from 0-2000°C ($^{33/34}\kappa$ =

1344 $\ln(^{33}\beta)/\ln(^{34}\beta)$, $^{36/34}\kappa = \ln(^{36}\beta)/\ln(^{34}\beta)$; after Cao and Liu, 2011). The horizontal red lines indicate the

1345 high temperature limits (as T$\rightarrow \infty$) based on the atomic mass of the sulfur isotopes derived from

1346 RPFRs (Matsuhisa et al., 1978).

1347 **Figure 8**: Triple isotope plot of theoretical fractionation factors for aqueous sulfite species relative to

1348 aqueous sulfur dioxide at 25°C. The A and B subscripts for disulfite (conformer computed with the

1349 shortest S-S bond length) refer to the 3-fold and 4-fold coordinated sites within the dimer,

1350 respectively (gray squares). The $S_2O_5^{2-}{}_T$ refers to the site-averaged fractionation factor for the dimer

1351 (black square). The exponents of mass dependence for select fractionation factors ($^{33/34}\theta$) are noted.

1352 **Figure 9:** Triple isotope plot of theoretical fractionation factors for aqueous sulfoxylate species

1353 relative to sulfoxylic acid, $S(OH)_2$, at 25°C. The exponents of mass dependence for individual

1354 fractionation factors ($^{33/34}\theta$) are noted.

1355 **Figure 10:** Triple isotope plot of theoretical fractionation factors for aqueous sulfide species relative

1356 to the atomic sulfide ion, S^{2-}, at 25°C. The exponents of mass dependence for individual fractionation

1357 factors ($^{33/34}\theta$) are noted.

1358 **Figure 11:** Comparison of theoretical fractionation factors to experimental constraints in the

1359 bisulfite-$SO_{2(g)}$ system as a function of temperature, highlighting the influence of bisulfite

1360 isomerization on fractionation behavior. Black data points (circles and diamonds) are from the

1361 experimental studies of Eriksen (1972a) and Eriksen (1972c). The open (white) square is our

1362 theoretical estimate for the bulk fractionation factor using the isomerization quotient at 0 m ionic

1363 strength from Risberg et al. (2007) following equation (10) in the text. The thick dashed curve

1364 represents our theoretical estimate (equation (10) in the text) using the isomerization quotients as a

1365   function of temperature at 1 m ionic strength (Horner and Connick, 1986; Littlejohn et al., 1992;

1366   Figure 2). The lighter dashed lines represent the uncertainty envelope derived solely from the

1367   propagation of the uncertainty of the isomerization quotient as a function of temperature that is

1368   based on the least squares linear regression in Figure 2.

1369   **Figure 12:** Fractionations at 25°C in the sulfite system from Eriksen (1972c) (white circles) and a

1370   modeled system based on our theoretical fractionation factors and mass balance calculations (solid

1371   or dashed curves). Solid curves ignore the bisulfite dimer and the thick dashed curves include the

1372   dimer assuming a total bisulfite concentration of 10 M (highest in the Eriksen experimental range)

1373   and a pH range of 0.5-4.5. The lightest dashed curves are identical to the thick dashed curves but

1374   include an artificially increased $^{34}\beta$ for the site-averaged dimer equivalent to 5 ‰ for illustration

1375   purposes.

1376   **Figure 13:** The major isotope fractionation factor between aqueous and gaseous sulfur dioxide. The

1377   curves represent our theoretical values and the data points represent experimental values from

1378   Eriksen (1972b) (black circles), Eriksen (1972c) (black diamonds), and Chmielewski et al. (2001)

1379   (white squares).

1380   **Figure 14:** Theoretical estimates/predictions of the major isotope fractionation factors among the

1381   anions in the sulfite system: sulfite *sensu stricto* (SO_3^{2-}) and the two isomers of bisulfite. The open

1382   (white) square and the thick dashed curve are the predicted bulk fractionation factors between

1383   bisulfite and sulfite using the isomerization quotients at ionic strengths of 0 m (Risberg et al., 2007)

1384   and 1 m (Horner and Connick, 1986; Littlejohn et al., 1992), respectively, following equation (13) in

1385   the text.

1386   **Figure 15:** The major isotope fractionation factor between aqueous and gaseous hydrogen sulfide

1387   (H_2S). The curves represent our theoretical values and those of Czarnacki and Halas (2012) and the

1388   data points represent experimental values from the literature.

1389   **Figure 16:** The major isotope fractionation factor between the two predominate aqueous sulfide

1390   species, $H_2S_{(aq)}$ and $HS^-_{(aq)}$, where curves represent our theoretical values and the data points are

1391   experimental constraints. The dashed white square is the estimate from Geßler and von Gehlen

1392   (1986) and the solid white square is our own re-estimate using their data and the dissociation

1393   quotients as a function of ionic strength from Hershey et al. (1988) (see section 5.4.3 for further

1394   explanation).

1395   **Figure 17:** Comparison of our theoretical estimations of fractionations between sulfate and sulfide

1396   (gray curves; solid and dashed indicate H_2S and HS^-, respectively) and the available experimental

1397   constraints at high temperature (200-400°C, indicated by dashed vertical lines). The black curve is

1398   derived from a compilation of experimental data by Ohmoto and Lasaga (1982). The data points

1399   (circles) are the recent experimental values derived from the $FeS_{2pyrite}$-H_2S-SO_4^{2-} system, where black

1400   circles indicate demonstrably equilibrated experiments via mass dependent relationships (see

1401   section 5.4.4 for further explanation).

1402   **Figure 18:** Comparison of our theoretical estimations of fractionations between sulfate and sulfide

1403   (gray curves; solid and dashed indicate H_2S and HS^-, respectively) and the available experimental

1404   constraints plotted from ambient to high temperature (0-2000°C). Labeling is same as in Figure 17.

1405   Also included for reference are the largest fractionations reported in microbial sulfate reduction

1406   experiments at ambient T: (1) Pure culture experiments: white squares (Leavitt et al., 2013) and

1407   white diamonds (Sim et al., 2011a) and (2) experiments with natural populations (Canfield et al.,

1408   2010): water incubations = black squares and sediment incubations = black diamonds.

1409   **Figure 19:** The major isotope fractionation factor for the intramolecular isotope fractionation in

1410   thiosulfate (experimental: white circles, our theoretical: dashed black curve), fractionations between

1411   the outer ("sulfanyl") sulfur in thiosulfate and $H_2S_{(aq)}$ (experimental: gray circles, our theoretical: gray

1412   curve), and the inner ("sulfonate") sulfur in thiosulfate and $H_2S_{(aq)}$ (experimental: black circles, our

1413   theoretical: black curve). Experimental data have been derived by Chu et al. (2004) from the

1414   experiments of Uyama et al. (1985).

1415   **References**

1416 Becke A. D. (1993) Density functional thermochemistry: the role of exact exchange. *J. Chem. Phys.* **98**,
1417   5648–5652.

1418 Beyad Y., Burns R., Puxty G. and Maeder M. (2014) A speciation study of sulfur(iv) in aqueous
1419   solution. *Dalton Trans.* **43**, 2147–52.

1420 Bigeleisen J. and Mayer M.G. (1947) Calculation of equilibrium constants for isotopic exchange
1421   reactions. *J. Chem. Phys.* **15**, 261-267.

1422　Bourne D.W.A., Higuchi T. and Pitman I.H. (1974) Chemical equilibria in solutions of bisulfite salts. *J.*
1423　　　 *Pharm. Sci.* **63**, 865-868.

1424　Bowles M. W., Mogollón J. M., Kasten S., Zabel M. and Hinrichs K.-U. (2014) Global rates of marine
1425　　　 sulfate reduction and implications for sub-sea-floor metabolic activities. *Science* **344**, 889–91.

1426　Bradley A. S., Leavitt W. D. and Johnston D. T. (2011) Revisiting the dissimilatory sulfate reduction
1427　　　 pathway. *Geobiology* **9**, 446–457.

1428　Brandt C. and van Eldik R. (1995) Transition Metal-Catalyzed Oxidation of Sulfur(IV) Oxides.
1429　　　 Atmospheric-Relevant Processes and Mechanisms. *Chem. Rev.* **95**, 119–190.

1430　Canfield D. E. and Teske a (1996) Late Proterozoic rise in atmospheric oxygen concentration inferred
1431　　　 from phylogenetic and sulphur-isotope studies. *Nature* **382**, 127–132.

1432　Canfield D. E., Farquhar J. and Zerkle A. L. (2010) High isotope fractionations during sulfate reduction
1433　　　 in a low-sulfate euxinic ocean analog. *Geology* **38**, 415–418.

1434　Cao X. and Liu Y. (2011) Equilibrium mass-dependent fractionation relationships for triple oxygen
1435　　　 isotopes. *Geochim. Cosmochim. Acta* **75**, 7435–7445.

1436　Cao X. and Liu Y. (2012) Theoretical estimation of the equilibrium distribution of clumped isotopes in
1437　　　 nature. *Geochim. Cosmochim. Acta* **77**, 292–303.

1438　Chacko T., Cole D. R. and Horita J. (2001) Equilibrium Oxygen, Hydrogen and Carbon Isotope
1439　　　 Fractionation Factors Applicable to Geologic Systems. *Rev. Mineral. Geochemistry* **43**, 1–81.

1440　Chen K. and Morris J. (1972) Kinetics of Oxidation of Aqueous Sulfide by O2. *Environ. Sci. Technol.* **6**,
1441　　　 529–537.

1442　Chmielewski A. G., Derda M., Wierzchnicki R. and Mikolajczuk A. (2002) Sulfur isotope effects for the
1443　　　 {SO2(g)-SO2(aq)} system. *Nukleonika* **47**, S69–S70.

1444　Chu X-L. and Ohmoto H. (1991) Kinetics of isotope exchange reactions involving intra- and
1445　　　 intermolecular reactions: I. Rate law for a system with two chemical compounds and three
1446　　　 exchangeable atoms. *Geochim. Cosmochim. Acta* **55**, 1953–1961.

1447　Chu X., Ohmoto H. and Cole D. R. (2004) Kinetics of sulfur isotope exchange between aqueous sulfide
1448　　　 and thiosulfate involving intra- and intermolecular reactions at hydrothermal conditions. *Chem.*
1449　　　 *Geol.* **211**, 217–235.

1450　Clayton R. N. and Mayeda T. K. (1996) Oxygen isotope studies of achondrites. *Geochim. Cosmochim.*
1451　　　 *Acta* **60**, 1999–2017.

1452　Cline J. and Richards F. (1969) Oxygenation of hydrogen sulfide in seawater at constant salinity,
1453　　　 temperature and pH. *Environ. Sci. Technol.* **3**, 838–843.

1454　Connick R. E., Tam T. M. and Von Deuster E. (1982) Equilibrium constant for the dimerization of
1455　　　 bisulfite ion to form disulfite(2-) ion. *Inorg. Chem.* **21**, 103–107.

1456　Crabtree K. N., Martinez O., Barreau L., Thorwirth S. and McCarthy M. C. (2013) Microwave detection
1457　　　 of sulfoxylic acid (HOSOH). *J. Phys. Chem. A* **117**, 3608–3613.

1458 Craig H. (1957) Isotopic standards for carbon and oxygen and correction factors for mass-
1459   spectrometric analysis of carbon dioxide. *Geochim. Cosmochim. Acta* **12**, 133–149.

1460 Cramer C.J. (2002) *Essentials of Computational Chemistry: Theories and Models*. Jon Wiley & Sons, New
1461   York.

1462 Czarnacki M. and Hałas S. (2012) Ab initio calculations of sulfur isotope fractionation factor for H2S
1463   in aqua–gas system. *Chem. Geol.* **318–319**, 1–5.

1464 Deines P. (2003) A note on intra-elemental isotope effects and the interpretation of non-mass-
1465   dependent isotope variations. *Chem. Geol.* **199**, 179–182.

1466 Ellis A.J. and Giggenbach W. (1971) Hydrogen sulphide ionization and sulphur hydrolysis in high
1467   temperature solution. *Geochim. Cosmochim. Acta* **35**, 247-260.

1468 Eriksen T. E. (1972a) Sulfur Isotope Effects. I. The Isotopic Exchange Coefficient for the Sulfur
1469   Isotopes 34S-32S in the System SO2g-HSO3-aq at 25, 35, and 45 degrees C. *Acta Chem. Scand.*
1470   **26**, 573–580.

1471 Eriksen T. E. (1972b) Sulfur Isotope Effects. II. The Isotopic Exchange Coefficient for the Sulfur
1472   Isotopes 34S-32S in the System SO2g-Aqueous Solutions of SO2. *Acta Chem. Scand.* **26**, 581–
1473   584.

1474 Eriksen T. E. (1972c) Sulfur Isotope Effects. III. Enrichment of 34S by Chemical Exchange Between
1475   SO2g and Aqueous Solutions of SO2. *Acta Chem. Scand.* **26**, 975–979.

1476 Eriksen T.E. and Lind J. (1972) Spectrophotometric determination of sulfur-dioxide and thiosulfate in
1477   aqueous-solutions of hydrogen sulfite. *Acta Chem. Scand.* **26**, 3325-3332.

1478 Ermatchkov V., Kamps Á. P. S. and Maurer G. (2005) The chemical reaction equilibrium constant and
1479   standard molar enthalpy change for the reaction {2HSO3(aq) ⇌ S2O 2-5 (aq) + H2O(1)}: A
1480   spectroscopic and calorimetric investigation. *J. Chem. Thermodyn.* **37**, 187–199.

1481 Falk M. and Guguere P.A. (1958) On the nature of sulphurous acid. *Can. J. Chem.* **36**, 1121-1125.

1482 Farquhar J., Johnston D. T., Wing B. A., Habicht K. S., Canfield D. E., Airieau S. and Thiemens M. H.
1483   (2003) Multiple sulphur isotopic interpretations of biosynthetic pathways: implications for
1484   biological signatures in the sulphur isotope record. *Geobiology* **1**, 27–36.

1485 Foresman J.B. and Frisch Æ. (1996) *Exploring Chemistry with Electronic Structure Methods, 2ⁿᵈ Ed.*
1486   Gaussian, Inc., Wallingford, CT.

1487 Frisch M. J., Trucks G. W., Schlegel H. B., Scuseria G. E., Robb M. A., Cheeseman J. R., Scalmani G.,
1488   Barone V., Mennucci B., Petersson G. A., Nakatsuji H., Caricato M., Li X., Hratchian H. P., Izmaylov
1489   A. F., Bloino J., Zheng G., Sonnenberg J. L., Hada M., Ehara M., Toyota K., Fukuda R., Hasegawa J.,
1490   Ishida M., Nakajima T., Honda Y., Kitao O., Nakai H., Vreven T., Montgomery J. A. Jr., Peralta J. E.,
1491   Ogliaro F., Bearpark M., Heyd J.J., Brothers E., Kudin K. N., Staroverov V. N., Keith T.,Kobayashi
1492   R., Normand J., Raghavachari K., Rendell A., Burant J. C., Iyengar S. S., Tomasi J., Cossi M., Rega N.,
1493   Millam J. M., Klene M., Knox J. E., Cross J. B., Bakken V., Adamo C., Jaramillo J., Gomperts R.,
1494   Stratmann R. E., Yazyev O., Austin A. J., Cammi R., Pomelli C., Ochterski J. W., Martin R. L.,
1495   Morokuma K., Zakrzewski V. G., Voth G. A., Salvador P., Dannenberg J.J., Dapprich S., Daniels A.

1496   D., Farkas Ö., Foresman J.B., Ortiz J. V., Cioslowski J., Fox D. J. (2010) Gaussian 09, Revision B.01.
1497   Gaussian, Inc., Wallingford CT.

1498   Fry B., Gest H. and Hayes J. M. (1986) Sulfur isotope effects associated with protonation of HS- and
1499   volatilization of H2S. *Chem. Geol. Isot. Geosci. Sect.* **58**, 253–258.

1500   Gerding H. and Nijveld W.J. (1936) Raman Spectrum of Gaseous and Liquid Sulphur Dioxide and its
1501   Solutions in Water. *Nature* **137**, 1070-1070.

1502   Geßler R. and Gehlen K.V. (1986) Investigation of sulfur isotope fractionation between H2S gas and
1503   aqueous solutions. *Fresenius' Zeitschrift für Anal. Chemie* **324**, 130–136.

1504   Goldberg R.N. and Parker V.B. (1985) Thermodynamics of solution of SO2(g) in water and of aqueous
1505   sulfur-dioxide solutions. *J. Res. Nat. B. Stand.* **90**, 341-358.

1506   Golding R.M. (1960) 741. Ultraviolet Absorption Studies of the Bisulphite-Pyrosulphite Equilibrium. *J.*
1507   *Chem. Soc.* 3711–3716.

1508   Hermann B., Kern M., La Pietra L., Simon J. and Einsle O. (2015) The octahaem MccA is a haem c-
1509   copper sulfite reductase. *Nature* **520**, 706-709.

1510   Hershey J. P., Plese T. and Millero F. J. (1988) The pK$_1$* for the dissociation of H$_2$S in various ionic
1511   media. *Geochim. Cosmochim. Acta* **52**, 2047–2051.

1512   Hoffmann M. R. and Lim B. C. (1979) Kinetics and mechanism of the oxidation of sulfide by oxygen:
1513   catalysis by homogeneous metal-phthalocyanine complexes. *Environ. Sci. Technol.* **13**, 1406–
1514   1414.

1515   Horner D. A. and Connick R. E. (1986) Equilibrium quotient for the isomerization of bisulfite ion from
1516   HSO3- to SO3H-. *Inorg. Chem.* **25**, 2414–2417.

1517   Horner D. A. and Connick R. E. (2003) Kinetics of oxygen exchange between the two isomers of
1518   bisulfite ion, disulfite ion (S2O52-), and water as studied by oxygen-17 nuclear magnetic
1519   resonance spectroscopy. *Inorg. Chem.* **42**, 1884–1894.

1520   Hulston J. R. and Thode H. G. (1965) Variations in the S33, S34, and S36 Contets of Meteorites and
1521   Their Relation to Chemical and Nuclear Effects. *J. Geophys. Res.* **70**, 3475–3484.

1522   Jørgensen B. B. (1977) The sulfur cycle of a coastal marine sediment (Limfjorden, Denmark).
1523   *Limnology and Oceanography* **22**, 814–832.

1524   Jørgensen B. B. (1990) A thiosulfate shunt in the sulfur cycle of marine sediments. *Science* **249**, 152–
1525   154.

1526   Jørgensen B. B., Bang M. and Blackburn T. H. (1990) Anaerobic Mineralization in Marine-Sediments
1527   From the Baltic-Sea-North-Sea Transition. *Mar. Ecol. Ser.* **59**, 39–54.

1528   Jørgensen B. B. (1982) Mineralization of organic matter in the sea bed – the role of sulphate
1529   reduction. *Nature* **296**, 643–645.

1530 Jørgensen B. B. and Nelson D.C. (2004) Sulfide oxidation in marine sediments: Geochemistry meets
1531   microbiology. In *Sulfur Biogeochemistry – Past and Present* (eds. J.P. Amend, K.J. Edwards, T.W.
1532   Lyons). GSA Special Papers 379, pp. 63-81.

1533 Leavitt W. D., Halevy I., Bradley A. S. and Johnston D. T. (2013) Influence of sulfate reduction rates on
1534   the Phanerozoic sulfur isotope record. *Proc. Natl. Acad. Sci. U. S. A.* **110**, 11244–9.

1535 Lee C., Yang W. and Parr R. G. (1988) Development of the Colle– Salvetti correlation-energy formula
1536   into a functional of the electron-density. *Phys. Rev. B* **37**, 785–789.

1537 Li X. and Liu Y. (2011) Equilibrium Se isotope fractionation parameters: A first-principles study.
1538   *Earth Planet. Sci. Lett.* **304**, 113–120.

1539 Li X., Zhao H., Tang M. and Liu Y. (2009) Theoretical prediction for several important equilibrium Ge
1540   isotope fractionation factors and geological implications. *Earth Planet. Sci. Lett.* **287**, 1–11.

1541 Littlejohn D., Walton S. A. and Chang S.-G. (1992) A Raman Study of the Isomers and Dimer of
1542   Hydrogen Sulfite Ion. *Appl. Spec.* **46**, 848–851.

1543 Liu Q., Tossell J.A. and Liu Y. (2010) On the proper use of the Bigeleisen-Mayer equation and
1544   corrections to it in the calculation of isotopic fractionation equilibrium constants. *Geochim.*
1545   *Cosmochim. Acta* **74**, 6965–6983.

1546 Lyons D. and Nickless G. (1968) The lower oxy-acids of sulphur. In *Inorganic Sulfur Chemistry* (ed. G.
1547   Nickless), pp. 509-534. Elsevier, New York.

1548 Makarov S. V., Kudrik E. V., van Eldik R. and Naidenko E. V. (2002) Reactions of methyl viologen and
1549   nitrite with thiourea dioxide. New opportunities for an old reductant. *J. Chem. Soc. Dalt. Trans.*,
1550   4074–4076.

1551 Makarov S. V., Sal'nikov D. S. and Pogorelova A. S. (2010) Acid-base properties and stability of
1552   sulfoxylic acid in aqueous solutions. *Russ. J. Inorg. Chem.* **55**, 301–304.

1553 Martell A.E. and Smith R.M. (1982) *Critical Stability Constants, Volume 5: First Supplement*. Springer
1554   Science+Business Media, New York.

1555 Matsuhisa Y., Goldsmith J. R. and Clayton R. N. (1978) Mechanisms of hydrothermal crystallization of
1556   quartz at 250°C and 15 kbar. *Geochim. Cosmochim. Acta* **42**, 173–182.

1557 McQuarrie D.A. (2000) *Statistical Mechanics.* University Science Books, Sausalito, California.

1558 Migdisov A. A., Williams-Jones A. E., Lakshtanov L. Z. and Alekhin Y. V. (2002) Estimates of the second
1559   dissociation constant of H2S from the surface sulfidation of crystalline sulfur. *Geochim.*
1560   *Cosmochim. Acta* **66**, 1713–1725.

1561 Miller M. F. (2002) Isotopic fractionation and the quantification of 17O anomalies in the oxygen
1562   three-isotope system: An appraisal and geochemical significance. *Geochim. Cosmochim. Acta* **66**,
1563   1881–1889.

1564 Millero F. J., Hershey J. P., Johnson G. and Zhang J.-Z. (1989) The Solubility of SO2 and the Dissociation
1565   of H2S03 in NaC1 Solutions. *J. Atmos. Chem.* **8**, 377–389.

1566 Napolion B., Huang M. J. and Watts J. D. (2008) Coupled-cluster study of isomers of H2SO2. *J. Phys.*
1567   *Chem. A* **112**, 4158–4164.

1568 Ohmoto H. and Lasaga A. C. (1982) Kinetics of reactions between aqueous sulfates and sulfides in
1569   hydrothermal systems. *Geochim. Cosmochim. Acta* **46**, 1727–1745.

1570 Oliveira T. F., Vonrhein C., Matias P. M., Venceslau S. S., Pereira I. a C. and Archer M. (2008) The
1571   crystal structure of Desulfovibrio vulgaris dissimilatory sulfite reductase bound to DsrC
1572   provides novel insights into the mechanism of sulfate respiration. *J. Biol. Chem.* **283**, 34141–
1573   34149.

1574 Ono S., Wing B., Johnston D., Farquhar J. and Rumble D. (2006) Mass-dependent fractionation of
1575   quadruple stable sulfur isotope system as a new tracer of sulfur biogeochemical cycles.
1576   *Geochim. Cosmochim. Acta* **70**, 2238–2252.

1577 Otake T., Lasaga A. C. and Ohmoto H. (2008) Ab initio calculations for equilibrium fractionations in
1578   multiple sulfur isotope systems. *Chem. Geol.* **249**, 357–376.

1579 Parey K., Warkentin E., Kroneck P. M. H. and Ermler U. (2010) Reaction cycle of the dissimilatory
1580   sulfite reductase from archaeoglobus fulgidus. *Biochemistry* **49**, 8912–8921.

1581 Richet P., Bottinga Y. and Javoy M. (1977) A review of hydrogen, carbon, nitrogen, oxygen, sulphur,
1582   and chlorine stable isotope fractionation among gaseous molecules. *Ann. Rev. Earth Planet. Sci.*
1583   **5**, 65-110.

1584 Risberg E. D., Eriksson L., Mink J., Pettersson L. G. M., Skripkin M. Y. and Sandström M. (2007) Sulfur
1585   X-ray absorption and vibrational spectroscopic study of sulfur dioxide, sulfite, and sulfonate
1586   solutions and of the substituted sulfonate ions X3CSO3- (X = H, Cl, F). *Inorg. Chem.* **46**, 8332–48.

1587 Rustad J. R. and Bylaska E. J. (2007) Ab initio calculation of isotopic fractionation in B(OH)3(aq) and
1588   BOH4-(aq). *J. Am. Chem. Soc.* **129**, 2222–2223.

1589 Rustad J. R., Nelmes S. L., Jackson V. E. and Dixon D. A. (2008) Quantum-Chemical Calculations of
1590   Carbon-Isotope Fractionation in CO 2 (g), Aqueous Carbonate Species, and Carbonate Minerals.
1591   **2**, 542–555.

1592 Rustad J. R., Bylaska E. J., Jackson V. E. and Dixon D. A. (2010) Calculation of boron-isotope
1593   fractionation between B(OH)3(aq) and B(OH)4 -(aq). *Geochim. Cosmochim. Acta* **74**, 2843–
1594   2850.

1595 Sakai H. (1968) Isotopic properties of sulfur compounds in hydrothermal processes. *Geochem. J.* **2**,
1596   29–49.

1597 Santos A. A., Venceslau S. S., Grein F., Leavitt W. D., Dahl C., Johnston D. T. and Pereira I. A. C. (2015) A
1598   protein trisulfide couples dissimilatory sulfate reduction to energy conservation. *Science (80-.).*
1599   **350**, 1541–1545.

1600 Schauble E.A. (2004) Applying Stable Isotope Fractionation Theory to New Systems. *Rev. Mineral.*
1601   *Geochemistry* **55**, 65–111.

1602 Schoonen M. A. A. and Barnes H. L. (1988) An approximation of the second dissociation constant for
1603   hydrogen sulfide. *Geochim. Cosmochim. Acta* **52**, 649–654.

1604　Sim M. S., Bosak T. and Ono S. (2011a) Large Sulfur Isotope Fractionation Does Not Require
1605　　　　Disproportionation. *Science* **333**, 74–77.

1606　Sim M. S., Ono S., Donovan K., Templer S. P. and Bosak T. (2011b) Effect of electron donors on the
1607　　　　fractionation of sulfur isotopes by a marine Desulfovibrio sp. *Geochim. Cosmochim. Acta* **75**,
1608　　　　4244–4259.

1609　Simons J. (1991) An experimental chemist's guide to ab initio quantum chemistry. *J. Phys. Chem.* **95**,
1610　　　　1017–1029.

1611　Steiger T. and Steudel R. (1992) Sulfur-Compounds. 149. Structures, relative stabilities and
1612　　　　vibrational-spectra of several isomeric forms of sulphoxylic acid (H2SO2) and its anion (HSO2-
1613　　　　)- An ab initio study. *J. Molec. Struct. (THERMOCHEM.)* **257**, 313-323.

1614　Steudel R. and Prenzel A. (1989) Raman Spectroscopic Discovery of the Hydrogenthiosulphate Anion,
1615　　　　HSSO3-, in Solid NH4HS2O3 [1]. *Z. Naturforsch., B: Chem. Sci.* **44**, 1499-1502.

1616　Steudel R. and Steudel Y. (2009) Microsolvation of thiosulfuric acid and its tautomeric anions [HSSO
1617　　　　3]- and [SSO2(OH)]- studied by B3LYP-PCM and G3X(MP2) calculations. *J. Phys. Chem. A* **113**,
1618　　　　9920–9933.

1619　Svarovsky S. A., Simoyi R. H. and Makarov S. V. (2001) A possible mechanism for thiourea-based
1620　　　　toxicities: Kinetics and mechanism of decomposition of thiourea dioxides in alkaline solutions.
1621　　　　*J. Phys. Chem. B* **105**, 12634–12643.

1622　Swain C. G., Stivers E. C., Reuwer Jr. J. F. and Schaad L. J. (1958) Use of hydrogen isotope effects to
1623　　　　identify the attacking nucleophile in the enolization of ketones catalyzed by acetic acid. *J. Am.
1624　　　　Chem. Soc.* **80**, 5885–5893.

1625　Syverson D. D., Ono S., Shanks W. C. and Seyfried W. E. (2015) Multiple sulfur isotope fractionation
1626　　　　and mass transfer processes during pyrite precipitation and recrystallization: An experimental
1627　　　　study at 300 and 350°C. *Geochim. Cosmochim. Acta* **165**, 418–434.

1628　Szaran J. (1996) Experimental investigation of sulphur isotopic fractionation between dissolved and
1629　　　　gaseous H2S. *Chem. Geol.* **127**, 223–228.

1630　Tossell J. A. (1997) Theoretical studies on possible sulfur oxides with +2 oxidation states in aqueous
1631　　　　solution. *Chem. Geol.* **141**, 93–103.

1632　Urey H.C. (1947) The thermodynamic properties of isotopic substances. *J. Chem. Soc. (Lond.)*, 562-
1633　　　　581.

1634　Uyama F., Chiba H., Kusakabe M., and Sakai H. (1985) Sulfur isotope exchange reactions in the
1635　　　　aqueous system: thiosulfate-sulfide-sulfate at hydrothermal temperature. *Geochem. J.* **19**, 301-
1636　　　　315.

1637　Vairavamurthy A., Manowitz B., Luther G. W. and Jeon Y. (1993) Oxidation-State of Sulfur in
1638　　　　Thiosulfate and Implications for Anaerobic Energy-Metabolism. *Geochim. Cosmochim. Acta* **57**,
1639　　　　1619–1623.

1640　Vairavamurthy M.A. and Zhou W. (1995) Characterization of a transient +2 sulfur oxidation state
1641　　　　intermediate from the oxidation of aqueous sulfide. In *Geochemical Transformations of*

1642   *Sedimentary Sulfur* (eds. M.A. Vairavamurthy and M.A.A. Schoonen). American Chemical Society,
1643   Washington, D.C. pp. 280-292.

1644   Voegele A. F., Tautermann C. S., Loerting T. and Liedl K. R. (2003) On the Formation of the Sulfonate
1645   Ion from Aqueous SO2 Solution. **3**, 1–9.

1646   Williamson M.A. and Rimstidt J. D. (1992) Correlation between structure and thermodynamic
1647   properties of aqueous sulfur species. *Geochim. Cosmochim. Acta* **56**, 3867–3880.

1648   Wing B. A. and Halevy I. (2014) Intracellular metabolite levels shape sulfur isotope fractionation
1649   during microbial sulfate respiration. *Proc. Natl. Acad. Sci.* **111**, 18116–18125.

1650   Wolfsberg M., Van Hook W.A., Paneth P., Rebelo L.P.N. (2010) *Isotope Effects in the Chemical,*
1651   *Geological, and Bio Sciences.* Springer, New York.

1652   Yiin B.S., Walker D.M., and Margerum D.W. (1987) Non-Metal Redox Kinetics General-Acid-Assisted
1653   Reactions of Chloramine with Sulfite and Hydrogen Sulfite. *Inorg. Chem.* **26**, 3435-3441.

1654   Young E. D., Galy A. and Nagahara H. (2002) Kinetic and equilibrium mass-dependent isotope
1655   fractionation laws in nature and their geochemical and cosmochemical significance. *Geochim.*
1656   *Cosmochim. Acta* **66**, 1095–1104.

1657   Zachariasen W.H. (1932) The crystal lattice of potassium pyrosulphite, K2S2O5, and the structure of
1658   the pyrosulphite group. *Phys. Rev.* **40**, 923.

1659   Zeebe R. E. (2009) Hydration in solution is critical for stable oxygen isotope fractionation between
1660   carbonate ion and water. *Geochim. Cosmochim. Acta* **73**, 5283–5291.

1661   Zhang Z. and Ewing G. E. (2002) Infrared spectroscopy of SO2 aqueous solutions. *Spectrochim. Acta -*
1662   *Part A Mol. Biomol. Spectrosc.* **58**, 2105–2113.

1663   Zhang J-Z. and Millero F.J. (1993) The products from the oxidation of H2S in seawater. *Geochim.*
1664   *Cosmochim. Acta* **57**, 1705-1718.

1665   Zopfi J., Ferdelman T.G. and Fossing H. (2004) Distribution and fate of sulfur intermediates—sulfite,
1666   tetrathionate, thiosulfate, and elemental sulfur—in marine sediments. In *Sulfur Biogeochemistry*
1667   *– Past and Present* (eds. J.P. Amend, K.J. Edwards, T.W. Lyons). GSA Special Papers 379, pp. 97-
1668   116.

Table 1

Table 1: Coefficients from polynomial fits to β-values computed at the B3LYP/6-31+G(d,p) level of theory in 30-40 H_2O clusters over 273.15-2273.15 K (0-2000°C). Values are computed using the coefficients via: $^{34}\beta$ or $^{33/34}\kappa$ or $^{36/34}\kappa$ = $A/T^4 + B/T^3 + C/T^2 + D/T + E$, where T is in Kelvin. Extra significant figures are given to minimize rounding errors. Values for $^{33}\beta$ and $^{36}\beta$ are computed from the $^{33/34}\kappa$ and $^{36/34}\kappa$ exponents, respectively, using: $^{33}\beta$ = $(^{34}\beta)^{33/34\kappa}$ and $^{36}\beta$ = $(^{34}\beta)^{36/34\kappa}$ at a given temperature. For the bisulfite dimer ($S_2O_5^{2-}$), the S-S bond length is noted in Å and A and B refer to: $(O_2S_A$-$S_BO_3)^{2-}$. Note: The values of E are intercepts at the high temperature limit (T→∞) and should theoretically converge on: $^{34}\beta_{[E]}$ = 1, $^{33/34}\kappa_{[E]}$= 0.51588, and $^{36/34}\kappa_{[E]}$ = 1.8904 (Matsuhisa et al., 1978).

Compound	nH₂O	$^{34}\beta$ A×10⁵	B×10⁴	C×10²	D×10²	E	$^{33/34}\kappa$ A×10⁵	B×10³	C×10⁻¹	D×10⁻³	E	$^{36/34}\kappa$ A×10⁶	B×10⁴	C×10⁻²	D×10⁻²	E
SO_4^{2-}	30	590.371	-126.799	109.869	-137.516	1.000347	-308690	46.1900	-2194.08	48.4610	0.515866	20.0957	-30.5253	146926	-30.9584	1.89050
(HS)SO₃ [1]	30	905.705	-147.268	105.824	-92.3176	1.000195	-360529	47.5396	-2038.76	40.6206	0.515848	24.2746	-31.9304	136605	-20.3357	1.89051
(HS)O₃ [2]	30	914.750	-148.129	106.124	-93.3723	1.000198	-37.0901	48.3512	-2051.71	35.6621	0.515861	24.4825	-32.1287	137230	-20.8157	1.89051
S-SO_3^{2-} (inner)	30	411.460	-96.9863	90.9001	-108.003	1.000274	-24.5634	37.7929	-1869.03	39.3817	0.515874	16.0257	-24.9975	125212	-25.2475	1.89048
SO_3^{2-} [1]	30	147.138	-57.1113	64.8862	-66.7662	1.000174	-12.1588	22.3335	-1256.77	5.84049	0.515915	6.59541	-13.9300	84468.4	-15.4418	1.89047
SO_3^{2-} [2]	30	131.638	-55.2533	64.0120	-65.9924	1.000172	-10.6590	21.1779	-1242.26	13.2399	0.515915	5.78271	-13.2584	83392.1	-19.5475	1.89062
(HO)SO₂ [1]	34	227.691	-62.3345	63.6829	-69.8409	1.000178	-16.2693	26.2215	-1364.47	27.2021	0.515871	10.5895	-17.2801	90887.8	-16.5777	1.89044
(HO)SO₂ [2]	34	243.446	-64.2295	63.9099	-72.0204	1.000184	-16.7025	26.7737	-1377.83	30.2698	0.515850	11.1722	-18.0159	93369.1	-20.3001	1.89056
$SO_{2(aq)}$	30	692.521	-108.509	71.7931	-103.029	1.000245	-48.0459	57.0980	-2177.40	55.0250	0.515831	32.5900	-38.5370	145870	-29.0384	1.89048
$SO_{2(g)}$	0	754.026	-114.672	71.5395	-105.747	1.000248	-55.2114	63.5980	-2337.13	44.8960	0.515869	36.7913	-42.6517	157869	-30.8486	1.89052
(HS)O₂⁻	30	360.997	-67.0840	54.3488	-27.5149	1.000048	-10.6136	18.2893	-982.056	3.89045	0.515901	6.77767	-12.0675	66138.9	-4.23454	1.89038
(HS)O₂·H	30	380.899	-66.3215	52.4857	-12.5409	1.000006	-12.2554	18.5304	-918.537	-13.8604	0.515944	6.69872	-11.4303	61927.7	-4.45807	1.89057
SO_2^{2-}	30	11.8836	-20.4170	30.3733	-24.9619	1.000006	-2.56730	9.61814	-733.960	10.4911	0.515889	2.31680	-7.04182	512282	-5.66457	1.89041
S(OH)₂	30	32.5192	-21.8550	29.2787	-26.1670	1.000068	-3.24888	10.4655	-768.717	32.7233	0.515828	1.90679	-6.37994	472473	-8.35974	1.89051
(HO)SO⁻	30	19.4614	-20.0430	28.5160	-24.7943	1.000065	-3.49639	9.82567	-688.628	-6.14640	0.515912	2.82153	-7.35610	508382	-7.70786	1.89041
$H_2S_{(aq)}$	30	462.536	-48.3382	20.1638	77.2695	0.999749	-11.2082	8.59125	-133.040	-53.7633	0.515864	7.70591	-6.05029	103540	35.4036	1.89025
S-SO_3^{2-} (outer)	30	-24.5550	-2.01175	11.3562	-2.64754	1.000007	2.58474	1.26805	-386.465	41.8080	0.515830	-0.678068	-1.09468	218708	-6.10872	1.89050
HS⁻	30	213.257	-22.4384	12.2701	42.8805	0.999864	-5.47337	3.11818	-6.41346	-53.7300	0.515891	3.91822	-2.18380	-4.79300	37.4599	1.89025
$H_2S_{(g)}$	0	470.075	-48.9645	19.2083	82.5595	0.999735	-10.7593	8.05933	-103.577	-55.2088	0.515898	7.44511	-5.61973	7534.45	37.2276	1.89031
S²⁻	30	2.46274	-2.30464	7.54757	-0.688045	1.000001	3.46783	-1.51862	-140.010	32.1639	0.515819	-2.33264	1.06520	9415.48	-25.8717	1.89127
$S_2O_5^{2-}$ [1A] (2.468 Å)	30	364.444	-73.0226	61.6230	-79.4550	1.000199	-26.4546	35.9415	-1591.09	34.2723	0.515880	17.4385	-24.0306	107998	-26.5683	1.89057
$S_2O_5^{2-}$ [1B]		380.966	-91.5445	85.5763	-103.665	1.000264	-22.1841	34.9103	-1750.48	41.3451	0.515873	14.3817	-22.9546	116418	-24.3994	1.89050
$S_2O_5^{2-}$ [2A] (2.505 Å)	30	397.137	-76.6766	62.5608	-82.4519	1.000205	-28.2450	38.4494	-1704.01	56.0947	0.515839	19.1298	-25.6490	111886	-25.5825	1.89052
$S_2O_5^{2-}$ [2B]		336.782	-85.7470	82.5440	-98.3850	1.000252	-19.6417	32.2172	-1663.53	38.7957	0.515853	13.1699	-21.6553	112295	-23.4324	1.89050
$S_2O_5^{2-}$ [3A] (2.482 Å)	31	349.189	-71.2235	60.5973	-78.5580	1.000197	-25.7908	35.3032	-1571.94	34.7375	0.515861	17.4691	-23.8774	106250	-20.6730	1.89044
$S_2O_5^{2-}$ [3B]		369.152	-89.9354	84.7548	-102.548	1.000262	-22.2684	34.4752	-1734.75	35.7416	0.515877	14.0824	-22.6706	115791	-25.4411	1.89052
$S_2O_5^{2-}$ [4A] (2.542 Å)	40	433.004	-80.4687	63.5931	-85.0203	1.000210	-30.6365	40.2622	-1719.62	44.8114	0.515845	20.8286	-27.2845	116158	-25.8011	1.89054
$S_2O_5^{2-}$ [4B]		316.881	-82.9536	81.0520	-95.5356	1.000245	-19.0720	31.5150	-1638.88	37.0809	0.515868	12.3525	-20.7774	109538	-23.1387	1.89047
Intercept (E) Average						*1.0001*					*0.51587*					*1.8905*
Intercept (E) 1 s.d.						*0.0002*					*0.00003*					*0.0002*

Table 2

Table 2: Summary of $^{34}S/^{32}S$ based fractionation factors in the sulfite system from experiments and theoretical calculations at 25°C.

$1000\ln^{34}\alpha$	Experiment (‰)	Theoretical* (‰)
$SO_{2(aq)}$-$SO_{2(g)}$	0 ± 2 [a] 0.9 ± 0.4 [b] ~ 2.2 [c]	1.8
$HSO_{3\ T}^-$-$SO_{2(aq)}$	9 ± 1 [b]	9.4 ± 0.9 ($\mu = 0$ m) 6.9 ± 0.1 ($\mu = 1$ m)
$HSO_{3\ T}^-$-SO_3^{2-}	N/A	4.0 ± 0.9 ($\mu = 0$ m) 1.5 ± 0.1 ($\mu = 1$ m)

[a]Eriksen (1972b), [b]Eriksen (1972c); [c]Chmielewski et al. (2001); *Computed at the B3LYP/6-31+G(d,p) level in aqueous 30-34H_2O clusters. The calculated values involving bisulfite were computed using isomer proportions from quotients determined at ionic strength of 0 m (Risberg et al., 2007) and 1 m ionic strength (Horner and Connick, 1986). Uncertainties on the calculated values solely represent the propagated uncertainties on the isomerization quotients reported at 25°C in the references.

Figure 1
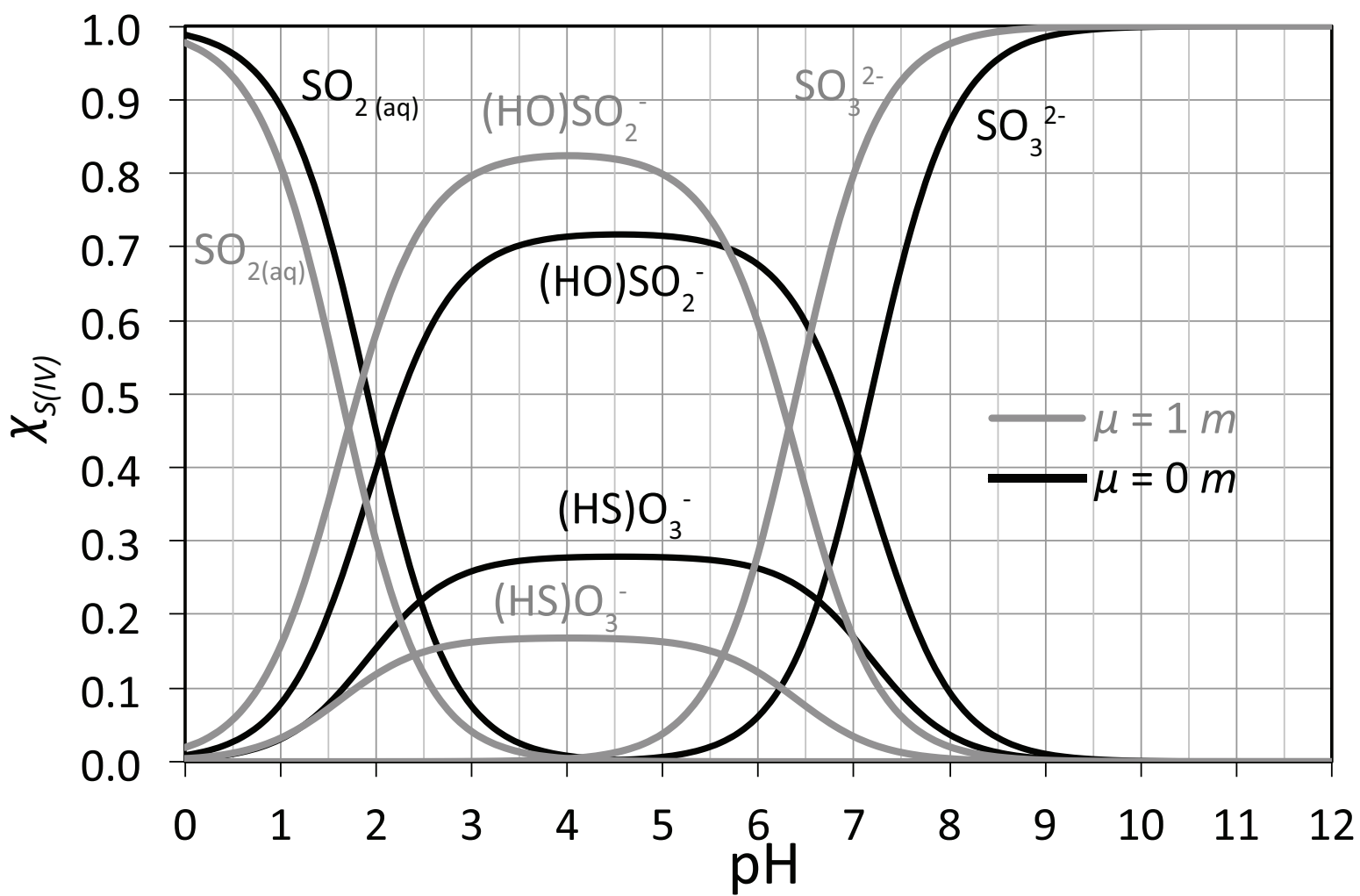
Figure 2
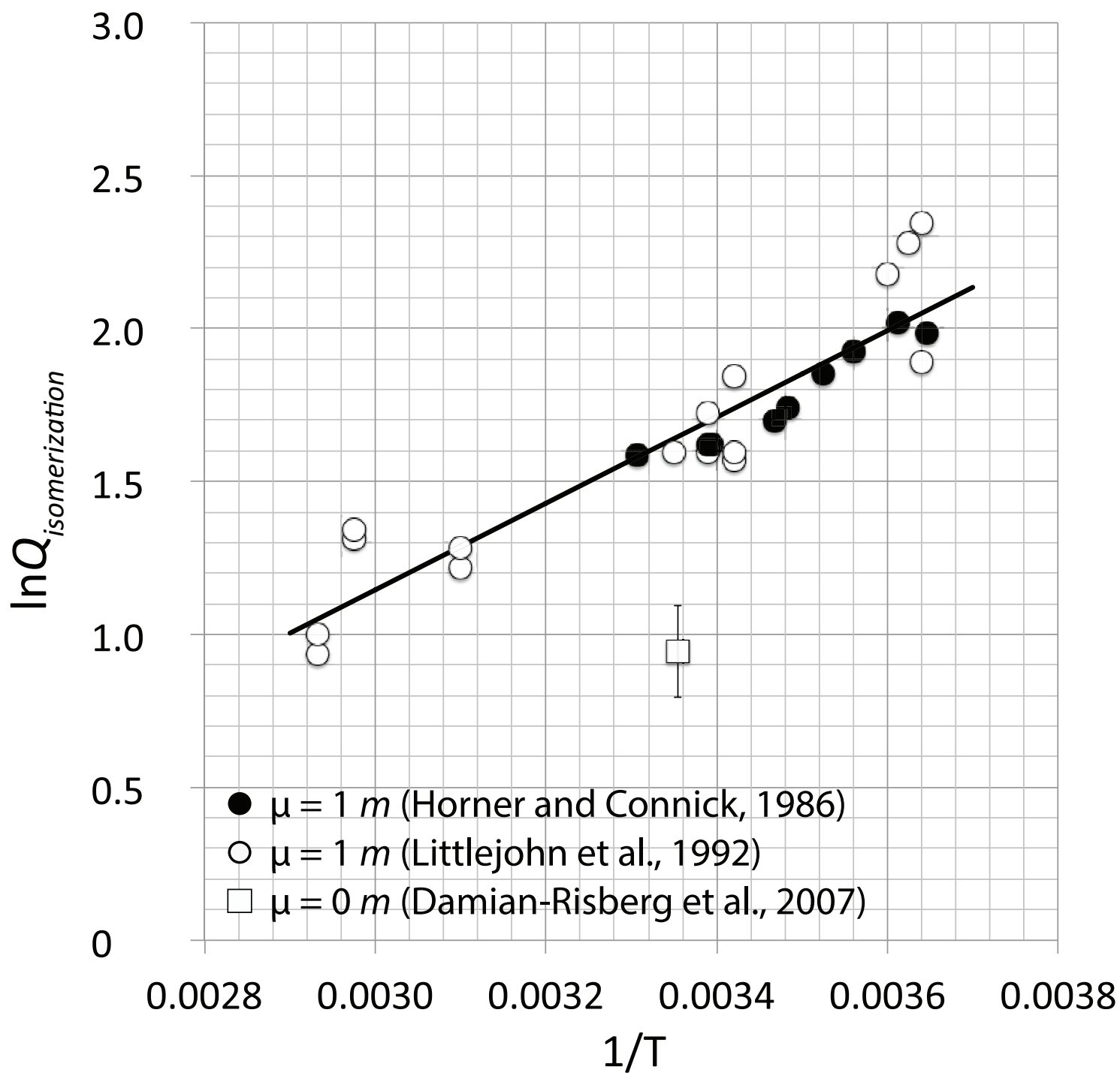
Figure 3
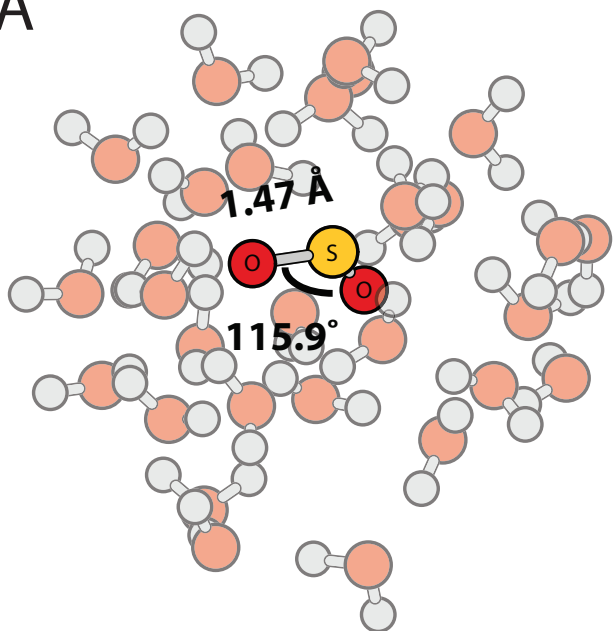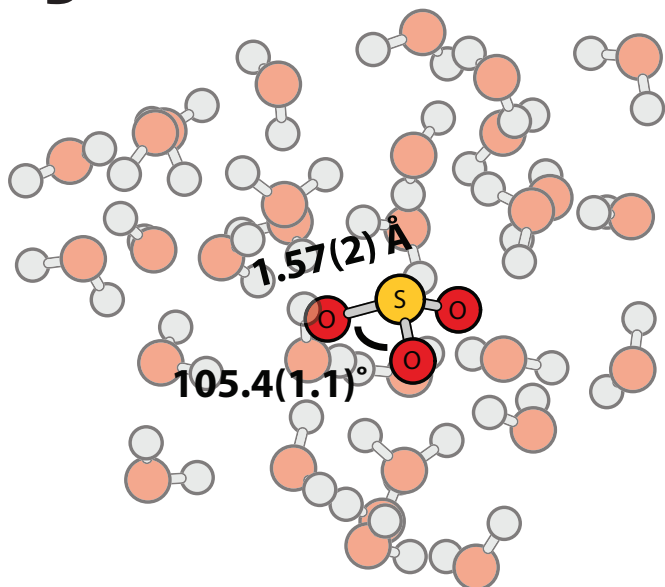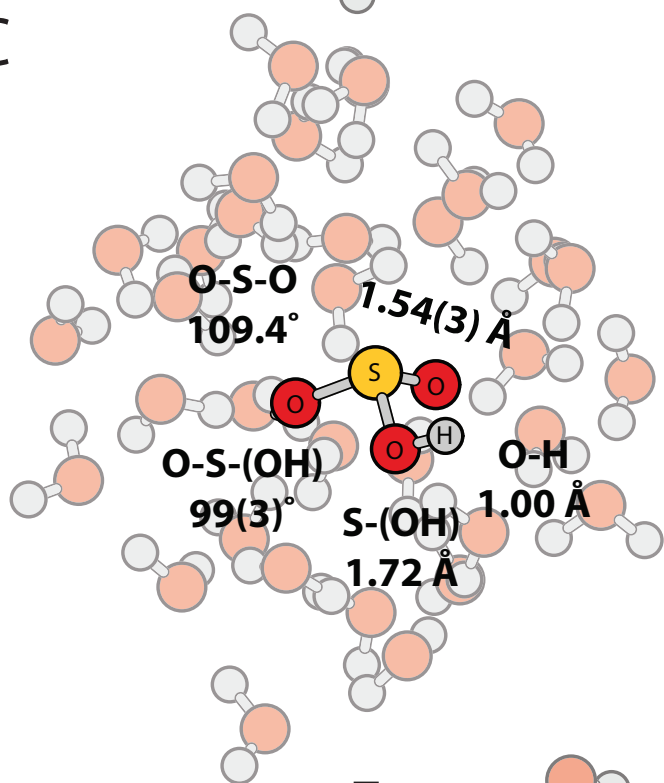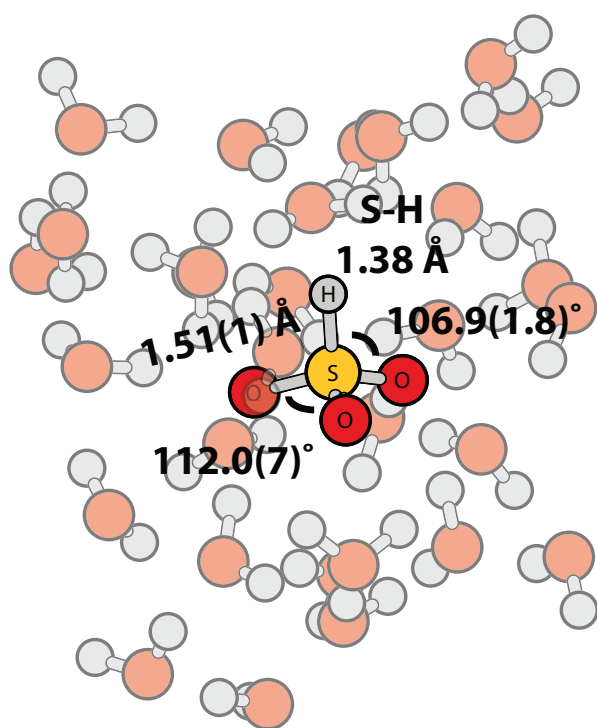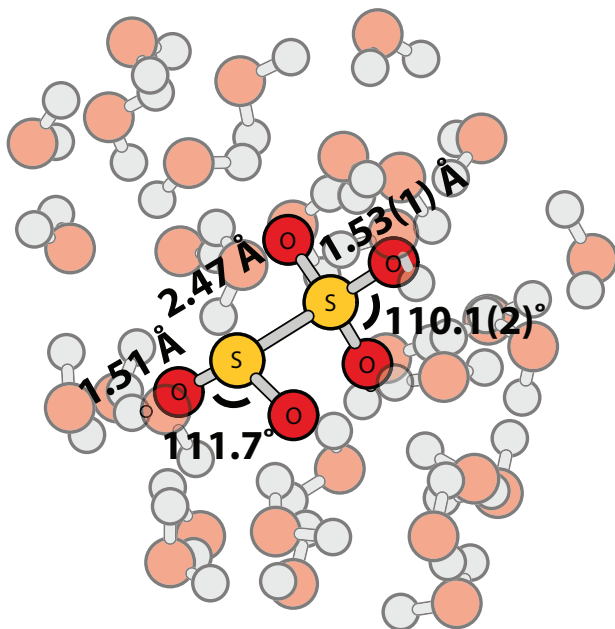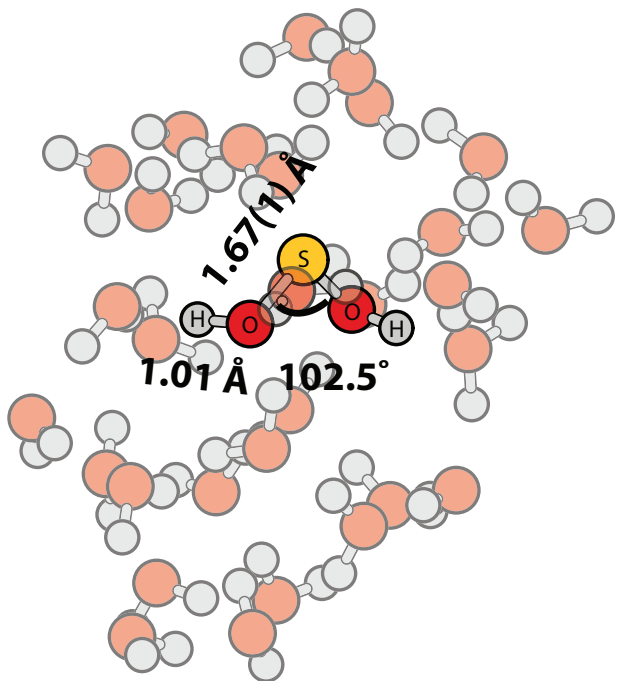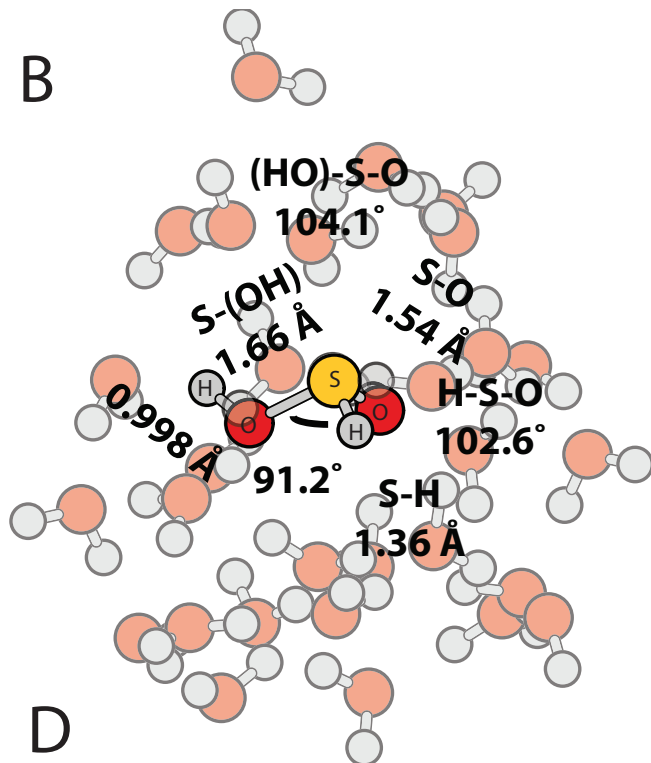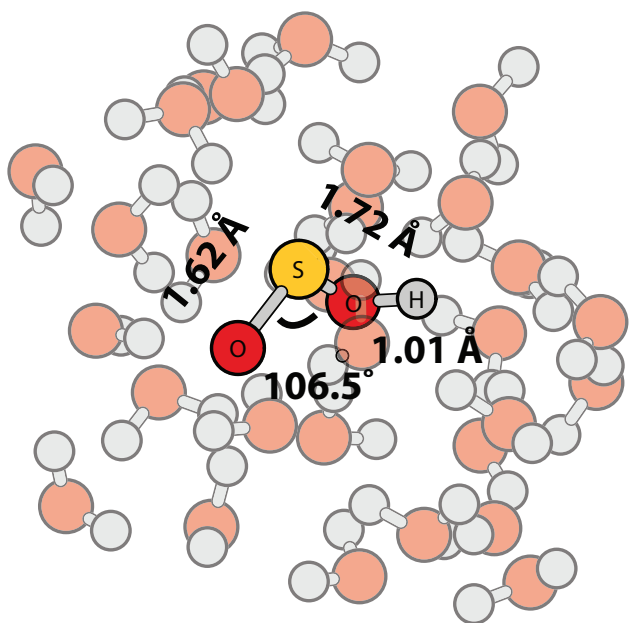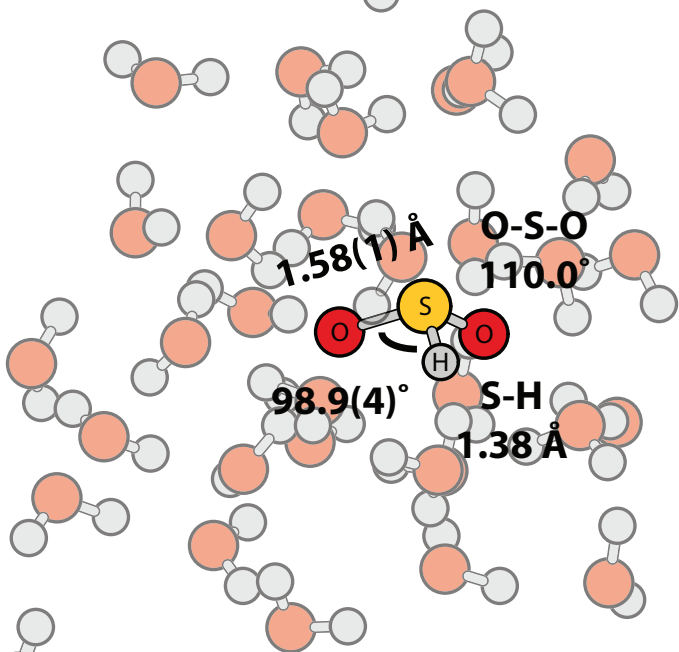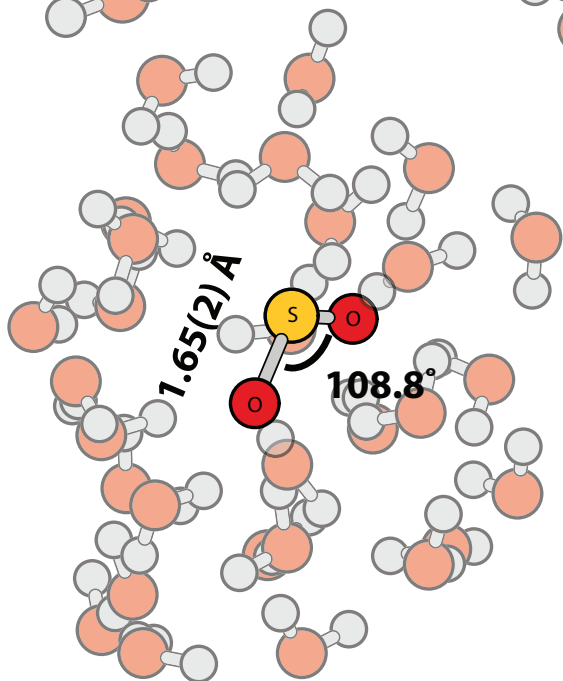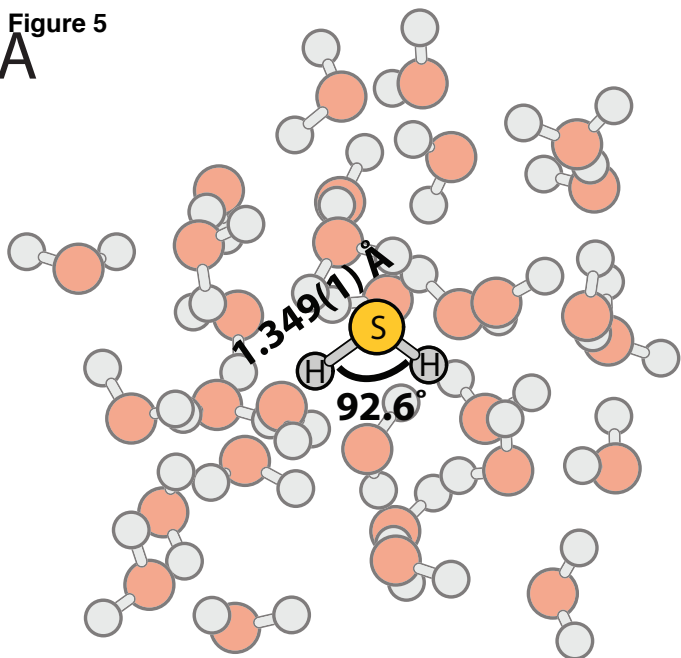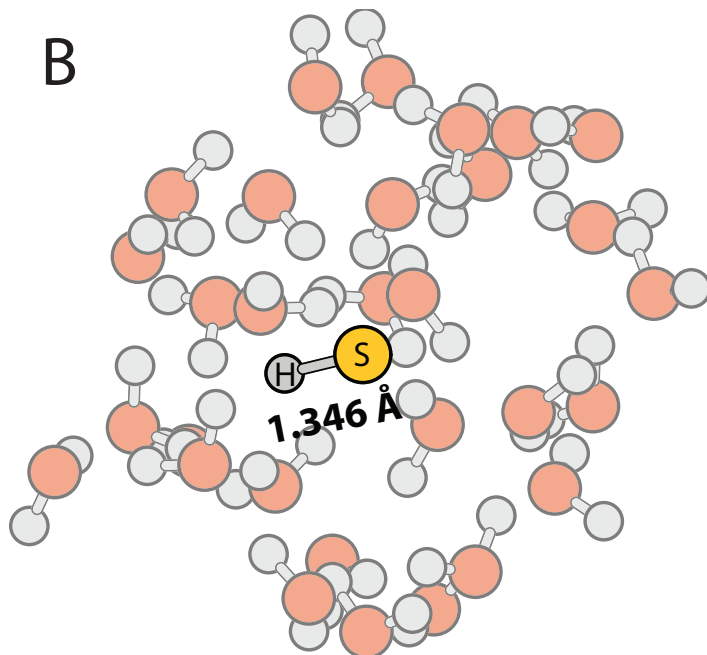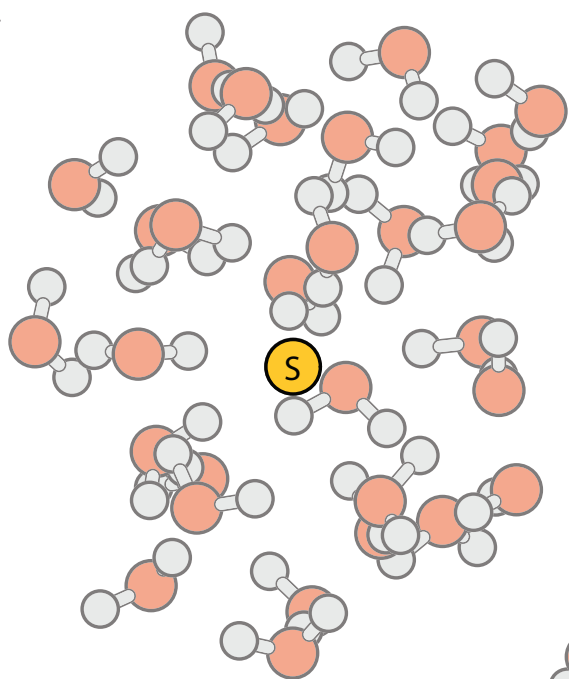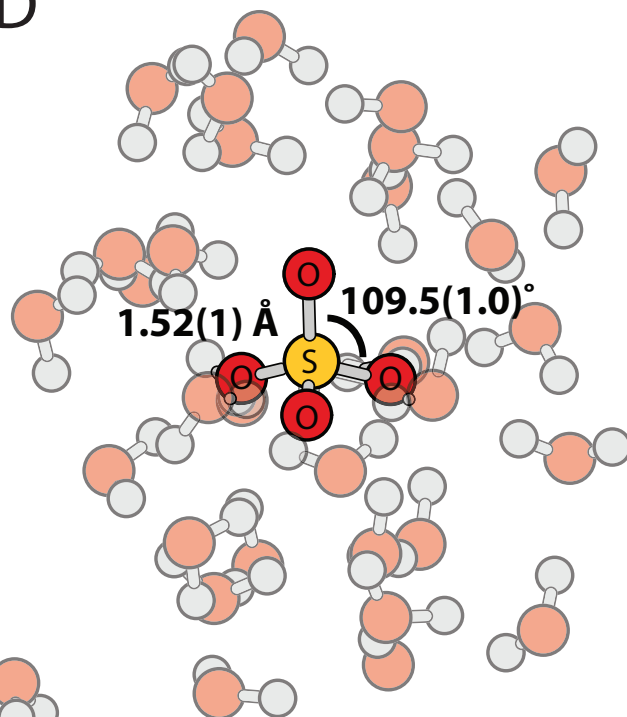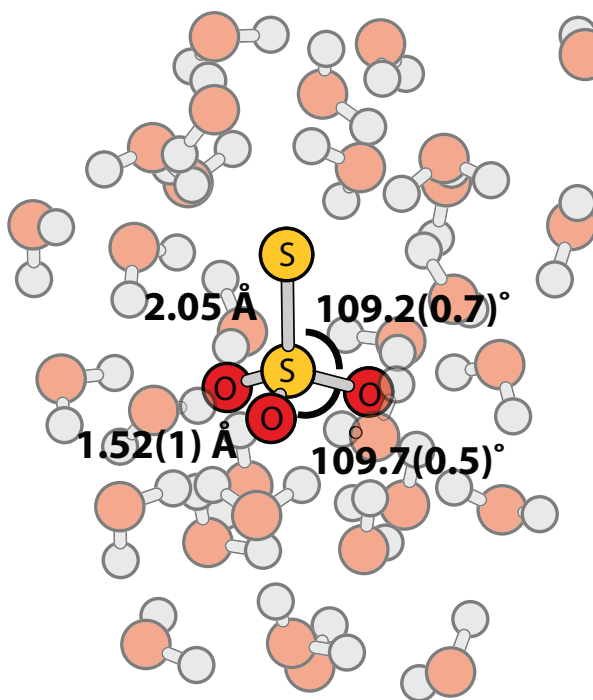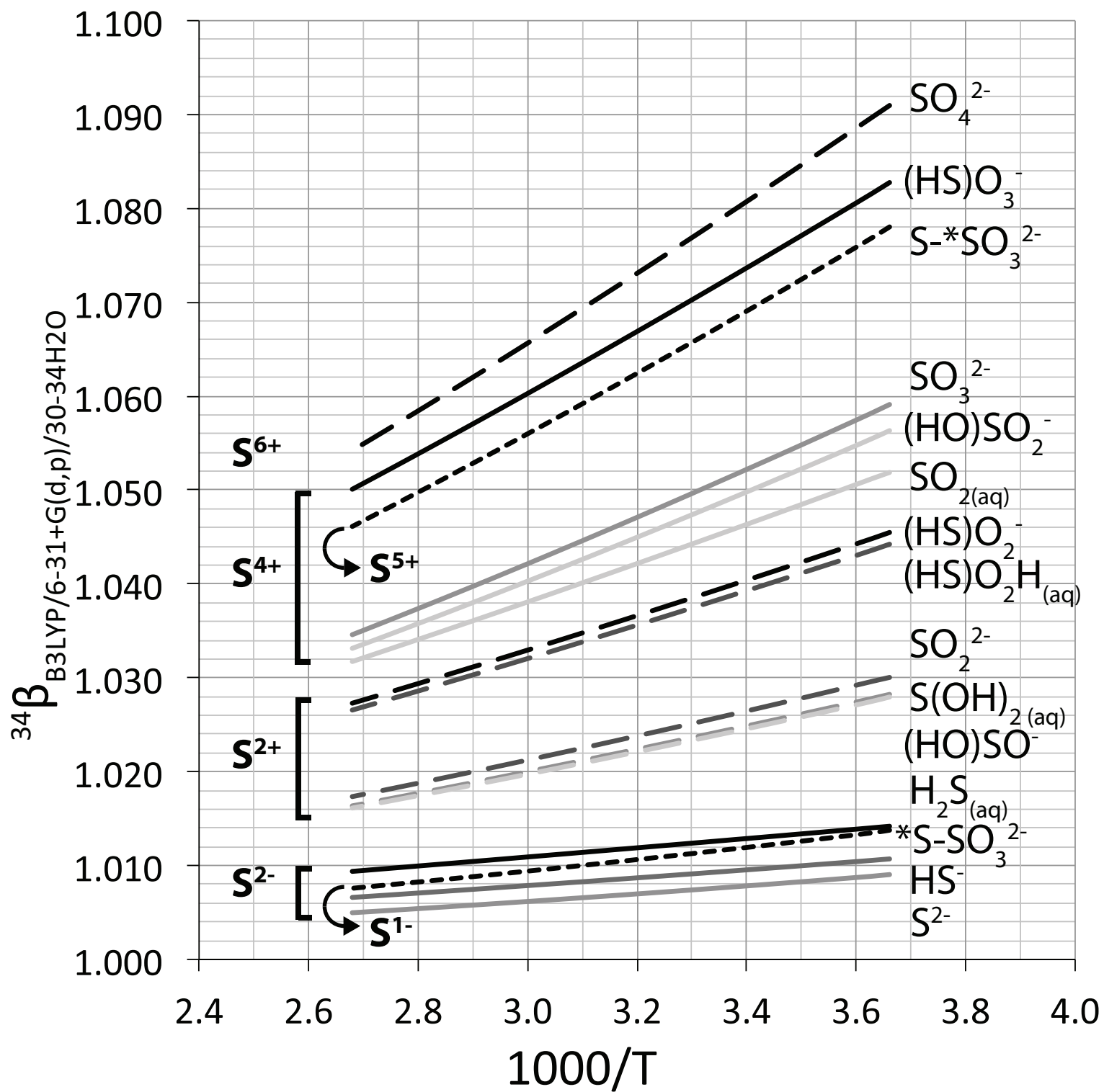
Figure 4

A

1.67(1) Å
1.01 Å   102.5°

B

(HO)-S-O
104.1°
S-(OH)
1.66 Å
S-O
1.54 Å
0.998 Å
H-S-O
102.6°
91.2°
S-H
1.36 Å

C

1.72 Å
1.62 Å
1.01 Å
106.5°

D

1.58(1) Å
O-S-O
110.0°
98.9(4)°
S-H
1.38 Å

E

1.65(2) Å
108.8°

Figure 5

Figure 6

Figure 8_revised

Sulfite System (S^{4+})

Legend:
- △ $(HS)O_3^-$
- ● SO_3^{2-}
- ◇ $(HO)SO_2^-$
- ◆ $SO_{2\,(aq)}$
- ▣ $(O_2S_A\text{-}S_BO_3)^{2-}$
- ■ $S_2O_5^{2-}$

$^{33/34}\theta = 0.51488$

$^{33/34}\theta = 0.51652$

$^{33/34}\theta = 0.51609$

B

A

x-axis: $1000\ln(^{34}\alpha)$ (‰)

y-axis: $1000\ln(^{33}\alpha)$ (‰)

Figure 9_revised

Sulfoxylate System (S^{2+})

$^{33/34}\theta = 0.51526$

$(HS)O_2^-$

$(HS)O_2H_{(aq)}$

$^{33/34}\theta = 0.51546$

$^{33/34}\theta = 0.51538$

SO_2^{2-}

$(HO)SO^-$ $S(OH)_{2\,(aq)}$

$^{33/34}\theta = 0.51410$

Axis labels:

$1000\ln(^{33}\alpha)$ (‰)

$1000\ln(^{34}\alpha)$ (‰)

Figure 10_revised

Sulfide System (S^{2-})

$^{33/34}\theta = 0.51565$

$H_2S_{(aq)}$

$^{33/34}\theta = 0.51573$

HS^-

S^{2-}

$1000\ln(^{33}\alpha)$ (‰)

$1000\ln(^{34}\alpha)$ (‰)
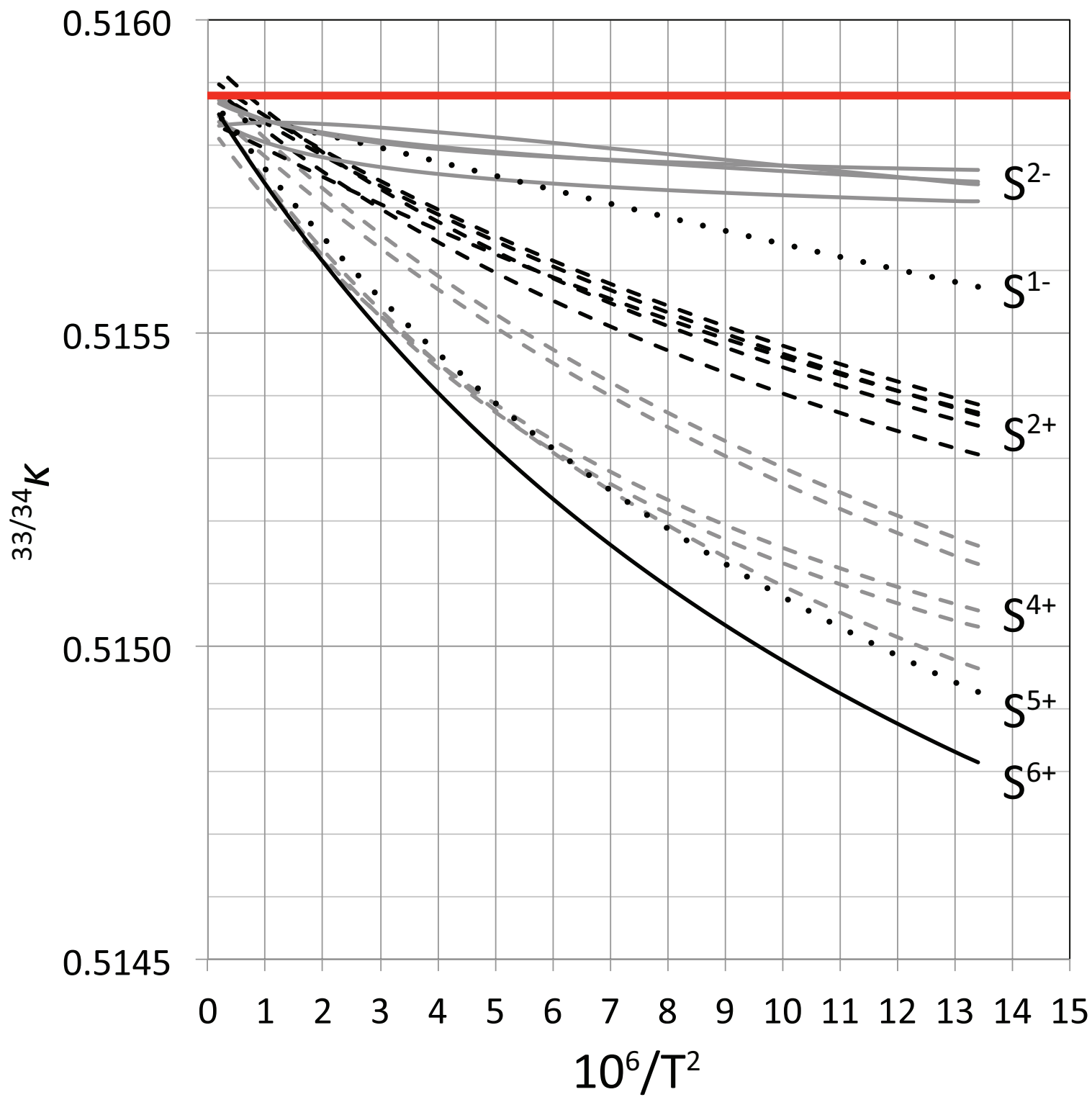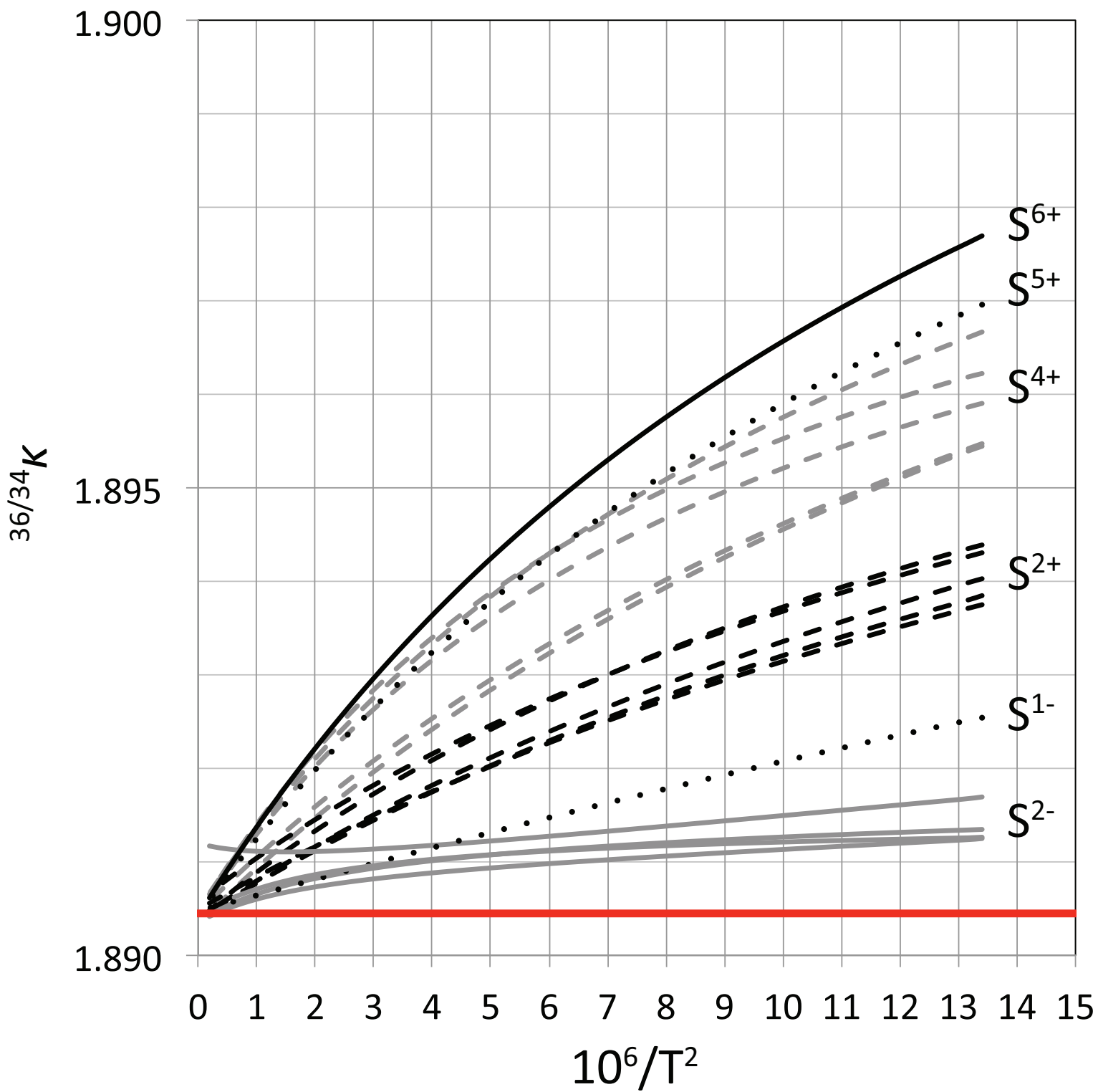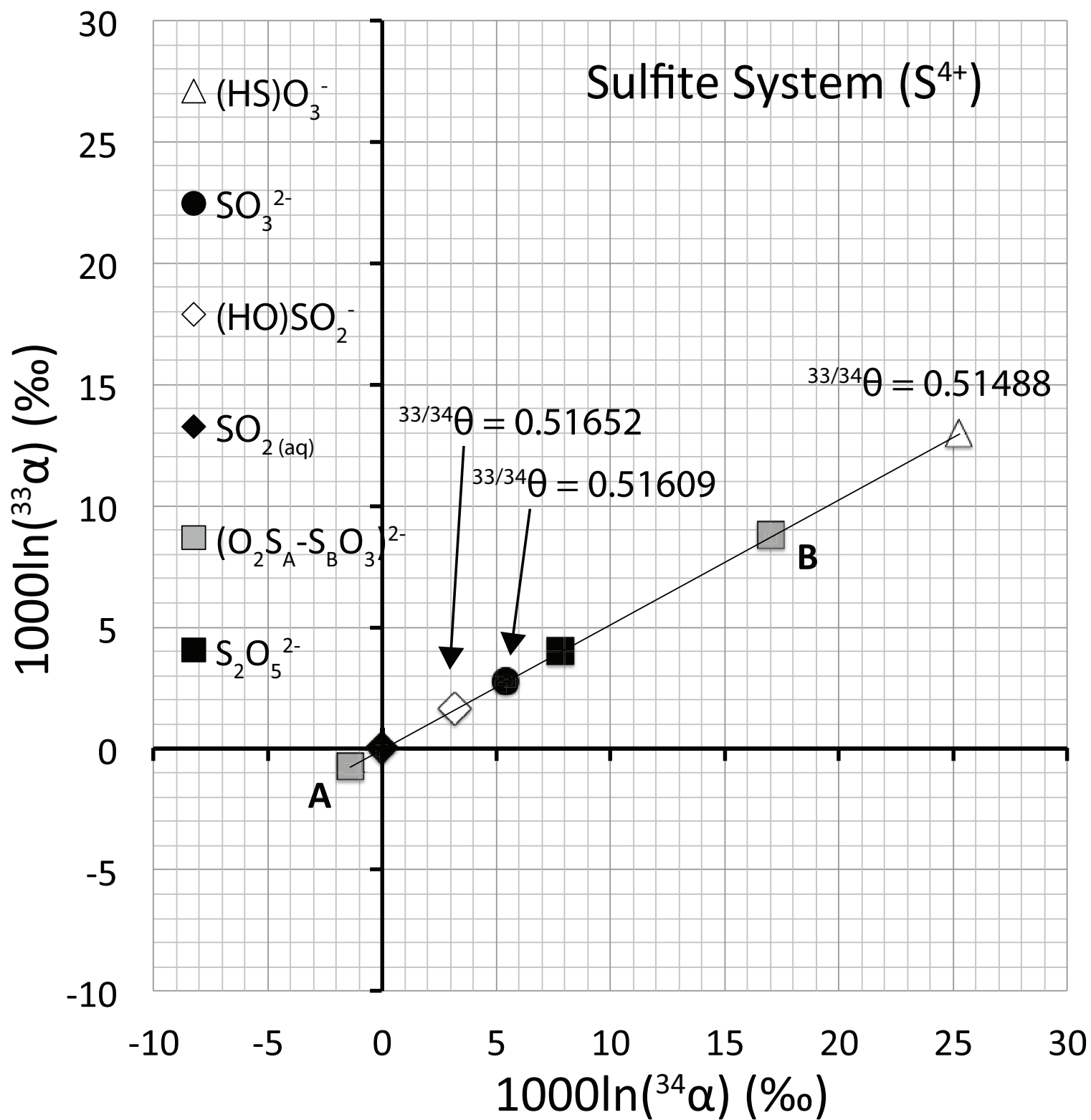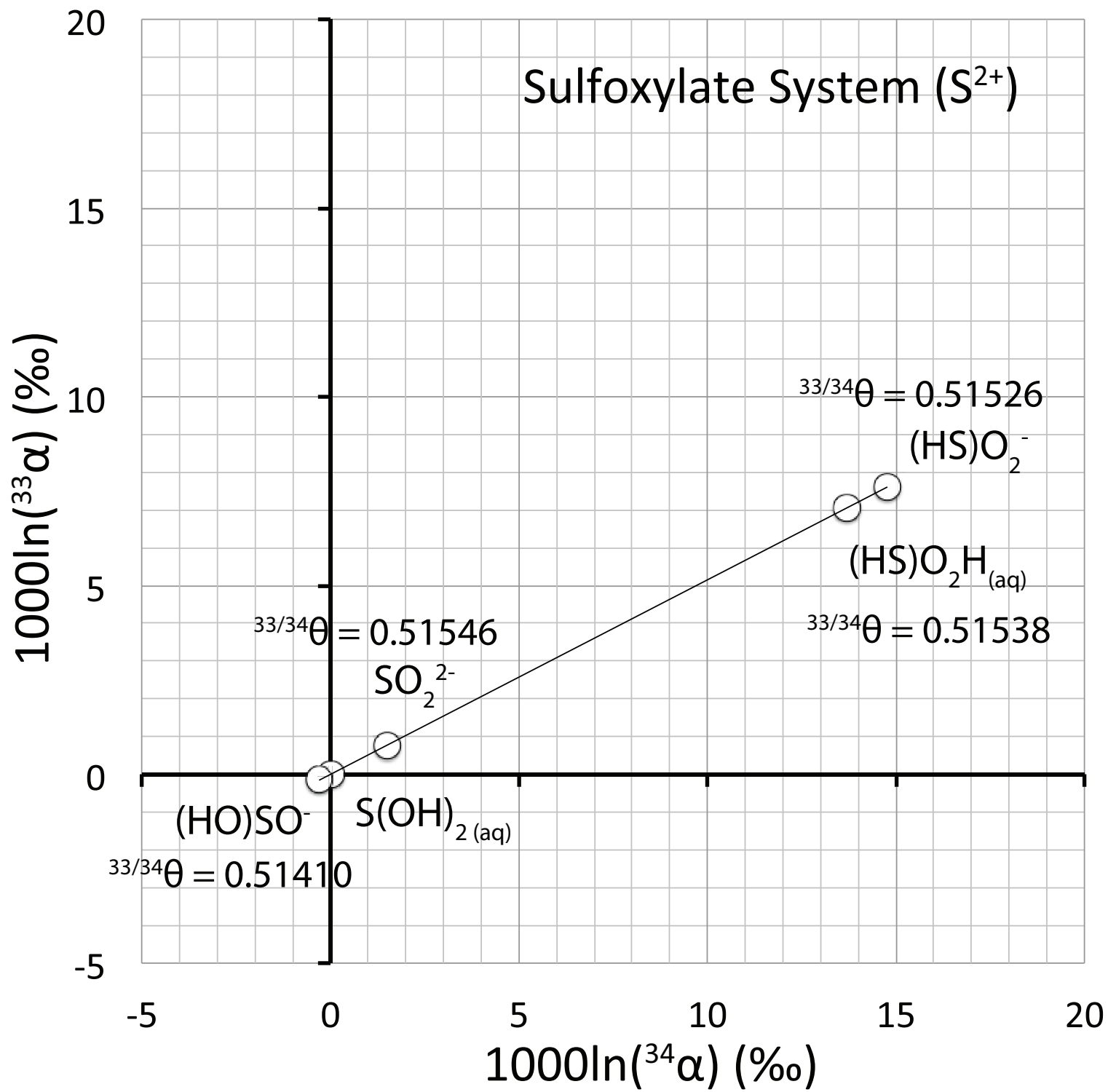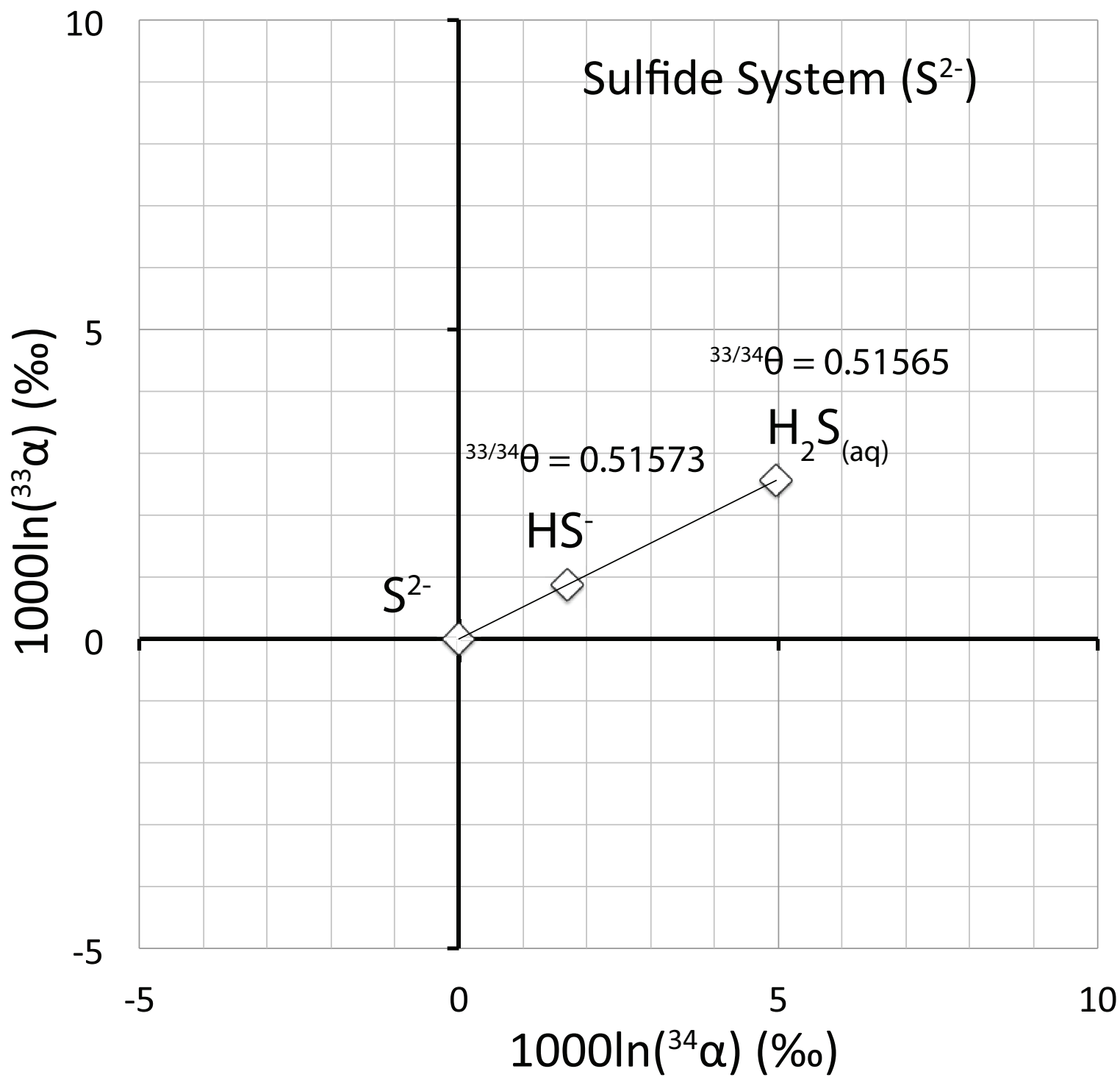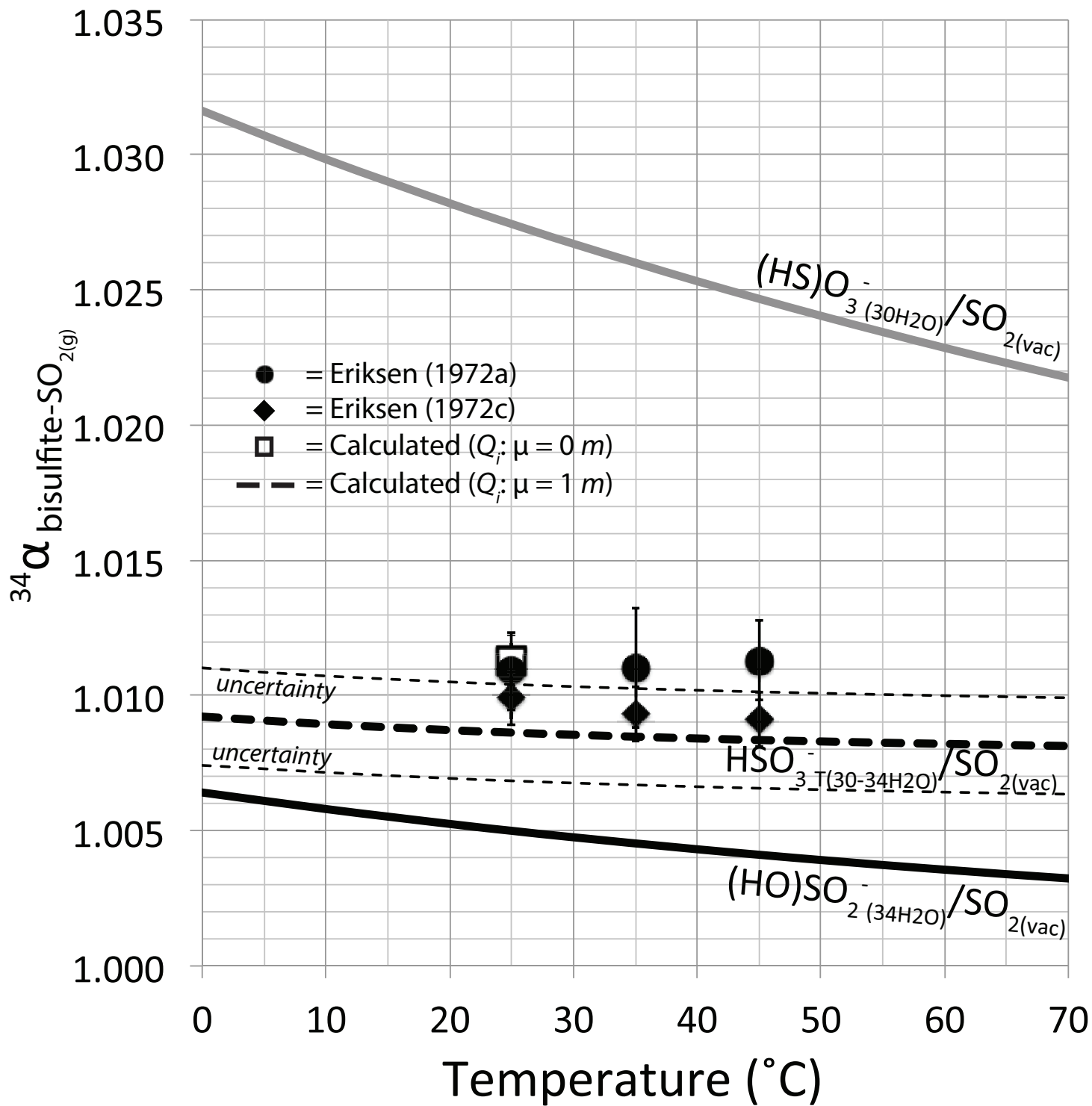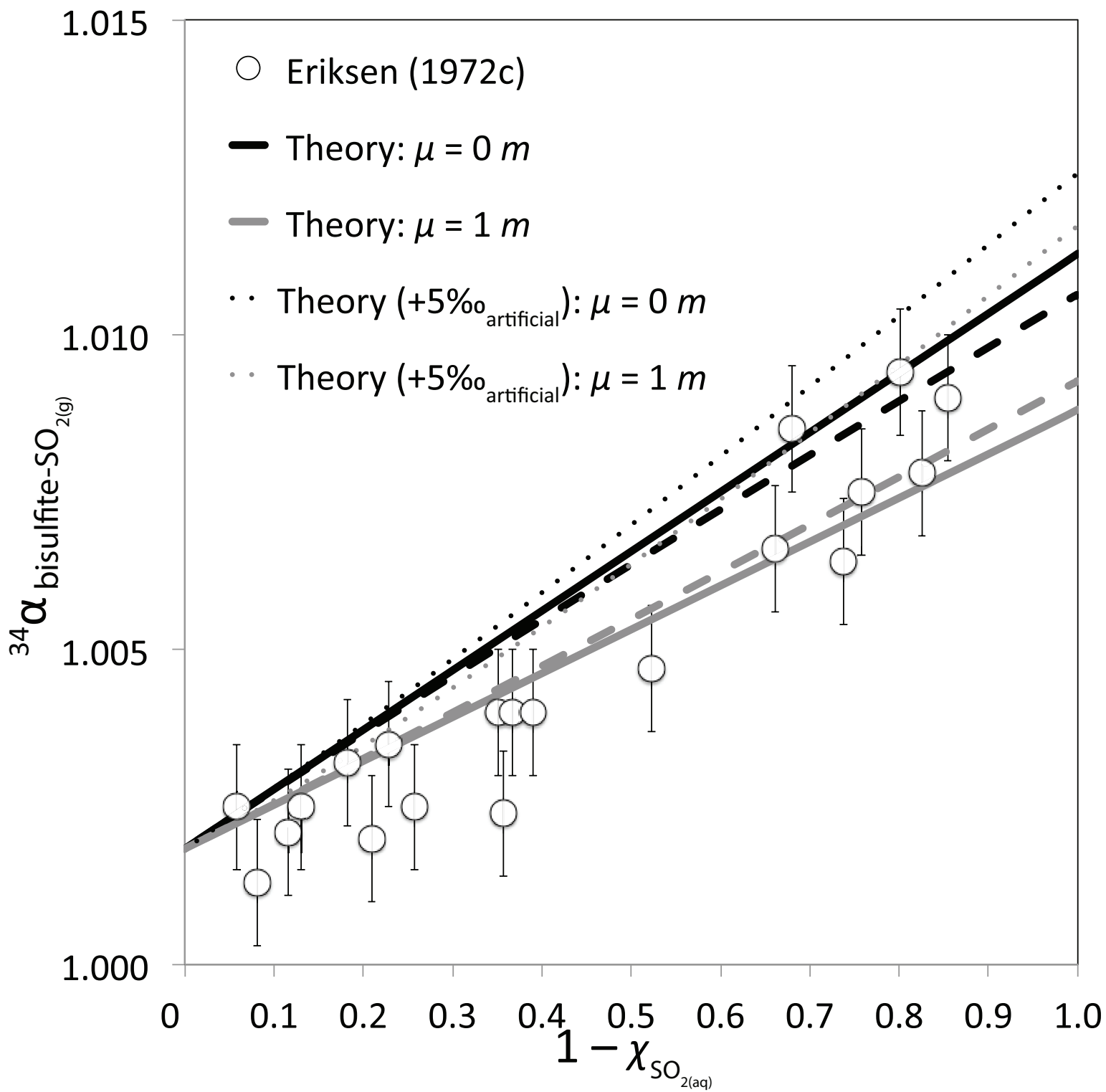
Figure 11
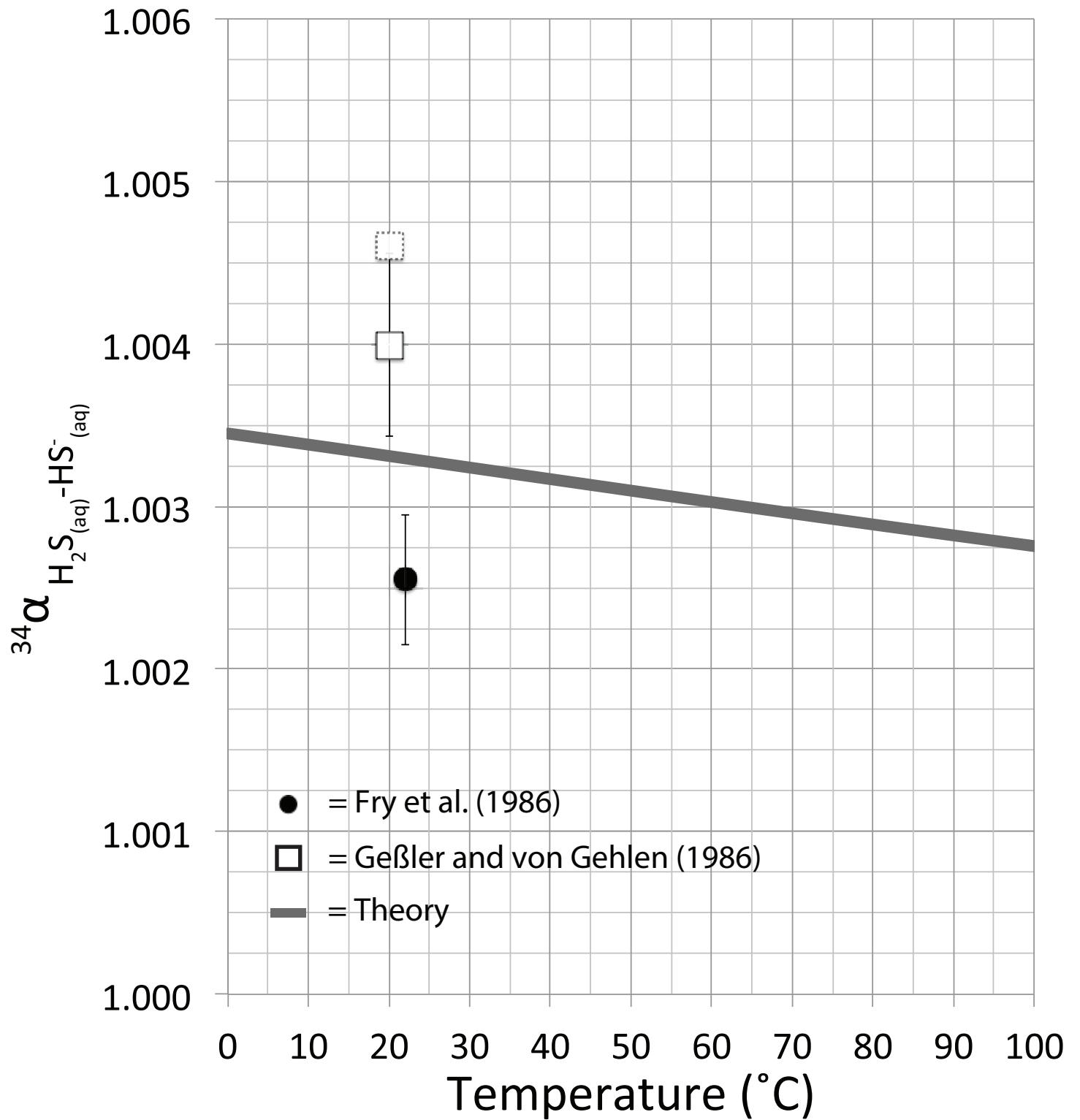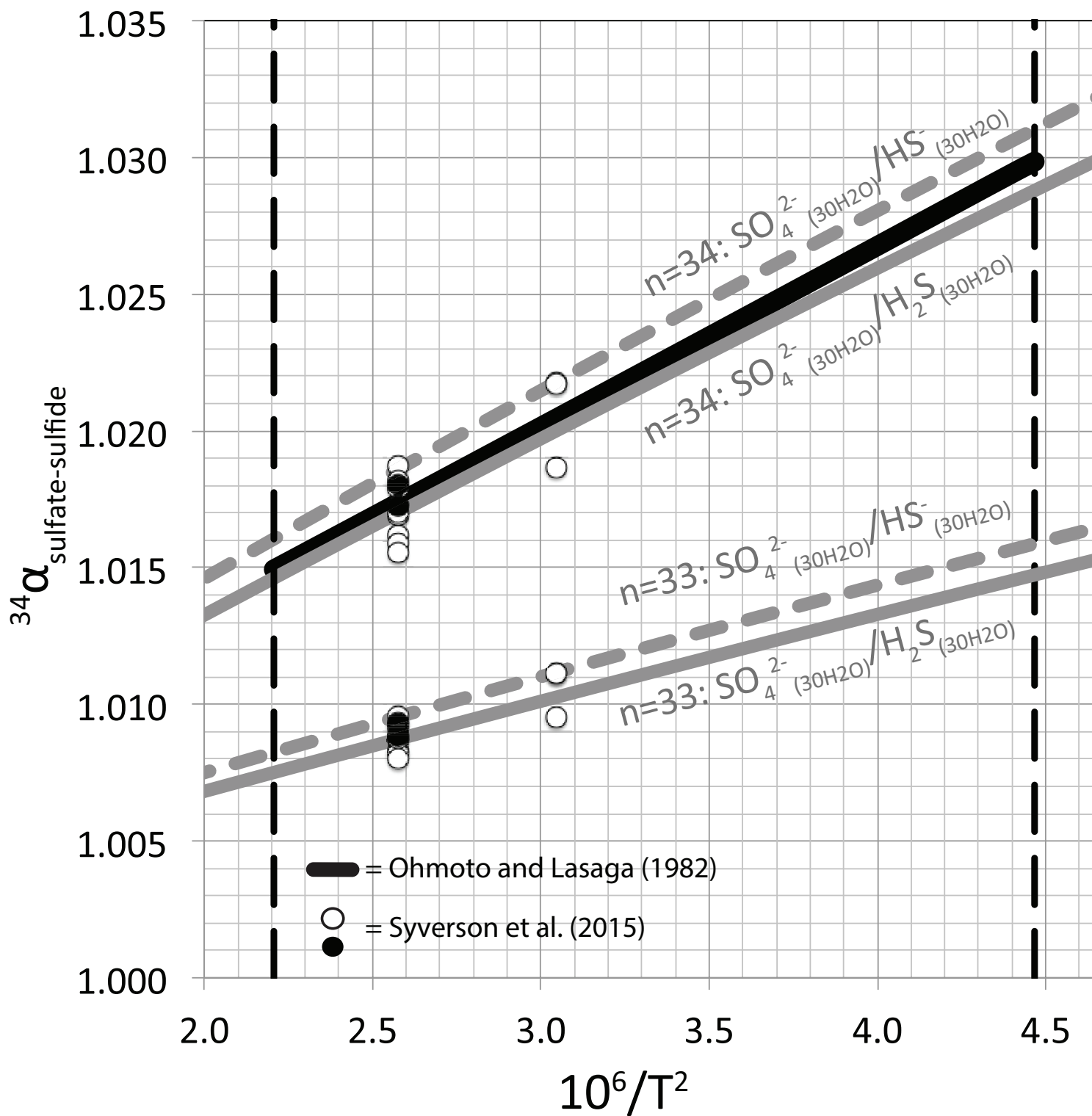
Figure 12

Figure 13
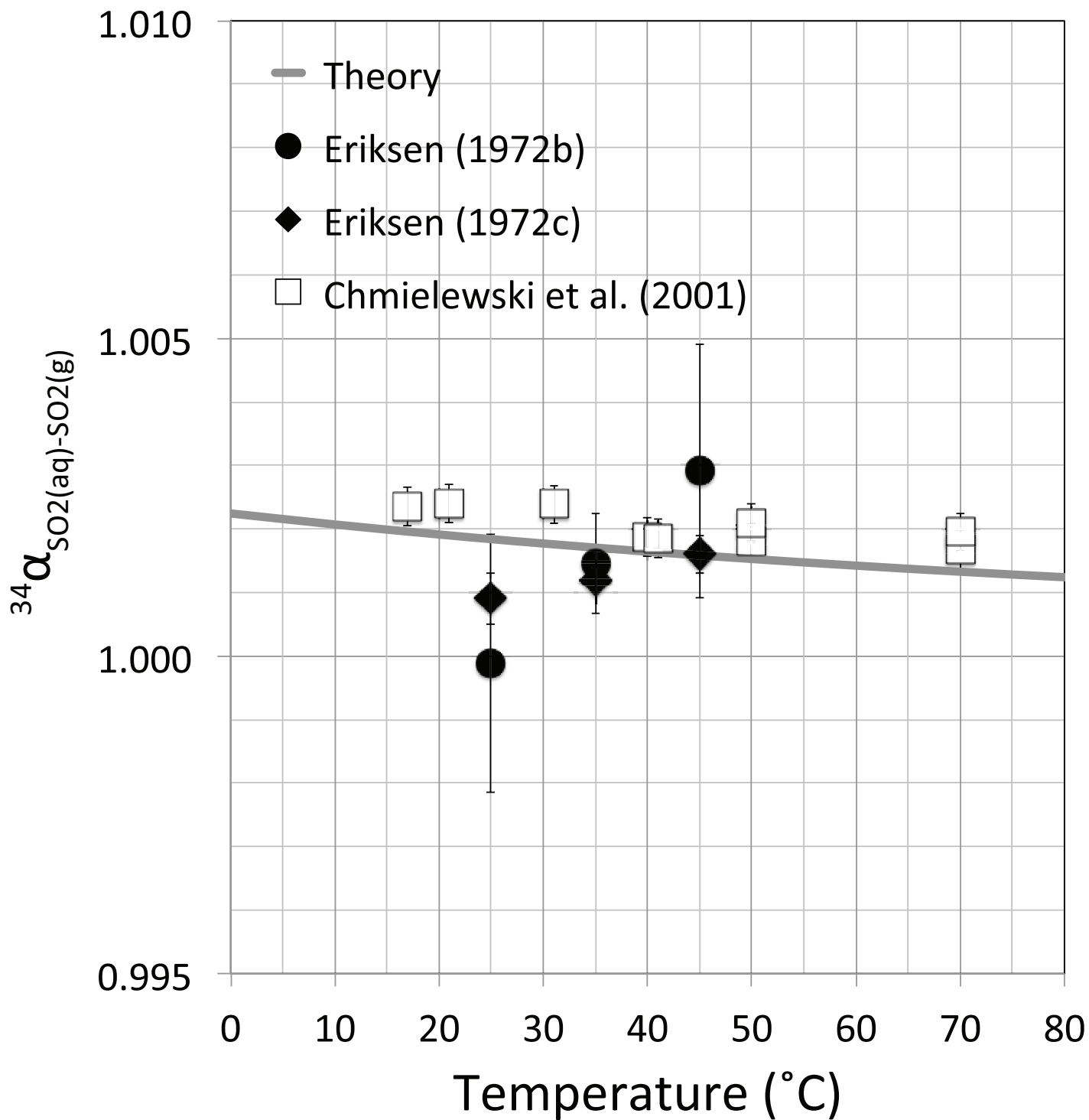
Figure 14
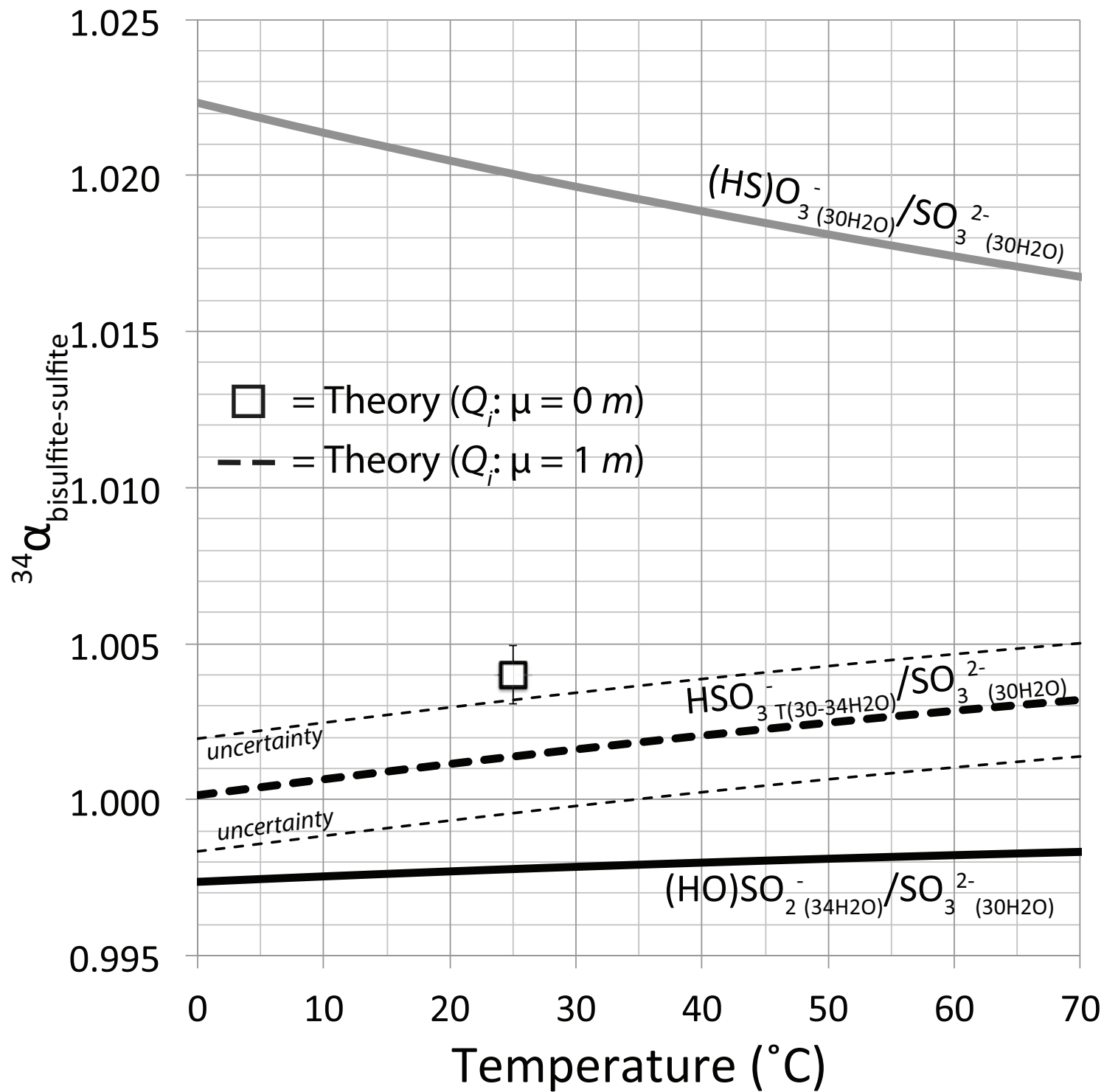
Figure 15
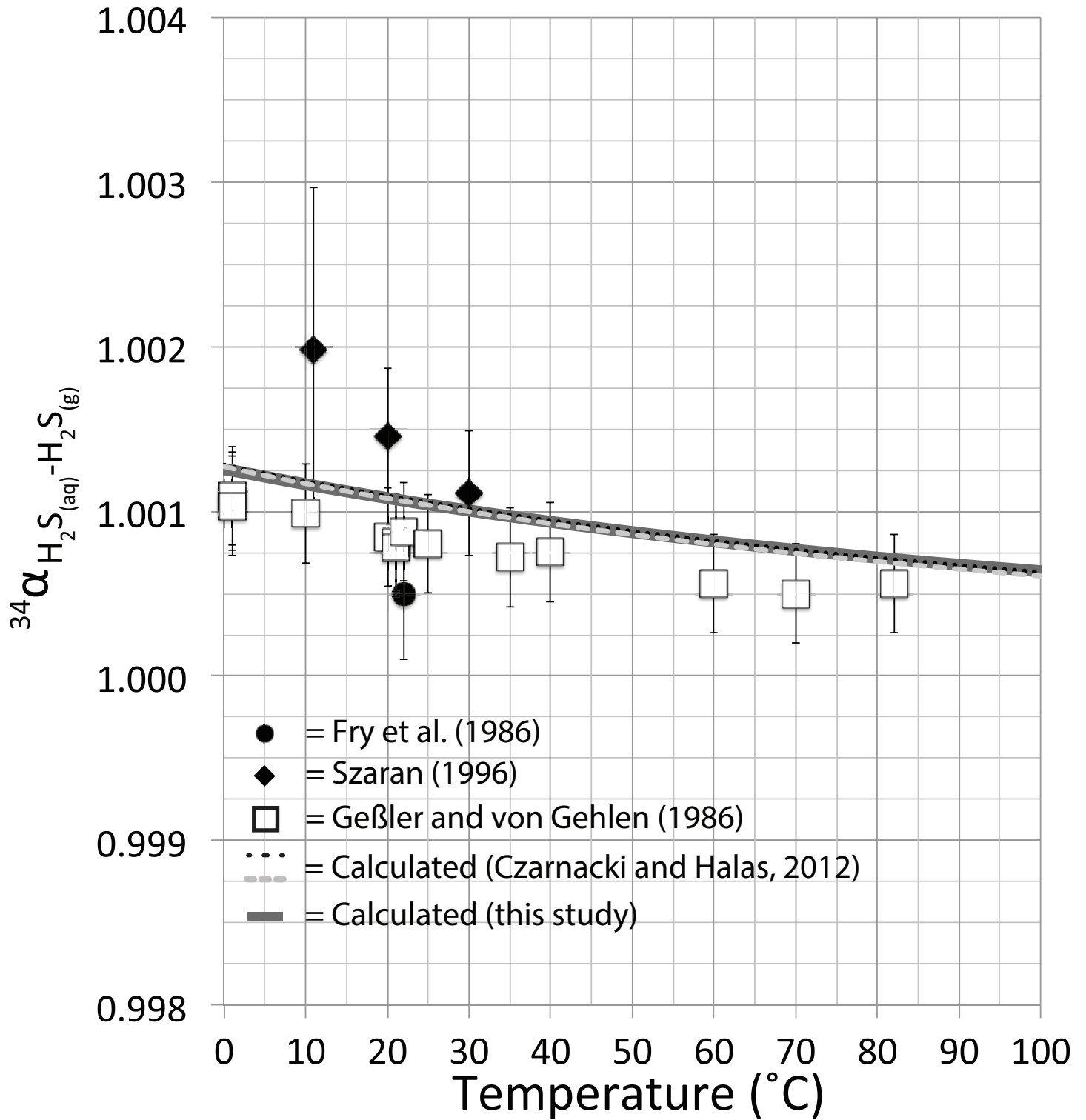
Figure 16

Figure 17

Figure 17
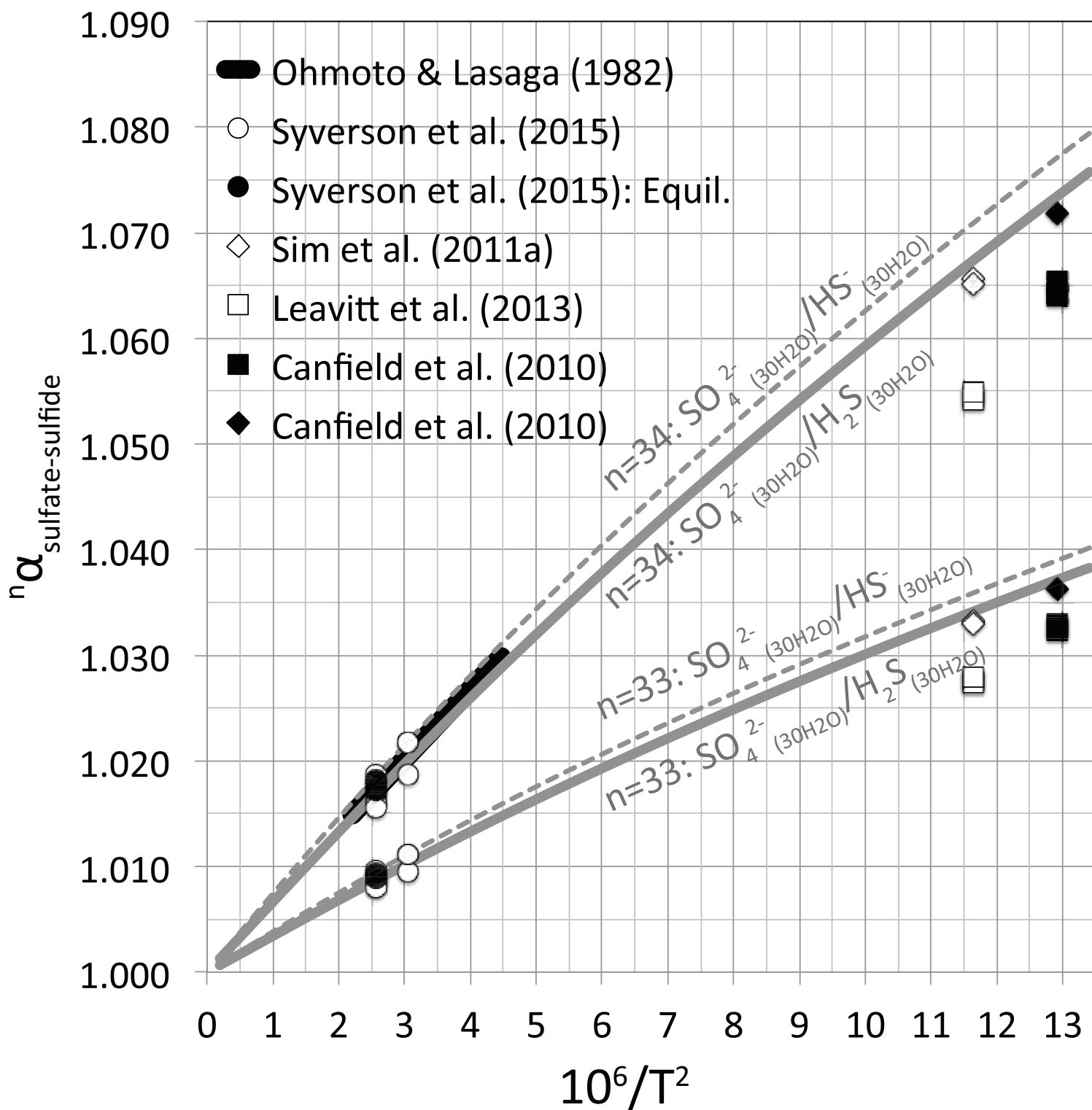
Figure 18

Figure 19

Figure showing $^{34}\alpha$ versus $1000/T$ with labeled trends: $S\text{-}^*SO_3^{2-}{}_{(30H2O)}/^*S\text{-}SO_3^{2-}{}_{(30H2O)}$, $S\text{-}^*SO_3^{2-}{}_{(30H2O)}/H_2S_{(30H2O)}$, and $^*S\text{-}SO_3^{2-}{}_{(30H2O)}/H_2S_{(30H2O)}$.
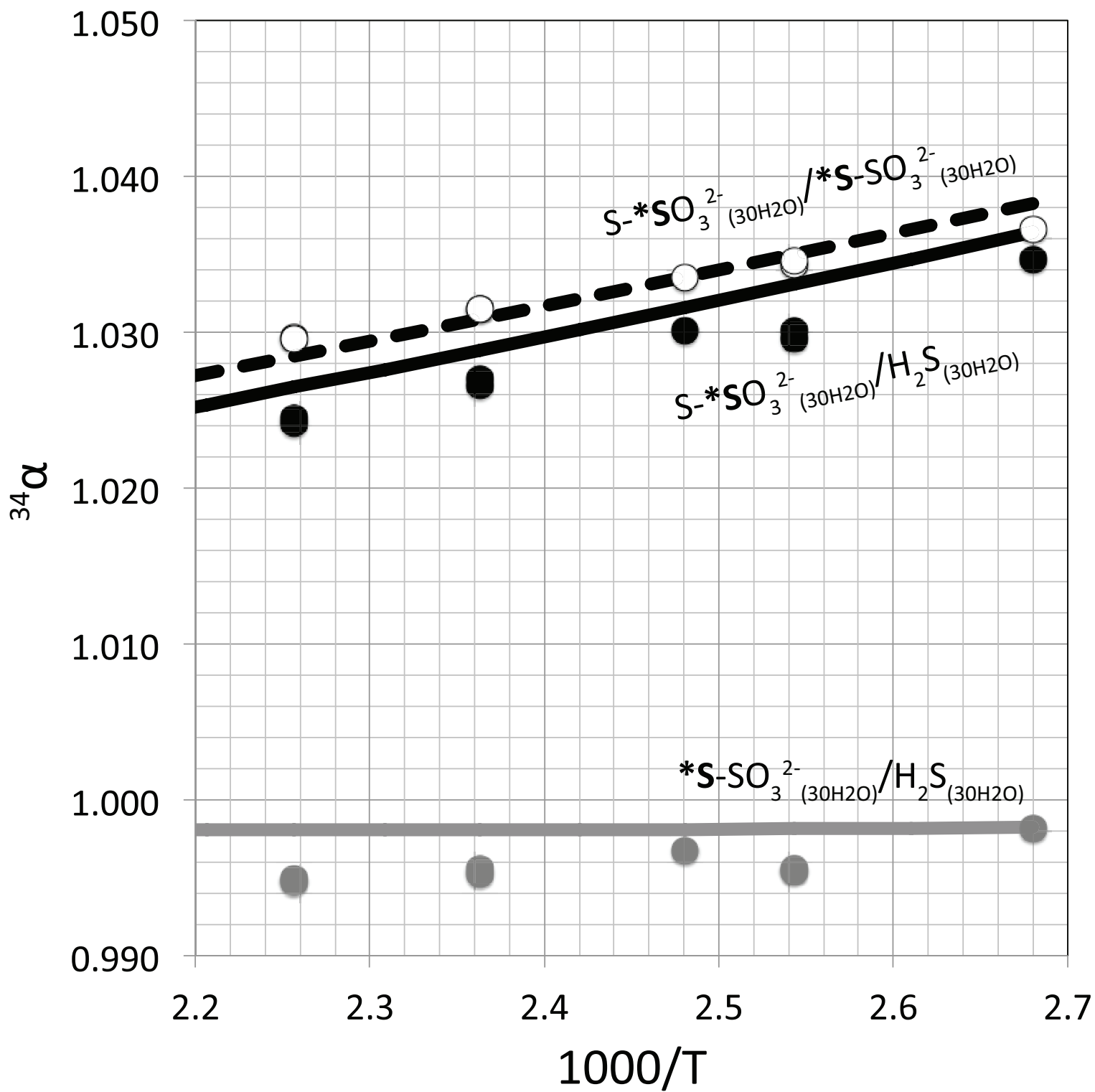
Supplementary Figures and Tables

Click here to download Electronic Annex: Supplementary Figures and Tables_Eldridge et al_GCA.docx

Supplementary Data: Vibrational Frequencies